UNIVERSITY OF
CALGARY

UNIVERSITY OF CALGARY

Network Modelling of Gas Relative Permeability in Heavy Oil

by

Farzam Javadpour

A THESIS

SUBMITTED TO THE FACULTY OF GRADUATE STUDIES IN PARTIAL

FULFILMENT OF THE REQUIREMENTS FOR THE DEGREE OF

MASTER OF SCIENCE IN CHEMICAL ENGINEERING

DEPARTMENT OF CHEMICAL AND PETROLEUM ENGINEERING

CALGARY, ALBERTA

May, 2001

Abstract

Some of the solution gas drive heavy oil reservoirs (foamy oil reservoirs) in Canada, Venezuela, China, and Oman have experienced unusual high primary oil recovery factor (>10%), low producing gas oil ratio, low reservoir pressure decline, and high oil production rate. One of the hypotheses to explain the behaviour is that the gas mobility in foamy oil flow is much lower than that in conventional oil, leading to improved recovery performance. In this study, immiscible micro-displacement in porous media was modeled by using a network of pores of converging-diverging geometry. The effect of viscosity of one phase (oil) on the mobility of another phase (gas) is included in the model. The developed model is used to simulate the motion of the dispersed gas bubbles in an initially oil filled network, and to determine gas relative permeability. The obtained results showed that gas relative permeability decreased drastically by increasing the oil viscosity. In addition, it is shown that dispersion of gas leads to lower relative permeability to gas. Dispersed gas flow and low gas mobility are believed to lead to improved recovery in foamy oil reservoirs.

Acknowledgement

I would like to express my sincere gratitude to my advisor Dr. M. Pooladi-Darvish, for his guidance, support, and patience throughout this work.

I am also indebted to Dr. A. Kantzas for useful discussion in network modeling, and Dr. B. Maini for valuable discussions in gas bubble movements and also accepting to be in my defence committee.

I would like to thank other defence committee members, Dr. A. Jeje and Dr. R. G. Wan for taking out time to read my thesis.

I wish to acknowledge all the staff of the Department of Chemical and Petroleum Engineering for their help and assistance during this work.

The financial support provided by the National Science and Engineering Research Council of Canada (NSERC) and Alberta Energy Research Institute (AERI) is greatly appreciated.

the memory of my mom,

Pari Kazemaini

Table of contents

Title page i

Approval page ..... "

Abstract .....

Acknowledgment ..... 'v

Dedication v

Table of contents vi

List of Tables xii

List of Figures ..... x'"

Nomenclature ..... xv'"

CHAPTER ONE: Introduction 1

1.1. Background 1

1.1.1. Geomechanical effect 2

1.2.2. Effect of reservoir fluids 2

1.1.3. Kinetics of bubble nucleation and growth 3

1.1.4. Effect of flow-dependent properties 3

1.2. Objective 4

1.3. Layout 5

CHAPTER TWO: Microscopic Immiscible displacement-

Background 6

2.1. Porous media 6

2.2. Equilibrium and motion of menisci 7

2.3. Immiscible displacement processes 9

2.3.1. Free imbibition 10

2.3.2. Quasi-static imbibition 11

2.3.3. Imbibition with constant influx and nearly constant Ca values 11

2.3.4. Dynamic invasion 11

2.3.5. Quasi-static displacement of ganglia 12

2.3.6. Dynamic displacement of ganglia 13

2.4. Mobilization and quasi-static displacement of a solitary ganglion 13

2.5. Major classes of local events leading to the formation of new ganglia 18

2.5.1. Pinch-off 18

2.5.2. Dynamic break-up 19

2.5.3. Choke-off or snap-off 19

2.5.4. Coalescence of ganglia 19

2.6. Two-phase flow of dispersed gas phase 20

CHAPTER THREE: Literature review on network models 22

3.1. Introduction 22

3.2. Historical background 24

3.2.1. Percolation based network models 24

3.2.2. Converging-diverging network models 36

3.2.3. Other types of network models 41

CHAPTER FOUR: Converging-diverging network model 43

4.1. Model definition 43

4.2. Analogy concepts 48

4.3. Two-phase flow conductance 51

4.4. Pressure drop across an interface 54

4.5. Effective conductance and pressure drop across an interface 55

4.5.1. Effective conductance 55

4.5.2. Effective pressure drop 56

4.6. Interface movement at the GUC's 57

4.7. Interface movements at the nodes 58

4.7.1. Occurrence of xeron 58

4.7.2. Occurrence of hygron 60

4.8. Boundary conditions 63

4.8.1. Boundary conditions at the inlet and outlet of the 2-D network 63

4.8.2. Boundary conditions at the sides of the network 65

4.9. Development of system of equations (Dias, 1984) 65

CHAPTER FIVE: Model features and assumptions 70

5.1. Porous medium 70

5.1.1. Model dimensions 70

5.1.2. Pore geometry 72

5.1.3. Pore size distribution 72

5.1.4. Coordination number (network connectivity) 73

5.1.5. Length of periodicity (node-to-node distance) 73

5.1.6. Network size 74

5.2. Fluid phases 74

5.2.1. Number of fluid phases 74

5.2.2. Newtonian and non-Newtonian fluids 75

5.2.3. Compressible and incompressible fluids 75

5.3. Driving and resisting forces 76

5.3.1. Capillary forces 76

5.3.3. Viscous forces 76

5.3.4. Gravity forces 76

5.4. Pore-level processes ..... ?[7]

5.4.1. Viscous coupling 77

5.4.2. Precursor wetting film 77

5.4.3. Gas bubble nucleation 78

5.4.4. Gas bubble expansion 79

5.4.5. Gas bubble movement 81

CHAPTER SIX: Determination of relative permeability and simulation algorithm 84

6.1. Determination of gas relative permeability *(k^)* 84

6.1.1. Background 84

6.1.2. Derivation of "steady state" gas pseudo-relative permeability 85

6.1.3. Methodology of ^determination in a network model 88

6.2. Simulation algorithm 91

6.2.1. Model initialization 92

6.2.2. Two-phase flow calculations 96

CHAPTER SEVEN: Results and discussion 101

7.1. Model verification 101

7.2. Model results 102

7.2.1. Effect of network size 103

7.2.2. Effect of gas saturation 106

7.2.3. Effect of capillary number 107

7.2.4. Effect of gas bubble size 110

7.2.5. Effect of aspect ratio (AR) 116

7.2.6. Effect of contact angles 118

7.2.7. Effect of Interfacial Tension (IFT) 119

7.2.8. Effect of viscosity ratio 121

CHAPTER EIGHT: Conclusions and recommendations **127**

8.1. Conclusions 127

8.2. Recommendations 129

References **130**

List of tables

Table	Description	Page
5.1	Model features	71
6.1	Experimental and theoretical analysis of the used porous medium	92
6.2	Input parameters and the range of the investigated Parameters	97

List of figures

Figure	Description	Page
2.1	Mobilization of a solitary ganglion (From dias, 1984)	15
3.1	Illustration of the basic percolation problem. Given a connectivity rule and a random pattern of occupied sites (black) on a lattice of sites. In the figure, a fraction 0.5 of the sites was occupied. (From Wagner, 1997)	26
4.1	A typical unit cell (UC) of the porous medium model (From Payatakes et al., 1980)	45
4.2	Two-dimensional depiction of a cubic network of unit cells. A Conceptual Equivalent Void System (CEVS), a Unit Cell (UC) and an Equivalent Unit Cell (EUC) are identified, as well as an 8-CEVS ganglion (solid line circle) and a 2-CEVS ganglion (dashed line circle). (From Dias, 1984)	48
4.3	Depiction of a 7x6 network showing the nodes numbering system and in the inset the branches numbering system. (Modified from Dias, 1984)	49
4.4	(a) Depiction of an 8-CEVS ganglion on a two-dimensional square network and (b) its electric analog network. (From Dias, 1984)	51
4.5	Representation of a gate unit cell (GUC) divided into ten compartments showing KG and KP used to calculate	

the effective conductance and the effective pressure drop

respectively. Extended part is divided into 2 compartments 56

4.6 Sequential pictures of a 6-pore ganglion during the xeron-

hygron cycle for *fy* = 0.6 (From Hinkley, 1983) 59

4.7 Stages of a 2-CEVS ganglion motion simulation.

Occurrence of a hygron. (From Dias, 1984) 61

4.8 Sequential pictures of a 2-pore ganglion during the

xeron-hygron cycle for ″ ° / = 0.6 (From Hinkley, 1983) 62

5.1 A portion of a 2-D model with 2-CEVS bubbles distributed regularly ... 80

6.1 Schematic representation of the gas bubble movements.

(Modified from Dias, 1984) 89

6.2 Schematic representation of dispersed gas bubbles in a network 90

6.3 Typical unit cell of porous medium

model (Dias, 1984) 93

6.4 Plot of the throat size probability distribution function $F_d(d)$ 94

6.5 (a) Depiction of an 8-CEVS ganglion on a two-dimensional

square network and (b) its electric analog network (Dias, 1984) 94

6.6 Block diagram of the gas relative permeability code 100

7.1 Typical model results of k_g versus time

(16-CEVS bubble, S_g=13%, IFT=15mN/m,

ᴹ * / =1e-5, Cfl = 1e-4, *9* = 25) 102

7.2 Effect of network size on k_{rg}

(16-CEVS bubble, S_g=13%, IFT=20mN/m, Ca = 1e-4, θ_e = 25)..... 104

7.3 Effect of network size on residual oil saturation in oil-water system.

(From Vizika et al., 1994)..... 105

7.4 k_{rg}, versus gas saturation (9-CEVS bubble, IFT=20mN/m,

μ_g/μ_o =1e-5, Ca = 1e-5, θ_e = 25)..... 106

7.5 Effect of capillary number on gas relative permeability at different

viscosity ratios (9-CEVS bubble, Sg=12%, IFT=20mN/m, θ_e = 25)... 107

7.6 Effect of capillary number and viscosity ratio on relative

permeability in oil-water system (From Avraam

and Payatakes, 1995)..... 108

7.7 Effect of capillary number on relative permeability in

oil-water system. (From Constantinides and Payatakes, 1996)..... 109

7.8 Effect of capillary number on relative permeability in

gas-condensate system. (From Mott et al., 2000)..... 110

7.9 Effect of gas bubble size on gas relative permeability

(Ca=1e-4, Sg=12%, IFT=20mN/m, θ_e = 25)..... 111

7.10 Comparison of bubble growth for gradual decline in pressure

(100 psi/hr) for various cases. (From Kumar, 2000)..... 113

7.11 Illustration of bubble break-up mechanisms by tip splitting [(a) and (b),

and break-up of elongated gas bubbles [(c) and (d)].

(From Bora et al., 2000) 114

7.12 Effluent foam texture for (a) a weak foam (d_BL=700 |am) and (b) a strong foam (d_Bi_=300 urn). (From Ettingerand Rodke, 1992) 115

7.13 Effect of average bubble densities and sizes on gas velocity for pre-generated and in-situ-generated foam flow experiments (From Ettingerand Radke, 1992) 116

7.14 Effect of aspect ratio (AR) on gas relative permeability (16-CEVS bubble, Sg=13%, / Mo = 1e-5, Ca=1e-4, IFT=20mN/m, ϑ_e = 25) 117

7.15 Effect of contact angle (equilibrium, advancing, and receding) on gas relative permeability (16-CEVS, Sg=13%, / Mo = 1e-5, Ca=1e-4, IFT=20mN/m). Advancing and receding contact angles are 5 degrees higher and lower than the equilibrium contact angles, respectively 119

7.16 Effect of interfacial tension (IFT) between oil and gas on gas relative permeability (16-CEVS bubble, Sg=13%, / Mo = 1e-5, Ca=1e-4, ϑ_e = 25) 120

7.17 Effect of interfacial tension on the relative permeability in gas/condensate system. (From Li and Firoozabadi, 2000) 121

7.18 Effect of viscosity ratio on relative permeability in oil-water system.
(From Odeh, 1959) 122
7.19 Effect of viscosity ratio on relative permeability in oil-water system.
(From Constantinides and Payatakes, 1996) 123
7.20 Gas relative permeability at different oil viscosities.
(From Wall and Khurana, 1972) 124
7.21 Comparison of relative permeability ratio in heavy and light oil.
(From Pooladi-Darvish and Firoozabadi, 1999) 125
7.22 Effect of viscosity ratio on gas relative permeability.
(9-CEVS bubble, Sg=12%, IFT=20mN/m, $\theta_c = 25$) 126

Nomenclature

a	=	maximum diameter of sinusoidal function, *[im*
AR	=	Aspect Ratio
c,,$c_2$and c_3	=	geometrical constants
Ca	=	capillary number
CEVS	=	Conceptual Equivalent Volume Space
d	=	throat diameter, minimum diameter of sinusoidal function, *\im*
D	=	effective chamber diameter, (im
EVS	=	Elemental Volume Space
EUC	=	Extended Unit Cell
G	=	conductance
GUC	=	Gate Unit Cell
h	=	wave length, um
ti	=	unit cell length, um
K	=	absolute permeability, fim^2
k_{gg}	=	effective gas permeability due to flow of gas phase
k_{go}	=	effective gas permeability due to flow of oil phase
k_r	=	relative permeability, fraction
IFT	=	interfacial tension, mN/m
j	=	Gaussian curvature, |^m"[1]
/	=	node-to-node distance, |j.m

L	=	length of liquid column, m
N	=	number of unit cells
N_b	=	total number of branches
NGUC	=	total number of GUC
N_p	=	total number of interior nodes
p	=	pressure, kpa
P_c	=	capillary pressure, kpa
$\boldsymbol{p}$	=	node voltage source vector
$\boldsymbol{q}_{uc}$	=	flow rate through unit cell, um^3/s
$\boldsymbol{q}$	=	branch current
$\boldsymbol{q}$	=	node flow source vector
$\boldsymbol{r}$	=	radius of capillary,
$\boldsymbol{R}$	=	resistor
$\boldsymbol{R}_e$	=	Reynolds number
t	=	time, s
UC	=	Unit Cell
$\boldsymbol{v}_p$	-	branch voltage
v,	=	voltage source (for gate unit cell)
v[	=	additional voltage source (for boundary pressure)

Greek

/u	=	viscosity, mpa.s
v	=	kinematics viscosity, m^2/s
v	=	superficial velocity, m/s
p	=	density, kg/m^3
G	=	contact angle
k	=	viscosity ratio
a	=	interfacial tension, mN/m
Ai>	=	pressure drop across an oil-water interface, kpa
AP_{uc}	=	pressure drop along a unit cell, kpa
A/	=	time increment, s
<)	=	porosity, fraction

Subscripts

a	=	advancing
dr	=	drainage
e	=	equilibrium
eff	=	effective
g	=	gas
ib	=	imbibition
nw	=	non-wetting phase
o	=	oil

ow	=	oil-water
r	•	receding
w	-	water, wetting phase
x	-.	x-direction
y		y-direction
z	=	z-direction

Superscripts

0	zero velocity
T	transpose

CHAPTER ONE

Introduction

Heavy oil will be a major energy source in the future as conventional oil production rates decline and energy consumptions increase. Production cost of the heavy oil reservoirs is more than conventional oil. Therefore, there are a lot of researches in order to find more economical production method for heavy oils. Smith (1988) published a paper about an unusual solution gas drive behaviour in a heavy oil reservoir. In that reservoir the production rate under primary recovery was favourably high, and the produced gas favourably low. This type of reservoir is called foamy oil reservoir.

1.1. Background

Some of the solution gas-drive heavy oil reservoirs in Canada (Smith, 1988; and Loughead and Saltukaroglu, 1992), and Venezuela (Heurta et al., 1996), China and Oman (Firoozabadai, 2001) have experienced unusually high primary production rates and other anomalous behaviour including high primary oil recovery factor (>10%), low producing gas oil ratio, low reservoir pressure decline, and high oil production rate.

To explain this behaviour, three fundamental reasons have been suggested. Geomechanical effects, special fluid properties and unusual flow dependent

properties of oil and gas have been suggested to explain the observed behaviour of foamy oil reservoirs.

1.1.1. Geomechanical effects

In many Canadian reservoirs it is believed that wormholes are generated during the initial phase of cold production and are responsible for enhanced production rates. Geomechanical effects are important through creation of wormholes, sand dilation, pore de-blocking, and so on. Some of the related references on this subject are: Dusseault and El-Sayed (2000), Economodes et al. (2000), Yuan et al. (1999 and 1998), Dusseault et al. (1998), Wang and Yuan (1998), Tremblay et al. (1997), and Dusseault (1993).

1.1.2. Effect of reservoir fluids

Another set of investigations study the special behaviour of reservoir fluids. Presence of micro-bubbles (Smith, 1988; Trienen et al., 1997; Bora and Maini, 1997), and the effect of these tiny bubbles on oil viscosity (Smith, 1988; Poon and Kisman, 1992; Islam and Chakma, 1990; Claridge and Prats, 1995; Sheng et al., 1999; Shen and Batycky, 1999) are the main issues that have been investigated in this category. Other reasons and effects such as pseudo-bubble point pressure (Kraus et al., 1993; Geilikman et al., 1995) was the target of some of the research works in this category.

1.1.3. Kinetics of bubble nucleation and growth

Experimental and modelling studies of Li (1993) suggest that the non-equilibrium processes between solution gas and free gas is affected by kinetics of bubble nucleation, and that gas diffusivity is important in describing the unusual behaviour of the solution gas drive heavy oil reservoirs.

1.1.4. Effect of flow-dependent properties

In this category it is believed that the low mobility of gas is the main reason of the unusual behaviour in solution gas drive heavy oil reservoirs. In conventional thinking of two-phase flow, where fluid distribution is a function of capillary forces and relative permeability functions depend only on fluid saturations for a specific rock, one would expect relatively similar relative permeability values for the two experiments that run in the same rock system but with fluids with different viscosity. However, the experimental and modeling studies have clearly shown that relative permeability to gas would change by changing the oil viscosity in the same rock system.

In recent works, it has been observed that matching of field data (Kumar and Pooladi-Darvish, 2000) as well as laboratory depletion data (Pooladi-Darvish and Firoozabadi, 1999 and Kumar et al., 2000) required assigning extremely low values of gas relative permeability. The relative permeability functions of these studies however, were obtained through history matching. One might ask, what

relative permeability functions should be chosen for a particular system? Can this be known a *priori?* This research work concentrates on obtaining the answer to such questions. As a first step, it is important to find what parameters affect relative permeability functions, and how these factors are ranked in their importance. This is investigated in this research project. A microscopic scale (network) model is developed and used in order to investigate the effect of different parameters, in particular oil viscosity on two-phase flow in porous media.

1.2. Objective

Possibly, all the above mentioned reasons play a role in describing the unusual behaviour of the solution gas drive heavy oil reservoirs. However, due to the complexity of the problem we will focus only on the gas and oil flow behaviour in porous media. The objective of this research is to find the effect of different parameters in particular oil viscosity on gas relative permeability. Microscopic scale (pore level) models are proposed in order to investigate the effect of pressure forces on gas bubble interfaces movements in two-phase flow.

Network models have been developed to represent the complex shape of a natural porous medium. These models are simplified mathematical representation of the real porous material. The objective of a porous network model is to provide a reasonable idealization of the complex geometry of the real porous medium, so that the related fluid flow can be treated mathematically at a

manageable level of complexity.

1.3. Layout

The thesis starts with the theoretical and experimental background of the microscopic immiscible two phase flow (Chapter 2). In this chapter the nature of two-phase flow in porous media, in particular equilibrium and menisci motion in pore level, different flow regimes, ganglia displacement and major classes of local events on the ganglion movement is presented. In Chapter 3, a review on the available network models is given. The converging-diverging network model of the porous media is explained in detail in Chapter 4. This chapter presents model definition, single and two-phase fluid flow conductance, pressure drop across an interface, interface movement, boundary conditions, and development of the system of equations. In Chapter 5, model capabilities and assumptions of the network model will be presented. Chapter 6 demonstrates the method of obtaining gas relative permeability from the model results, and the simulation algorithm. Model results, discussion and verifications are presented in Chapter 7. Each graph will be followed with an explanation. Finally, in Chapter 8 the conclusions of this investigation and recommendations for the future work will be given.

CHAPTER TWO

Microscopic immiscible displacement-Background

In this chapter, immiscible displacement of oil by water will be explained. Immiscible displacement at pore level or specifically interface movements of a solitary ganglion and major classes of local events leading to formation of new ganglia will be explained. All the explanations in this chapter are based on oil ganglion movements by water. However, we assumed that oil ganglion motion rules are valid for the gas bubble movements in the rest of this study. The justification for this assumption is given at the end of this chapter when two-phase flow of gas and oil is described.

2.1. Porous media

Flow in natural or industrial porous media arise in many diverse fields of science and engineering such as agriculture, biomedical, construction, ceramic, chemical, underground hydrocarbon reservoirs, powder metallurgy, food and soil sciences. Here, attention is focused on a pertinent class of prototype porous media, namely rock formation of oil reservoir. Micro-model and network model of porous media which have much simpler structures are usually used in experimental and theoretical studies of displacement processes, respectively.

In the remainder of this work, pore terminology will be used to denote the void space within the porous medium. Large pores with size comparable to that of the grains are called chambers (pore bodies) and the narrow pores connecting chambers are referred to as throats.

A porous medium could be characterized by its porosity, pore geometry, heterogeneity and anisotropy. The throat size distribution, the chamber size distribution, the chamber-to-throat size ratio (aspect ratio), the number of throats connected to a chamber (coordination number), and the shape of the pores (circular, square, triangular, converging-diverging, four-cusp, etc.) are the most relevant characteristics of pore geometry and topology (Payatakes et al., 1973, Payatakes et al.; 1980; Chandler et al., 1982; Koplic, 1982; Wilkinson and willemsen, 1983; Koplic and Lasseter, 1985; Goode, 1991; Patzek, 2000).

2.2. Equilibrium and motion of menisci

A contact line is formed at the intersection of two immiscible fluids and a solid. The mutual interaction between the three materials in the immediate vicinity of the contact line affects the static and dynamics of the entire flow field. West (1911) and Washburn (1921) were the first to analyze the displacement of one immiscible fluid by another through a circular capillary. The progress of a liquid flowing under its own capillary pressure in a horizontal cylindrical capillary can be theoretically described by the Washburn equation:

$$L^2 = \frac{art\cos 9}{2/} \qquad (2.1)$$

where L is the length of the liquid column at time t, $/u$ its viscosity, r is the radius of the capillary, a is the liquid-gas interfacial tension and 6 is the contact angle.

Equation 2.1 can be derived from Poiseuille's equation for viscous flow by assuming that pressure drop (AP) across the liquid-vapor interface is given by Young-Laplace equation (Equation 2.2) for a hemispherical interface.

$$AP = \frac{2(7C\ o\ s\ 0}{} \qquad (2.2)$$

where 6 in this equation is the "apparent" dynamic contact angle of the moving meniscus.

Dynamic contact angles have been the object of extensive studies. A good review on this subject is given by Dussan V. (1979). She observed when a meniscus advances away from the wetting phase, its advancing contact angle, 9_a, is larger than the intrinsic or equilibrium value, 6_e, and when a meniscus recedes towards the wetting phase, its receding contact angle, 9_r, is smaller than 0_e.

2.3. Immiscible displacement processes

Immiscible displacement is the displacement of one fluid by another immiscible fluid. The process is controlled and affected by a variety of factors. Depending on how the displacement process proceeds, many different regimes may arise.

In this work attention is focused on micro-displacement that is on flow phenomena at the pore scale. Due to small pore dimensions and low flow rates, the flow regime of interest is in the domain of creeping flow. The flow phenomena depend on the geometry and topology of the porous medium, on the physical properties of both fluids (viscosity, density, interfacial tension and contact angle), and the externally imposed macroscopic pressure drop. The flow is also history dependent, since it depends locally on the value of the non-wetting saturation as well as on the way in which the non-wetting phase is distributed. Two dimensionless groups are often used to characterize the displacement mode:

- The capillary number, Ca-$\frac{LI\ V}{\ ^{w}}$, where $//_{w}$ and v_{w} are the viscosity and <j superficial velocity of the wetting phase, respectively and ***a*** is the interfacial tension between the two fluids.
- The viscosity ratio ***(K*** = ^***-),*** where $/i_{nw}$ is the viscosity of the non-wetting phase.

Payatakes and Dias (1984) proposed a partial classification of the displacement phenomena in flow regimes. This classification was based on the values of capillary number, Ca and viscosity ratio, K, the connected or disconnected form of the non-wetting phase, and the transient or steady nature of the flow. A summary of their classification is given here. In this discussion it is assumed that the non-wetting phase is initially connected and fills the porous medium (save for a small amount of connate water). Wetting phase is brought into contact with the non-wetting phase so that the two fluids are now separated by a set of interfaces residing in pores near the front layer of the medium.

2.3.1. Free imbibition

Free imbibition occurs spontaneously when the wetting phase invades the porous medium driven by the capillary forces. These capillary forces resulting from the presence of the wetting and non-wetting interfaces remain within relatively narrow bounds throughout the displacement process, whereas the viscous resistance to the flow increases as the wetting phase invades the porous medium. The capillary number takes values of a wide range (10^{-9} to 10^{-4}). Since the process is driven by capillary suction, the wetting phase tends to pass through the narrowest accessible pores at every stage.

2.3.2. Quasi-static imbibition

Quasi-static imbibition is achieved in a similar fashion as free imbibition, only now a backpressure is applied in order to counter-balance the capillary suction and to obtain vanishingly small flow rates.

2.3.3. Imbibition with constant influx and nearly constant Ca values

This flow regime in many respects is similar to both free imbibition and quasi-static imbibition. A backpressure is applied across the porous medium and continuously adjusted to compensate for the changes of the viscous resistance as the wetting phase displaces the non-wetting phase. Therefore, the velocity and capillary number are kept relatively constant.

2.3.4. Dynamic invasion

Dynamic invasion is obtained by applying a sizeable pressure difference across the porous medium making the pressure forces the dominant driving force, whereas the capillary suction plays a secondary assisting role. Depending on the value of viscosity ratio, the invasion develops in different ways. In this regime, the capillary forces are negligible compared with the pressure forces, and several of the advancing interfaces tend to follow paths of least viscous resistance. Since, for the most part, chambers are substantially larger than throats, the process is controlled by the invasion of the largest accessible throats.

At the end of any invasion process, some of the non-wetting phase remains trapped in the form of ganglia. These ganglia could be as small as the size of one pore. Some of these ganglia may become mobilized if a new flood with a much larger capillary number (say $Ca = \0\sim^{4}$) is performed. The minimum capillary number required for mobilization of a ganglion is called the critical capillary number. It should be noticed that now, contrary to the cases of imbibition and dynamic invasion, the capillary forces resist the displacement of the non-wetting ganglia. Depending on the capillary number, the displacement of ganglia can take different characteristics. The developed model in this study is based on the ganglia movement. This model will be used for the study of gas bubble movement in a heavy oil saturated porous medium. The complete discussion of the model will be given in chapter 4.

2.3.5. Quasi-static displacement of ganglia

Quasi-static displacement of ganglia is observed when the value of Ca is slightly larger than the critical value for mobilization. This flow regime is characterized by the non-wetting phase invasion of one (and only one) of the downstream chambers and the wetting phase invasion of one (may be two) upstream chambers.

2.3.6. Dynamic displacement of ganglia

This occurs when the value of Ca exceeds the critical value by a sizable amount, and it presents characteristics somewhat different than those of quasi-static displacement of ganglia. Here, the ganglion may move through different pathways simultaneously as one or more interfaces advance simultaneously in the porous medium.

2.4. Mobilization of a solitary ganglion (Dias, 1984)

Consider a non-wetting ganglion stranded in a porous medium as it is shown in Figure 2.1a. If the macroscopic pressure difference is nil, V> = 0, both the wetting phase and the ganglion are immobile, and both p_w and p_{nw}, the pressure values in the wetting phase and non-wetting phase, respectively, are constant.

The condition for quasi-static equilibrium at each point of a non-wetting/wetting phase interface is given by:

$$P_n\text{*-}Pw=<r_{nw}\text{-}_wJ \qquad (^2\text{-}^3)$$

where, $p_{nw} - p_w = P_c = \frac{2\sigma_{nw}\cos\theta}{r}$ and for the solid/non-wetting/wetting contact line the equilibrium is given by Young's equation:

$$\cos\theta_c = \frac{\sigma_{nw} - \sigma_{ws}}{\sigma_{ns}} \qquad (2\text{-}4)$$

Here, J is the Gaussian curvature of the interface which is 2 over the radius of the curvature *(R),* θ_c is the equilibrium contact angle, σ_{nw} is the interfacial tension between the non-wetting and the wetting phase, σ_{ns} is the interfacial tension between the non-wetting phase and the solid and σ_{ws} is the interfacial tension between the wetting phase and the solid.

If the macroscopic pressure difference is increased to a non-zero ($\nabla p > 0$) but small value (below the value required to induce mobilization), the pressure in the wetting phase decreases along the ganglion, while the pressure p_n in the non-

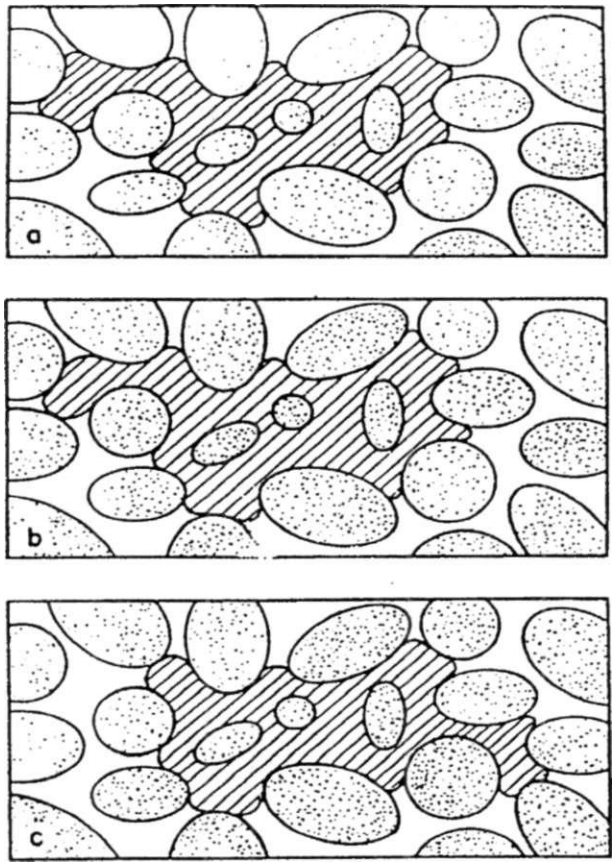

Figure 2.1: Mobilization of a solitary ganglion (From Dias, 1984)

wetting phase remains virtually uniform. In this case the pressure drop $(p_{nw}-p_w)$ across each downstream interface is different from the pressure drop across each upstream interface. In order to retain an equilibrium position, the ganglion responds as follows. The downstream interfaces advance in their respective throats, increasing their Gaussian curvature, and the upstream interfaces recede in the corresponding throats, such that their Gaussian curvatures decrease (Figure 2.1b). Due to the roughness of most prototype porous media, the contact angle may present hysteresis effects. With this effect, at the same time as the

downstream interface advances, the contact angle decreases tending to the limiting value of θ_r at zero velocity $0°$, and similarly, the contact angle for the upstream interfaces tends to $\theta°$. This new position can be considered, as an equilibrium position between external pressure forces and capillary forces, since the resulting capillary pressure imbalance tends to move the ganglion backward or forward, whereas the external pressure difference tends to move the ganglion forward.

The macroscopic pressure gradient may be increased even further and the ganglion rearranges and remains in an equilibrium position as long as all interfaces of the ganglion are stable. Melrose (1970) and Melrose and Brandner (1974) developed a criterion for the stability of a single interface in a water-wet system. In essence, this criterion says that an interface is stable as long as its curvature is within the range of $J_{imh}<J<J_{dr}$, where $J_{imh}=\frac{4\cos\theta°}{a}$ is the minimum stable Gaussian curvature (imbibition Gaussian curvature) and $J_{dr}=\frac{4\cos\theta°}{d}$ is the maximum stable Gaussian curvature (drainage Gaussian curvature). The parameter d is the throat diameter and a is the maximum pore diameter. Both J_{imh} and J_{dr} are functions of the contact angle, and local pore size and geometry.

Assume now that the macroscopic pressure difference is increased to exceed a critical value (|v>| >|V/>$_{tr}$| or $Ca>Ca_{cr}$) *at* which the curvature of one of the downstream interfaces exceeds its critical drainage Gaussian curvature J_{dr}. The ganglion becomes unstable and moves. The non-wetting phase invades one of the downstream chambers (this event is called xeron) and the wetting phase invades one (may be two or more if the xeron occurs in an unusually large chamber) of upstream chambers that used to be occupied by the non-wetting phase (this event is called hygron). This motion is a relatively fast one and was initially called a rheon by Heller (1968) and Melrose and Brandner (1974) (Figure 2.1c).

If the macroscopic pressure difference is kept constant, the ganglion may continue to move through a series of xerons and hygrons until it breaks in two daughter ganglia or it finds a new equilibrium position and gets stranded again.

This type of displacement, where only one of the downstream interfaces of the ganglion advances while one or maybe two upstream interfaces retract is called quasi-static displacement of ganglia. Quasi-static displacement of ganglia occurs when the applied macroscopic pressure gradient |Vp| is slightly larger than the value required to cause mobilization.

Ng and Payatakes (1980) developed a criterion for the quasi-static mobilization of ganglia. This criterion is based on the one developed by Melrose and Brandner (1974). Furthermore it is capable of determining not only whether mobilization occurs, but also through which pair of throats, the rheon is going to occur.

2.5. Major classes of local events leading to the formation of new ganglia

At the end of both dynamic invasion and imbibition one obtains many isolated blobs or clusters of the displaced fluid-their displacement is the main goal of the oil recovery enhancement. Usually, the mobilization and displacement of oil blobs require relatively high capillary number, of the order of $Ca > 10^{-4}$. The mobilization and displacement of oil blobs depend on several factors, including the shape and size of the blobs, the morphology of the porous medium, especially around the regions where the blobs reside, the viscosity ratio of the fluids, and the contact angles (Sahimi, 1993).

A moving blob might break into smaller blobs by one of the following mechanisms.

2.5.1. Pinch-off

In pinch-off, the velocity of the moving blob becomes small for a long enough time that the blob collapses and breaks into several smaller blobs.

2.5.2. Dynamic break-up

In dynamic break-up, a blob advances in two or more pore throats simultaneously, which can easily happen if the coordination number of the pore space is large enough. For this to happen, the value of capillary number should be large enough to move the blob into two different size throats.

2.5.3. Choke-off or snap-off

This mechanism was first discussed by Pickell et al. (1966). Choke-off signals the break-up of a small drop from the leading tip of a non-wetting constriction. In this process, as an oil drop moves through a throat into a chamber filled with the wetting phase, part of the oil drop snaps off into a smaller droplet and moves ahead of the primary drop. Choke-off becomes important when the ratio of the pore body and pore throat diameter (aspect ratio) is large (Wardlaw, 1980; Chatzis etal., 1982).

2.5.4. Coalescence of ganglia

Reconnection of ganglia occurs through collision followed by coalescence. When two droplets of the non-wetting phase collide with each other, a thin film of continuous wetting phase is trapped between the two drops. If this film is drained to such an extent that hydrodynamic disturbances and interfacial attractive forces eventually cause the film to collapse, coalescence would occur (McKay and Mason, 1963; Hartland, 1967).

Jeffrey and Davis (1971) identified five stages for a typical coalescence process between two droplets. First the drops approach one another under the influence of some external force. Then, a pendular film of the continuous phase is formed between the two drops. As time passes the film drains slowly until it ruptures. The process ends with the rapid combination of the contents of the two drops. The film drainage step tends to be the limiting stage.

2.6. Two-phase flow of dispersed gas phase

In this work, we are interested in the mobility of the gas-phase in the presence of oil. For the gas to move, however it does not need to form a continuous phase. The notion of mobility of a discontinuous phase is in departure from the traditional view that for a phase to be mobile it needs to be continuous. Experiments of Avraam and Payatakes (1995) have shown that substantial two-phase flow can occur while one of the phases is discontinuous. Pressure forces exerting on the discontinuous gas bubbles could lead to their flow. Pooladi-Darvish and Firoozabadi (1999) suggested that a discontinuous gas phase can lead to sustained but intermittent gas flow. Visual observation of gas-clusters on the surface of a sand-pack, as well as fluctuating pressure differentials across the sand-pack under solution gas drive suggested that there could be substantial gas flow while the gas-phase is discontinuous. These observations are in-line with filed experience in heavy oil reservoirs under solution-gas drive, where gas is produced in slugs. Within this framework, continuity of gas phase is not a

requirement for gas mobility (Firoozabadi, 2001). A similar flow mechanism was suggested by Dias (1984) for oil ganglion movement in water saturated porous medium. We have adopted the same displacement process to study the gas bubble movements in oil saturated porous medium.

CHAPTER THREE

Literature review on network models

3.1. Introduction

The world works differently at different scales, and earth sciences must therefore rely on different methods of modelling the diverse earth systems that range in size from atoms and molecules to the whole planet. The typical size of the pore considered in network studies is of the order of 20 ^m. One cubic centimetre of reservoir sandstone may have 200,000 pore bodies, and 500,000 pore throats (Patzek, 2000).

There are two different modelling approaches for the study of fluid flow through porous media. The first approach is based on the classical equations of transport phenomena supplemented with constitutive equations describing the transport and other important coefficients and parameters, which are called continuum models. The second approach, which is our interest in this study, is based on network models of pore space.

In order to represent the complex shape of a natural porous medium, network models have been developed. Network models are simplified mathematical representation of the real porous material. Sahimi (1993) defined network model as; "network model models the phenomena at the smallest scale, a pore or

fracture, and then employs large-scale simulation and modern concepts of the statistical physics of disordered systems, such as scaling and universality, to obtain the macroscopic properties of the system". The objective of a porous network model is to provide a reasonable idealization of the complex geometry of the real porous medium, so that the related fluid flow through that can be treated mathematically at a manageable level of complexity.

Network analysis methods make use of standard electric network analysis to solve the network flow field, with the recognition of the analogy between flow rate and current, pressure drop and voltage, hydraulic conductance and electric conductance, and capillary pressure and voltage source.

Pores in network models can be geometrically represented as circular, triangular, square (Patzek, 2000), converging-diverging (Payatakes et al., 1980), and four-cusp (Goode, 1991). Networks of constricted unit cells, allows inclusion of viscous forces and modelling of ganglion movement. These features make such model suitable for the study of gas bubble movement in oil saturated porous media.

The network model of this study is based on the converging-diverging unit cell network model. This model is used for the study of gas bubbles in highly viscous oil. This type of models is reviewed in Section 3.2.2 and is explained in detail in

Chapters 4 and 5. Other network models commonly used, are reviewed in the next sections.

3.2. Historical background

Fatt (1956) seems to be the first to use a multiple connected pore space (2-D) network of cylindrical tubes. He modeled the capillary pressure characteristics, by accounting for the dynamic properties of a single size tube and capillary radius distribution. The proposed model more closely represented real porous media than the bundle-of-tube models.

Network models can be categorized in two main types: (1) percolation based models and (2) converging-diverging models. In the next section percolation based models will be explained briefly and some of the developed models in this category will be reviewed. History of the development of converging-diverging network model will be presented briefly at the end of this chapter.

3.2.1. Percolation based network models

Percolation is about connectedness. Percolation phenomena are common in nature and occur in porous media (spontaneous imbibition without corner flow and with surface roughness), in multiphase systems (critical phenomena), in chemical systems (polymerization reactions), and in biological systems (the antibody-antigen immunological reactions). The special properties of a system,

which emerge at the onset of macroscopic connectivity within it, are known as percolation phenomena (Patzek, 2000).

Percolation models make use of percolation theory in conjunction with lattices composing of sites (pore bodies or chambers) and bonds (pore throats). The theory of percolation was first stated by Broadbent and Hammersley (1957) as the theory of properties of particles interacting with a random network. Good reviews of percolation theory are provided by Frisch and Hammersley (1963), and Essam (1980).

Transport processes in random media are related to percolation theory. The general formulation of the percolation problem is concerned with elementary geometrical objects (spheres, sticks, sites, bonds, etc.) placed at random in a *d*-dimensional lattice or continuum of infinite size. Objects are connected if the distance between points belonging to different objects is less than a connectivity radius *R.* Percolation theory deals with the size and structure of the clusters formed by objects that are connected to each other. If the density of connecting objects exceeds a threshold, an infinite cluster of connecting objects spans the space. The infinite space may represent a porous or fractured medium that is saturated with one phase, and the objects may represent pores or fractures in the medium that are filled with a second phase. Flow of the second phase through the

medium is possible if the concentration of pores or fractures filled with the phase exceeds a threshold concentration.

The percolation problem describes the simplest possible phase transition with nontrivial critical behavior. The transition is purely geometrical in nature. Although the rules that govern the connectivity of elementary objects are well defined, the structure of the percolation cluster at the threshold concentration is far from being understood.

Percolation models are qualitative models of two-phase flow in which a random medium is represented by a two- or three-dimensional lattice, see Figure 3.1. The

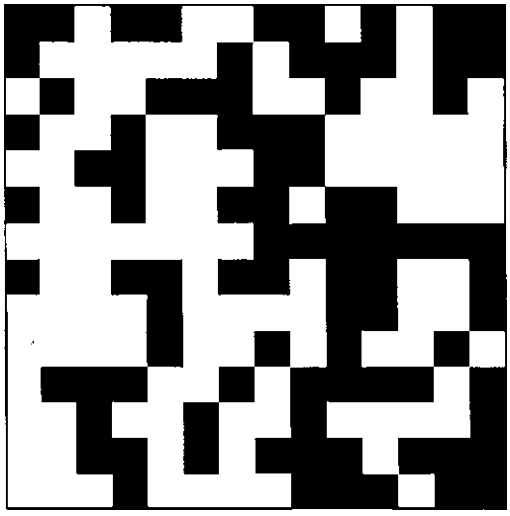

Figure 3.1: Illustration of the basic percolation problem. Given a connectivity rule and a random pattern of occupied sites (black) on a lattice of sites. In the figure, a fraction 0.5 of the sites was occupied. (From Wagner, 1997)

sites or bonds of the lattice represent regions in the medium that are either completely filled with one fluid, or completely filled with the other fluid.

Percolation models cannot account for viscous effects, and there is no parameter that corresponds to the viscosity ratio of displacing fluids. The use of percolation models is thus restricted to studies of displacement processes at low capillary numbers (Wagner, 1997). Therefore, this type of network models is not appropriate for the study of the effect of oil viscosity on gas mobility. However, due to the vast applications of the percolation based models, the following paragraphs present a short explanation of some of the developed percolation based models and their applications.

The applicability of percolation theory to the study of disconnection and entrapment in porous media was suggested by several research groups (Melrose and Brandner, 1974; Larson, etal., 1977).

Dullien et al. (1976) exploited the correspondence of the bond percolation probability theory and network penetration to find the penetration history in various 3-D networks. The obtained model was then used to predict the permeabilities, formation resistivity factors and rate of capillary rise.

Larson et al. (1977) and Larson et al. (1981) proposed a percolation model to study drainage in porous media and to calculate the dependence of the residual non-wetting saturation on the capillary number.

Chandler et al. (1982) proposed a different method to simulate the displacement of an incompressible fluid (oil) from a network of bonds and sites by a second immiscible and incompressible fluid (water). In this model, the lattice is initially filled with oil, and water is allowed to enter along one edge in the presence of the capillary pressure differences across the interface. The simulation is done in a discrete, stepwise process where at each step, the oil-water interface moves through exactly one element of the lattice. The formed ganglia during the invasion are stranded as soon as they are formed. In view of the incompressibility of the oil, the invasion of pores corresponding to these ganglia is not allowed. As pointed out by Chandler et al. (1982), this simulation method differs from the classical percolation problem. The simulation consists of a sequence of motions, where each step is determined by the results of the previous one, while classic percolation provides a static configuration. Nevertheless, the final state of the oil seemed to be qualitatively similar to a percolation cluster, which can be treated with classic percolation analysis.

Wilkinson and Willemsen (1983) proposed a simulation method that applies to quasi-static imbibition, which they called invasion percolation. A lattice composed

of chambers and throats is initially filled with oil. Each chamber is assigned a random size ranking in the interval [0,1]. Water is brought into contact with the oil forming a set of menisci occupying throats near the entrance to the lattice. Each of the menisci is assumed to be near the entrance of the next chamber. A backpressure is applied in order to attain quasi-static imbibition. The smallest interface chamber is selected and is flooded by water, provided that the equivalent diameter of the chamber is smaller than the chamber diameter corresponding to the backpressure. All the throats connected to this newly invaded chamber get invaded at this point, and the chambers into which these throats lead are now included among the interface chambers. The process is repeated until no more interface chambers with diameter less than chamber diameter are found.

In porous media, the invading fluid must be connected to the inlet to continue invading and the defending fluid must be connected to the outlet to be displaced. This dynamic percolation process is called invasion percolation (Wilkinson and Williamsen, 1983). If clusters of the defending fluid become disconnected from the outlet, process is called percolation with trapping (Dias and Wilkinson, 1986).

The statistical network model and percolation theory of capillary pressure and relative permeabilities in low capillary number displacements of the three phases

has been studied by Heiba et al. (1984). In this model, a bond-disordered Bethe tree represents the chaotic connectivity of the pore space.

Diaz et al. (1987) used a stochastic approach to network modeling to simulate quasi-static immiscible displacement in porous media. The obtained oil-water capillary pressure curve simulated for drainage closely resembles those measured experimentally. The agreement between the simulated and the measured secondary imbibition and secondary drainage curves was less satisfactory.

Kantzas and Chatzis (1988) used bond correlated-site percolation model of pore structure to simulate relative permeability curves. They investigated the effects of pore throat size distribution and pore body size distribution on relative permeability behaviour.

Heiba et al. (1992) used statistical concepts, some borrowed from percolation theory of disordered media, to develop a theory of two-phase relative permeabilities in regimes where one phase is strongly wetting. Inputs to the model are the distributions of pore-throat and pore body radii, and functions that relate pore-throat conductance and volume to its radius.

Sahimi (1993) categorized percolation models of capillary-controlled two-phase flow as; random-percolation models, random site-correlated bond percolation models, invasion percolation, and random percolation with trapping. In this paper, he reviewed theoretical and experimental approaches to flow, hydrodynamic dispersion, and miscible and immiscible displacement processes in reservoir rocks. Then, various structural models of homogeneous and heterogeneous rock were discussed. The fundamental roles of the interconnectivity of the rock and its wetting properties in dispersion and two-phase flows, and those of microscopic and macroscopic heterogeneity in miscible displacements were emphasized. More than 1000 papers have been reviewed in this review paper by Sahimi (1993).

Oren et al. (1994) used a numerical three-phase invasion percolation type network model to compute the oil recoveries by tertiary gas flooding for oil-water-gas systems.

Satik and Yortsos (1996) simulated single-bubble (cluster) growth with a pore-network model that includes heat transfer (convection and conduction), and capillary and pressure forces.

Dixit et al. (1996) developed a 3-D network model to derive capillary pressure curves from non-uniformly wetted (mixed and fractionally-wet) systems. In

continuation of this study Dixit et al. (1997) studied hysteresis phenomena in both strongly and weakly water-wet drainage and imbibition relative permeability curves. A 3-D network model is reported which takes into account initial water saturation, wettability alterations, film flow, phase trapping and variations in advancing and receding contact angles. The consequences of different combinations of pore scale displacement mechanisms (viz. snap-off and piston-like displacement) for relative permeability hysteresis have been calculated in their study. The authors extended these previous works to mixed wet systems (e.g. preserved/age cores), where hysteresis trends between the secondary imbibition and secondary drainage oil/water relative permeability curves have been observed (Dixit et al., 1998).

Mani and Mohanty (1998) developed a three-dimensional (3D) pore-level network model to calculate three-phase capillary pressure and relative permeability curves. The model combines a description of pore space morphological features and three-phase displacement physics to model capillarity-controlled gas invasion into a water-wet medium containing oil and water. They found that the gas/water capillary pressure curves in three-phase systems depend on the fluid saturations, the spreading coefficient, and the oil/water capillary pressure. Water relative permeability, for the strongly water wet system is only a function of water saturation. Gas and oil relative permeability curves depend on the history, the spreading coefficient, and the gas and oil saturation, respectively.

Fenwick and Blunt (1998) presented a network of three-phase flow in water-wet porous media. They showed that the mechanism for oil recovery is flow through connected oil layers in the pore space that are of the order of a micron in thickness.

Kharabaf, and Yortsos (1998) used a simple pore-network model to simulate the generation and mobilization of foam in porous media. The model simulates the dynamic invasion process, where gas invades a porous medium occupied by a surfactant solution. In their study, they focused on the properties of the displacement, the onset of foam flow and mobilization, the foam texture and displacement efficiencies and the fractions of flowing and trapped lamella, as a function of parameters, such as snap off probability.

Larcoche et al. (1999) developed a numerical tool to demonstrate the impact of small scale wettability heterogeneities on gas injection efficiency, for various patterns and spatial heterogeneity distributions. In this model, the pore space is simulated as a two or three dimensional lattice formed by pore bodies (nodes) interconnected by pore throats (bonds). When gas is injected, three phases coexist within the network. The three-phase displacement is dominated by drainage mechanisms. Oil is assumed to flow through wetting films in the oil-wet regions and through spreading films on water in the water-wet regions. Their

results demonstrated the effect of the size and distribution of wettability heterogeneities on water/oil displacement and three-phase gas injection.

Hughes and Blunt (1999) used pore-scale network modelling to simulate imbibition in fractures and the matrix/fracture interaction. They modeled matrix/fracture transfer by attaching a three-dimensional porous matrix of pores and throats to the two-dimensional fracture lattice of conceptual pores and throats.

A new kind of invasion percolation is introduced by Zara et al. (2000) in order to take into account the inertia of the invading fluid. The inertia strength is controlled by the number ***N*** of the invaded pores (or steps). The new model belongs to a different class of universality with the fractal dimensions of the percolating clusters depending on ***N.***

Patzek (2000) found that primary drainage is a pure bond invasion-percolation problem, while imbibition is a problem in mixed invasion-percolation and ordinary percolation with trapping.

Maximenko and Kadet (2000) modeled porous media by a network of capillaries. The percolation and effective-medium models were used to calculate the network conductivity. Newtonian and plastic flow cases were considered in their model.

They used this model to predict the efficiency of the polymer flooding. The obtained results were verified by means of experimental data.

Larsen et al. (2000) applied an iterative procedure linking the pore-level displacement mechanisms with a macroscopically defined WAG process. Flow at the pore level is described by the network model. At the field scale it is computed by means of a reservoir simulator. The link between these two levels is provided by relative permeability and saturation paths obtained from the network model and reservoir simulator, respectively. The network model was made up a regular lattice with 30x15x15 pores. The pores were assumed with square cross sections. The pore size distribution was considered uniform.

Alexandrov et al. (2000) developed a mechanistic foam flow model, which includes snap-off, and lamella mobilization and destruction. The pore space was partitioned into pores occupied by liquid only and pores occupied by foam (gas and lamellae).

In the next section, the literature review corresponding to the converging-diverging network model which is a different class of pore level models will be explained.

3.2.2. Converging-diverging network models

In this section the history of the development of converging-diverging network model will be presented. Detailed description will be presented in Chapter 4.

Payatakes et al (1973) developed a model for porous media comprised of mono-sized, or nearly mono-sized grains. In applying this model to a packed bed, the bed is assumed to consist of a series of unit cells connected in parallel. Each unit cell resembles a piece of a constricted tube with random dimensions.

Payatakes and Dias (1984) presented a comprehensive literature review on immiscible micro-displacement and ganglion dynamics in porous media. The topics of porous media itself, different flow regimes, displacement in single capillaries and doublet, modelling of immiscible displacement, ganglion formation, mobilization and quasi-static displacement of ganglion, dynamic displacement of ganglion, and dynamics of ganglion populations have been reviewed in this paper. More than 220 references have been reviewed in 95 pages.

Dias et al. (1986) developed a converging-diverging network model for the two-phase flow in porous media. The effects of capillary number and viscosity ratio on ganglion movement were studied.

Constantinides et al. (1991) developed a theoretical model of collision and coalescence of a pair of mobilized ganglia in porous media. The porous medium was modeled as a three dimensional network of randomly sized unit cells of the constricted-tube type. The details of the flow near and between the two colliding menisci were analyzed with a film drainage model, which took into account the presence of the constraining pore wall, the wetting film which surrounds the ganglia by occupying roughness feature on the pore wall, and the hydrodynamics interactions of the three liquid bodies. The authors couldn't find reliable conclusions on the effect of viscosity ratio on collision.

Flumerfelt et al. (1992) used a 1-D constricted tube network model to describe capillary pressure and flow-fraction pressure behaviour of dispersed phase systems (foams) in porous media. They found that the presence of internal liquid lamella between bubbles in displaced trains gives rise to significantly higher capillary and flow-fraction pressures compared to non-dispersed phase systems (i.e., conventional gas/liquid systems, no surfactant). They also concluded that low mobilities of foam systems are attributed to reductions in mobilized gas fraction.

Vizika et al. (1994) conducted experimental and theoretical studies on the role of viscosity ratio during low capillary number forced imbibition in porous media. They used micro-model and converging-diverging network model for the experimental

and theoretical studies, respectively. In their studies, in agreement with the experimental observations, the simulator predicted that the viscosity ratio affects the value of residual oil saturation even for very low Ca values. As viscosity ratio decreased, residual oil saturation also decreased, especially in the case of very strong water wet system.

Steady state two-phase flow was studied experimentally in a planar and a non-planar pore network model, etched in glass by Avraam et al. (1994). The two porous media have virtually the same pore geometry, but one had a planar network skeleton, whereas the other had a non-planar (two-layer) skeleton. The latter is a new type of model porous medium that permits detailed visual observation and quantitative measurements without sacrificing the 3D character of the pore network topology. The non-planarity is shown to have small qualitative but significant quantitative effects.

Constantinides and Payatakes (1996) developed a simulator to study the two-phase flow in consolidated porous media. The porous medium is modeled as a 3-D network of suitably shaped and randomly sized unit cells of the constricted tube type. In their studies, the wetting phase saturation, the viscosity ratio, the capillary number, and the probability of coalescence between two colliding ganglia were changed systematically, while the geometrical and topological characteristics of the porous medium and wettability (dynamic contact angles) were kept constant.

In the range of the investigated parameter values, they found that the observed flow behaviour is ganglion population dynamics (intrinsically unsteady, but giving a time-averaged "steady state"). They determined the fractional flow and relative permeabilities and correlated them with flow phenomena at pore level. Effects of the wetting phase saturation, the viscosity ratio, the capillary number, and coalescence factor on relative permeabilities were examined. The main conclusions from their study are:

- At "steady state" the oil is disconnected in the form of multi-sized ganglia. The motion of the oil occurs exclusively through the motion of ganglia. The motion and the complex interactions of the ganglia can be denoted as "steady state " ganglion dynamics.
- Ganglia show an increased tendency to move through large pores as the viscosity ratio (—), and/or capillary number (**"**) decreases.
- The "steady state" relative permeability to water is an increasing function of the water saturation, whereas the relative permeability to oil is an increasing function of viscosity ratio and capillary number, and a decreasing function of water saturation and the coalescence factor, keeping the other parameters constant.

A computer-aided simulator of immiscible displacement in strongly water-wet consolidated porous media that takes into account the effects of the wetting films was developed by Constantinides and Payatakes (2000). The porous medium was modeled as a three-dimensional network of randomly sized unit cells of the constricted-tube type. Precurser wetting films were assumed to advance through the micro-roughness of the pore walls. Precursor wetting film is the wetting film on the sand surface. In other words, there are two hydraulic resistances in this type of models, (1) hydraulic resistance of the main pore and (2) the hydraulic resistance of the space between the pore wall and the main fluid. The developed simulator was used to predict the residual oil saturation as a function of the pertinent parameters such as capillary number, viscosity ratio, and the fraction of pores with each type of wall micro-roughness. The obtained results were compared with those obtained in the absence of wetting films. The following conclusions were obtained:

- Wetting films cause extensive disconnection and entrapment of non-wetting fluid, especially for small capillary numbers ($Ca<10^{-6}$).
- The above action of wetting films intensifies as the oil/ water viscosity and/or the fraction of the pores in which wetting films advance through spontaneous imbibition increase.

As it was discussed in this section, converging-diverging network models, have been used widely to study the effect of viscosity ratio on flow characterization such as relative permeability.

3.2.3. Other types of network models

There are few other types of network models that have different characteristics and applications. In this section some of them are reviewed.

Singhal and Somerton (1970) described a simulation procedure where a network model for the reservoir rock was generated by the Monte-Carlo technique, using pore size distribution and structural parameters appropriate to the particular reservoir. The model has been used to study displacement behaviour in unconsolidated sand packs. The model results simulate the relative permeability behaviour of porous media quite satisfactorily but semi-quantitatively.

Simon and Kelesey (1971, 1972) used capillary tube networks in miscible displacement studies. Their model is capable to handle all miscible displacement mobility ratios. A heterogeneity factor is also introduced in their model to account for the reservoir heterogeneity.

Boamin et al. (1999) reported on a systematic approach to link pore model inputs and laboratory data to a calibration methodology, and the subsequent use of a

pore network model to match laboratory core-floods in a heterogeneous dolomite. It is found that spatial correlation effects determined from core samples using thin section and computed tomography (CT) data are important for a satisfactory match.

Yuan et al. (1999) proposed that the wormhole growth can be described by the probabilistic active walker (PAW) model, which is a generalization of the classical random walk model.

Li and Firoozabadi (2000) recently used network modelling for the phenomenological study of critical condensate saturation and relative permeability in gas/condensate system.

CHAPTER FOUR

Converging-diverging network model

In Chapter 3, different types of network models have been discussed. As it was mentioned converging-diverging network model has been used widely to study the effect of pressure forces on the relative permeability of the phases in multi-phase flow in porous media. In this chapter this type of network models will be explained in detail.

Basically network analysis methods make use of standard electric network analysis to solve the network flow field. The analogy between flow rate and current, pressure drop and voltage, hydraulic conductance and electric conductance, and capillary pressure drop and voltage source are used to develop the analogous electrical circuit. In this type of network models, the pressure fields for both the wetting and the non-wetting phases are solved simultaneously, and viscosity difference between the two phases is taken into account. Complete discussion will be given in next sections.

4.1. Model definition

For clarity, certain definitions of idealized elements of the porous medium are stated first. The pore space in porous media is composed of relatively large

chambers that are connected to each other through narrow throats. The void space comprised of a chamber and its adjacent throats will be denoted as an Elemental Void Space (EVS). It will be assumed that each throat is characterized by the diameter of its narrowest cross section d and each chamber characterized by its effective chamber diameter $(D,$ diameter of the sphere with equivalent volume). In most porous media such as sand-packs or sandstone, both d and D are random variables.

Consider a finite, three-dimensional cubic network of interconnected unit cells of the constricted tube type, called a unit block. The size of a unit block is given by the number of unit cells along each axis, $N_x x N_y x N_z$, and the node to node distance, /. Each branch is occupied by a unit cell (UC). Each unit cell has axial symmetry, and its wall profile is a sinusoidal function, as they are shown in Figure 4.1. The distance of the wall from the axis, r_w, at some position z is given by;

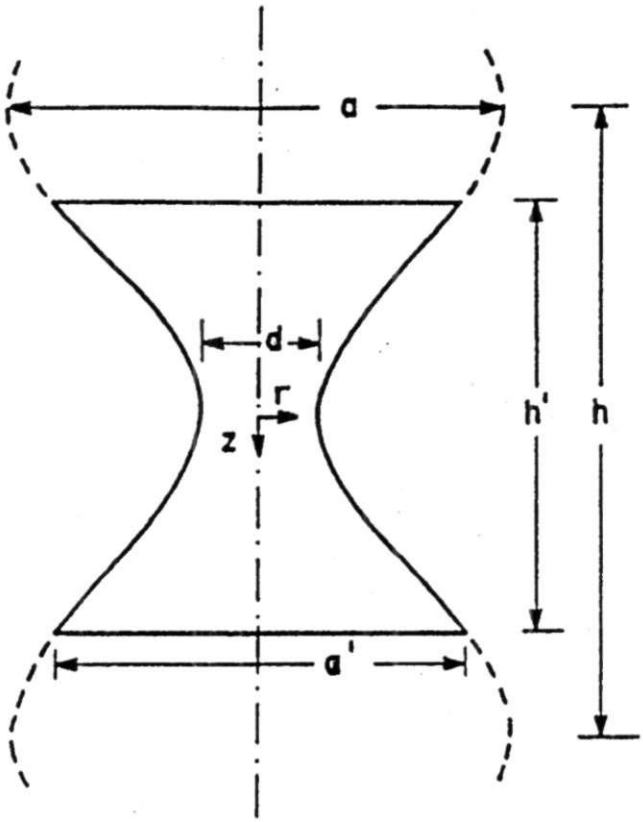

Figure 4.1: A typical unit cell (UC) of the porous medium model. (From Payatakes et al., 1980)

$$r_w(z) = \frac{1}{4}[(a+d) - (a-d)\cos(\frac{2\pi z}{h})] \tag{4.1}$$

where a and d are the maximum and minimum diameters of the sinusoidal function and h is its wavelength. Pore body diameter, a, and pore throat diameter, d, distribution functions are completely correlated by a geometrical factor, c, , so that;

$$a = c_x d \tag{4.2}$$

According to Payatakes, Tien, and Turian, 1973 (called P-T-T for abbreviation), the unit cell dimensions are set so that:

$$h = c_2 d \tag{4.3}$$

Payatakes (1980) has modified this formulation in order to keep realistic unit cell dimensions. The modified formulation properly accounts for porosity and number of constrictions per unit volume of the prototype. The unit cell in this modified P-T-T porous media model is comprised within the segment corresponding to $-h' \quad ti$ $(—<z<—)$ in Figure 4.1, where h' is the unit cell length $(h'<h)$ and is calculated by:

$$h' = c_2 c_3 d \tag{4.4}$$

where constants c_1, c_2, and c_3 are dependent on the particular porous medium, and are calculated based on experimental measurements of the porosity, the initial drainage curve and the grain size distribution.

This model applies to non-consolidated porous media such as sand or beads packs. For consolidated porous structures such as sandstone, and limestone, the

sinusoidal shape of the unit cell and the relations between its minimum and maximum diameters and length (Equations 4.1-4.4) should be relaxed. Furthermore, their size distributions should be calculated independently by pore cast analysis and/or porosimetry and imbibition/drainage curves. In this model we use the unconsolidated representation of P-T-T, which is in line with unconsolidated nature of many heavy oil reservoirs under cold production.

A two-dimensional representation of a random cubic network of constricted unit cells is given in Figure 4.2. Each node is connected to six unit cells (the pair unit cells normal to the paper is not shown). Unit cells are represented by bow-tie symbols whose sizes are proportional to the actual size of each unit cell. One node and adjacent six-half unit cells comprise a Conceptual Elemental Void Space (CEVS). According to the model, when a CEVS is occupied by gas, the gas bubble fills part of the six unit cells associated with the CEVS under consideration. The representation of a gas bubble occupying several adjacent pores is made in a similar way, filling the unit cells of the appropriate CEVS's according to the volume of gas held by each unit cell. A unit cell occupied by a gas-oil interface will be denoted as a Gate Unit Cell (GUC). (see Figure 4.2 for clarification)

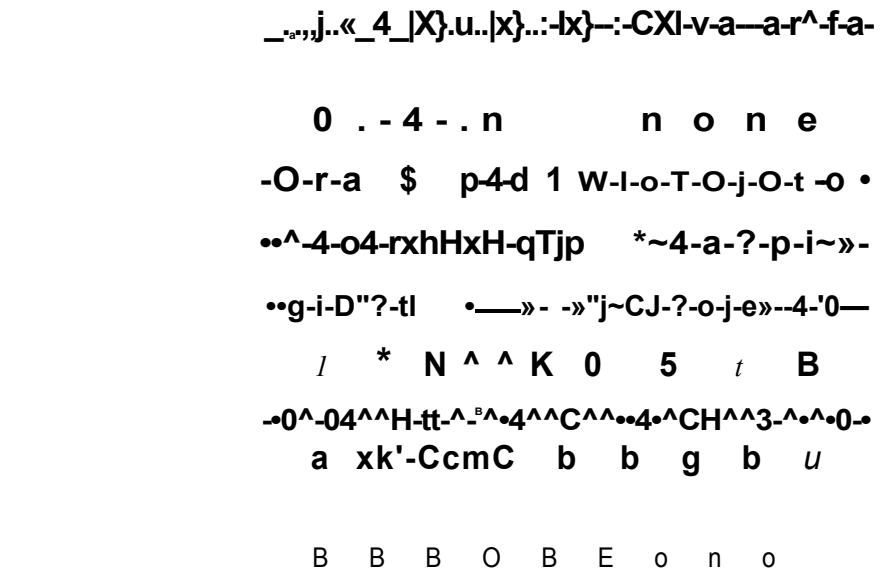

Figure 4.2: Two-dimensional depiction of a cubic network of unit cells. A Conceptual Equivalent Void System (CEVS), a Unit Cell (UC) and an Equivalent Unit Cell (EUC) are identified, as well as an 8-CEVS ganglion (solid line circle) and a 2-CEVS ganglion (dashed line circle). (From Dias, 1984)

4.2. Analogy concepts

For simplicity consider a N_x x N = 7 x 6 network such as the one represented in Figure 4.3. The network nodes are numbered in Figure 4.3, starting with the node at the lower-left-hand corner and proceeding from left to right and upwards.

Each branch of the network corresponding to a unit cell is numbered with relation to the node to which it is connected. Considering then node k, the four branches connected to it are numbered, (k,j), j=1,2,3,4 starting with left branch and proceeding clockwise around the node (see inset in Figure 4.3). This numbering

system results in duplicating of addresses for some unit cells. For example (k,3) and (k+1,1) refer to the same unit cell and similarly (k,2) and (k+Nx-1,4) also refer to the same unit cell. Such a network can be regarded as an electric network of resistors, each resistor corresponds to a unit cell with an associated conductance value, G. The flow rate through each unit cell, q_{uc}, corresponds to the branch current, q and the pressure drop along a unit cell, ΔP_{uc}, corresponds

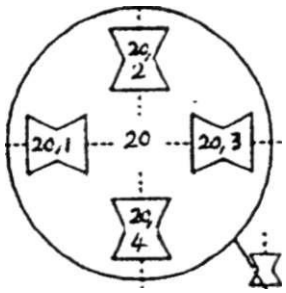

B B 0 B B

B / T r \ n a B B

B v B y B B B B

B B B B B B

-a-t ?- a -?- a - h x h - k h h x h

B B B B B B

y i - e w ?-M-t - e h - e h a -

B B B B B B

Figure 4.3: Depiction of a 7x6 network showing the nodes numbering system and in the inset the branches numbering system. (Modified from Dias, 1984)

to the branch voltage, v_p. For each gate unit cell, its overall resistance is taken as the sum of the resistance corresponding to the segment of the unit cell containing oil, plus the resistance corresponding to the segment that containing gas.

$$R_{gu} = K + R_g \qquad (4.5)$$

The capillary pressure difference across a gas-oil interface for each GUC, ΔP_c, is taken as a voltage source, v_c. Finally, the pressure at each boundary node, resulting from the applied macroscopic pressure gradient, is represented as an additional voltage source, v^*.

An 8-CEVS gas bubble in a 6x7 network is represented in Figure 4.4(a), with the corresponding electric analog shown in Figure 4.4(b). In Figure 4.4(b), unit cells filled with oil are shown as thin line resistors, whereas unit cells filled with gas are shown as thick line resistors. Gate unit cells are partly shown by a thin and a thick line resistors corresponding to the oil and gas, respectively. These two resistor lines are separated by a voltage source corresponding to the gas-oil interface.

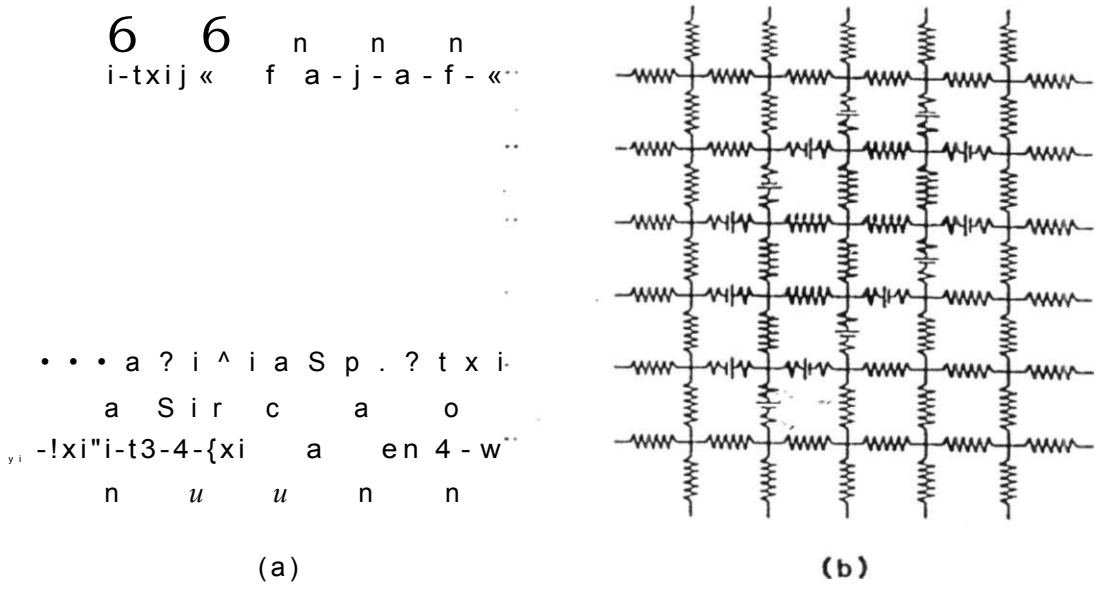

Figure 4.4: (a) Depiction of an 8-CEVS ganglion on a two-dimensional square network and (b) its electric analog network. (From Dias, 1984)

4.3. Two-phase flow conductance

For very low Reynolds number, R_e, and very small unit cell diameter, D, of interest, the entrance length, L_e (L_e=0.06 D R_e) in a unit cell is very small and negligible. Therefore, it is assumed that flow is fully developed in the unit cells of the network.

The following equation has been obtained between pressure gradient and flow rate through a unit cell by approximating the sinusoidal tube as a series of infinitely short cylindrical tubes which diameter varies as a sinusoidal function with axial position (Sheffield and Metzner, 1976).

$$\frac{dp}{dz} = \frac{8\mu}{n\,(r_w(z))^2}\,Q_{ue} \tag{4.6}$$

where z is the direction of flow through the unit cell and $r_w(z)$ follows a sine curve (Equation 4.1) in z-direction. By inserting Equation 4.1 and integrating Equation 4.6, the pressure-drop between any two points, z, and z_2, is obtained

$$\Delta p(z_1, z_2) = -\frac{2^{10}\,\mu\,c_z}{n\,a^4\,(c_1+1)} \cdot y(z_1, z_2) - q_{uc} \tag{4.7}$$

where,

$$y(z_1,z_2) = \frac{\sin x}{3(1-b^2)(1-b\cos x)} + \frac{5b}{6}\,\frac{\sin x}{2(1-b\cos x)^2} + \frac{b(U+4b^2)}{6(1-b^2)^2}\,\frac{\sin x}{1-6\cos x} + \frac{2+3b^2}{(n-b^2)^{5/2}}\tan^{-1}\left[\frac{(1-6^2)^{0.5}(\tan(x/2)}{1-b}\right] \tag{4.8}$$

where,

(4.9)

and,

$$x = \frac{In \quad z}{c_2 d} \tag{4.10}$$

For a gate unit cell, where the interface position is at $z_{,;}$

$$AP(z,) = AP(-^{\wedge}, 2_{/}) + AP(z_{/,}, |) \tag{4.11}$$

where *ti* is defined in Figure 4.1, and the conductance is;

$$G(z,) = \frac{n^2 d \backslash c_x \quad +1)^4}{{}^{o\ 0}_{2} \quad /"w^{\circ}2} \tag{4.12}$$

where **k** = is the viscosity ratio.

Equation 4.12 can be used for the single phase flow by considering ***K*** = = 1

As it is clear all the above equations represent flow in one direction. However, by using one-dimensional unit cells at different directions in a network, multi-dimensional (2-D and 3-D) flow can be studied. This is because in this network

model, flow is not allowed at the nodes. However, by using extended unit cell method (Section 4.7), interfaces can move from one unit cell to another.

4.4. Pressure drop across an interface

Dias et al. (1986) have shown that for a water-oil system the pressure drop across an interface is;

$$U>_{i}(z,) = 2a_{,,}^{\cos\ p} \tag{4.13}$$

where $z_{,}$ is the axial position of the solid-oil-water contact line, and

$$\cos /? = \frac{\cos 9 + \sin 9 \bullet \tan a}{(1 + \tan^{2}\ \ddot{a})^{0.5}} \tag{4.14}$$

and,

$$\tan a = \frac{}{dz} = \frac{}{2c,}(c,\ -1)\sin \tag{4.15}$$

where $\boldsymbol{0}$ is the contact angle. In this study, our fluid pairs are oil and gas. Instead of $<r_{,,,}$ we have $cr_{()g}$, and z. will be the axial position of the solid-oil-gas contact line.

4.5. Effective conductance and pressure drop across an interface

Conductance and pressure drop across an interface for a gate unit cell depend on position of the interface. The following approach is proposed by Dias (1984) to calculate conductance and pressure drop in a GUC. Each gate unit cell is divided into several compartments. For simplicity the compartments are equally spaced, that means, $z_k - z_{k-1} = z_{k+1} - z_k$, where z_k is the axial position of the division corresponding to compartment *k*. For higher accuracy, in this model each GUC is divided into 80 compartments. The extended unit cell is also divided into equally spaced compartments. Figure 4.5 shows an example of a unit cell divided into ten compartments. Figure 4.5 also shows an extended unit cell divided into 2 compartments, which will be explained in next sections.

4.5.1. Effective conductance

The effective conductance G_{eff} can be estimated as follows: take V_g to be the volume of gas contained in the gate unit cell at a given instant. Now, if we consider that V_{kGM}, and V_{kG} are the volumes of the part of the constricted tube up

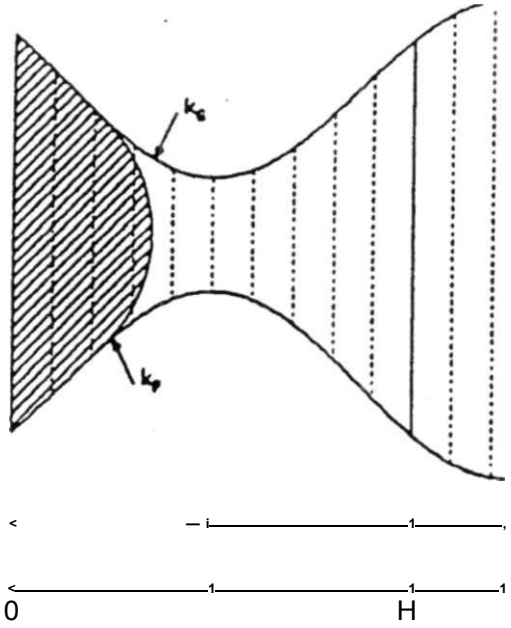

Figure 4.5: Representation of a gate unit cell (GUC) divided into ten compartments showing K_G and K_p used to calculate the effective conductance and the effective pressure drop respectively. Extended part is divided into 2 compartments.

to $z_{w;\_}$, and z_{kf}, respectively, then it is obvious that $V_{kf} > V_g > V_{kG\_\_x}$. G_{eff}, is estimated to be equal to the conductance that would be obtained if the pseudo-interface were situated at the plane positioned at z_G, where $z_G = \wedge(^{z}w;^{+z}*c-i)$ •

4.5.2. Effective pressure drop

The effective pressure drop, AP_{eff}, is calculated by considering that the interface is situated at the middle of the compartment k_P. The middle location is

calculate by z_p = ^(ˇki- ˚ˇw-\)> where z_{ki}, and z_{w}, are the axial positions of the divisions at both ends of the compartment k_p .

Figure 4.5 shows the position of k_g and k_r for a given volume of gas in a typical unit cell.

4.6. Interface movement at the **GUC's**

In this model, each interface moves by no more than one compartment in the corresponding gate unit cell. The procedure is;

- A time increment for each GUC, At, i=1,...,NGUC (NGUC is the total number of gate unit cells) is calculated by dividing the volume of the compartment containing the interface by the flow rate through gate unit cell "i".
- Comparing the obtained At for all GUC's, the lowest At will be the time step.
- By using the calculated minimum At, the volume of the gas in all GUCs will be updated according to their respective flow rates, and the total recorded elapsed time.
- This process will be repeated until one of the following events occurs;
  1. A gate unit cell fills with gas and gas invades the pore downstream (xeron).
  2. A gate unit cell gets emptied of gas and the pore is invaded by oil (hygron).

4.7. Interface movements at the nodes

In this section xeron and hygron occurrences, which are the interface movements in nodes will be discussed.

4.7.1. Occurrence of xeron

In order to find a more sound solution for interface movements at the nodes, it is helpful to look at actual laboratory studies of oil-ganglion motion. Figure 4.6, shows a sequence of photographs taken from movies made by Hinkley (1982). The experimental apparatus used by Hinkley consisted of a single layer of uniformly sized glass spheres organized in a square configuration and held between two glass plates. In Figure 4.6, a 6-pore rectilinear oil ganglion moves in response to a Ca = 3.8e-4. The ganglion reacts to the external forces, principally the external pressure difference, by shifting oil towards its down stream end. This produces a shape reminiscent of a hammerhead shark (HHS) shape (Figure 4.6a). Since the capillary number is above the critical capillary number, the drainage curvature is eventually exceeded. The ensuing xeron begins with a slow advancement of the oil interface which, gradually accelerates until it occupies most of the pore. In Figure 4.6a, the oil-water interface is about to invade the adjacent pore in the downstream side. Looking now at subsequent photographs (Figure 4.6b), this interface is actually invading the front pore, but not touching either one of the two spheres located down-stream. The interface proceeds in this way for some time (Figure 4.6c), until the volume of oil in this

pore is sufficiently large and all four spheres come in contact with oil (Figure 4.6d).

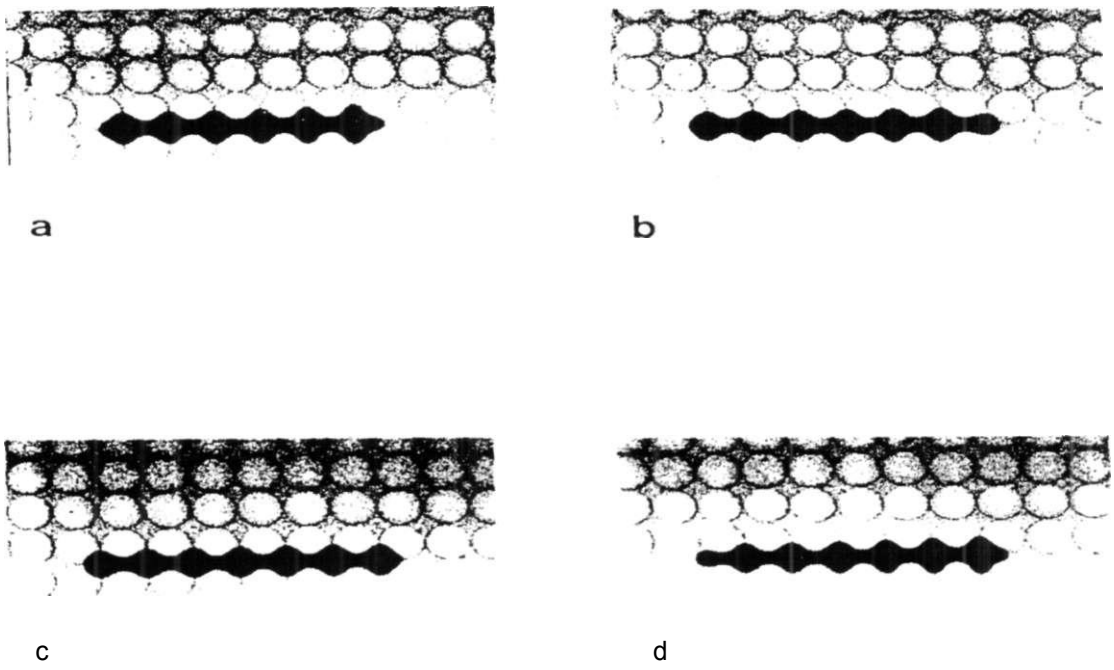

Figure 4.6: Sequential pictures of a 6-pore ganglion during the xeron-hygron cycle for = 0.6 (From Hinkley, 1983)

In the simulation algorithm these series of events are represented by allowing filled unit cell to take an extended unit cell configuration. When the gas reaches the end of a gate unit cell, and it is ready to flow to other adjacent unit cells (three adjacent unit cells in 2-D model), the unit cell takes its extended configuration $(-h' < z < h)$ (Figure 4.5) and the gas is allowed to fill the extended unit cell. At

this point, there is enough gas in the extended unit cell to fill portions of the adjacent unit cells corresponding to the volume of the three adjacent (down stream) unit cells. New interfaces are placed simultaneously at the downstream unit cells the excess gas is divided among them in proportion to their respective volumes. At the same time the extended unit cell regains its usual size $(\frac{-h'}{2} < z < \frac{}{2})$ and a xeron is said to have occurred.

4.7.2. Occurrence of hygron

To figure out about a gas-oil interface when the gate unit cell gets empty of gas, a similar analysis of an actual laboratory experiment will be done. Consider the 2-CEVS gas bubble represented in Figure 4.7 and consider the most upstream gate unit cell A. As it is shown in subsequent Figure 4.7b, the gas

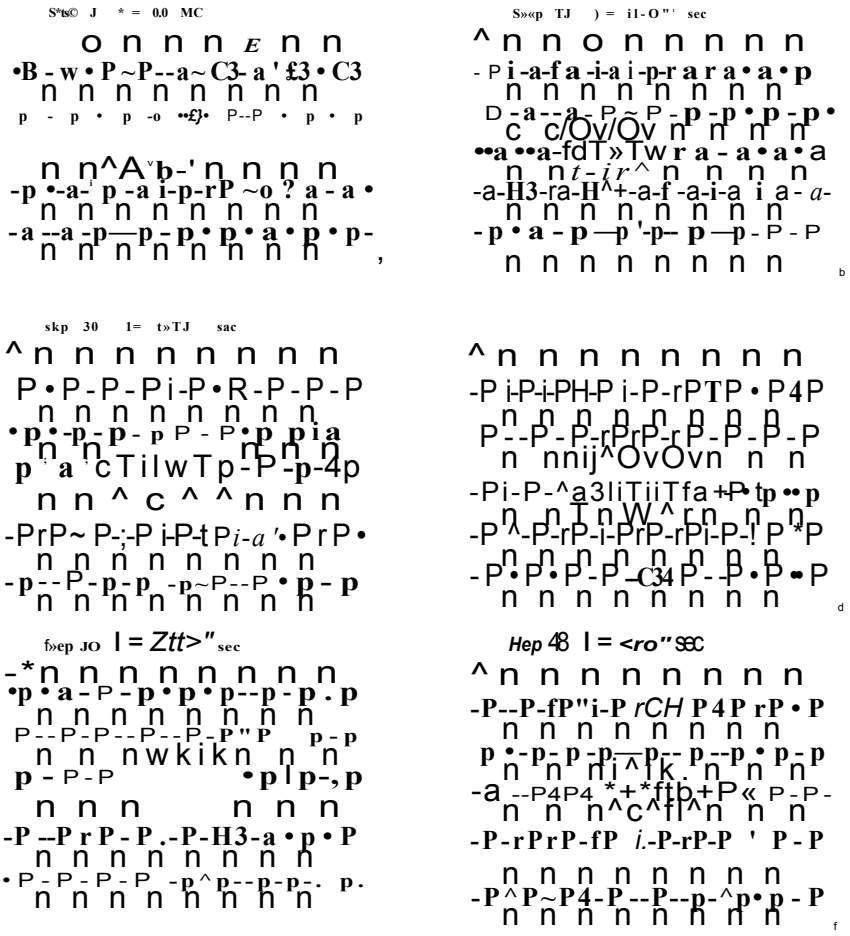

Figure 4.7: Stages of a 2-CEVS ganglion motion simulation. Occurrence of a hygron. (From Dias, 1984)

in this gate unit cell is receding, that is the volume of gas is decreasing. If this decrease leads to a negative volume of gas in the unit cell in question, the time increment is adjusted so that unit cell A is now filled with oil, Figure 4.7c. At the same time, unit cells B and C, which belong to the same CEVS as unit cell A, still contain some gas.

An analogous situation is seen in Figure 4.8 taken from the experimental work of Hinkley (1982). The sequence of photographs show a 2-pore oil ganglion

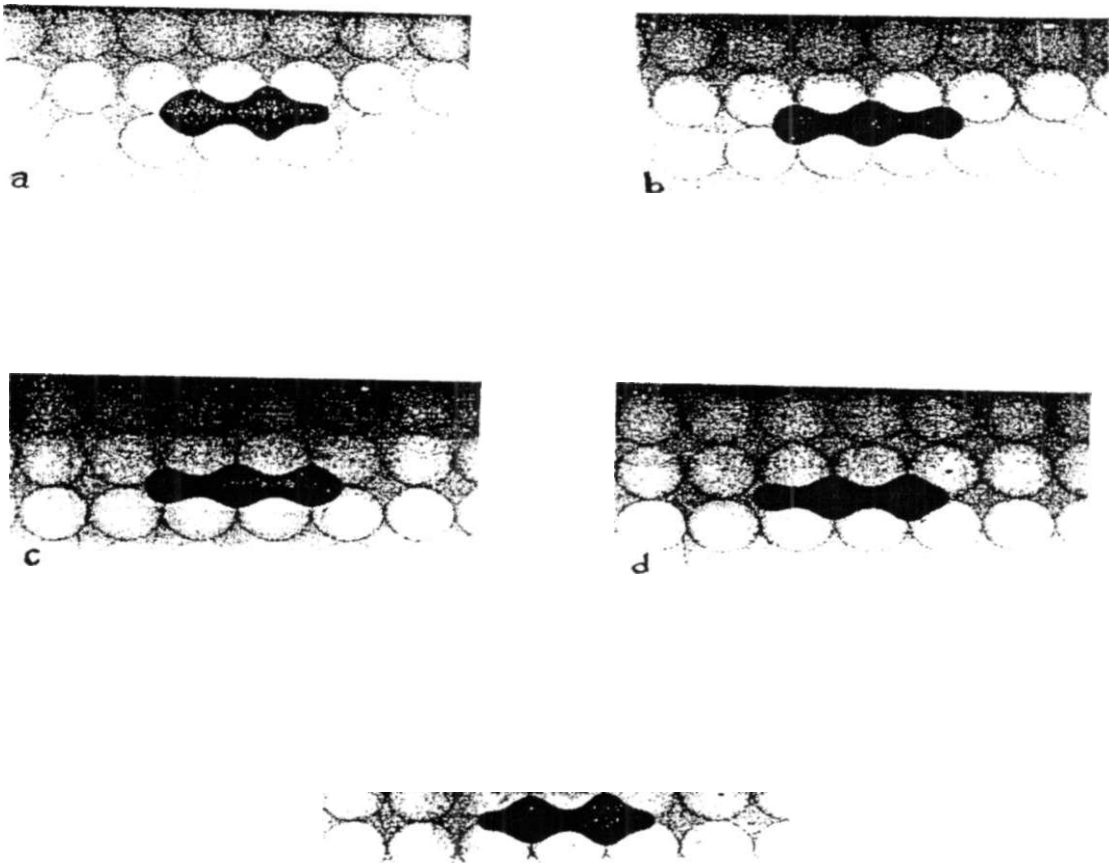

Figure 4.8: Sequential pictures of a 2-pore ganglion during the xeron-hygron cycle for = 0.6 **(From Hinkley, 1983)**

where the most upstream interface is about to leave the pore (Figure 4.8b), but there is still some oil left in both lateral connections. In the following photograph (Figure 4.8c), it is seen that the interface has now about to detach itself from the walls of the two upstream spheres. The interface proceeds in this way for some

time until it is detached completely from the upstream spheres (Figure 4.8d), until finally the interface leaves the pore (Figure 4.8e) completely.

The series of events are recreated by the simulation algorithm by placing an interface at the beginning of the gas-filled unit cell which is adjacent to the common node. This unit cell takes the form of an extended unit cell D (Figure 4.7d), and it is partially filled with the gas contained in unit cells B and C (Figure 4.7c). At this point a hygron is said to have taken place. The simulation now proceeds as usual until finally the volume of gas in this unit cell is equal to or less than the volume of a regular unit cell, at which point the EUC shape is dropped (Figure 4.7f).

4.8. Boundary conditions

For a two-dimensional network model we need boundary conditions for all four sides.

4.8.1. Boundary conditions at the inlet and outlet of the 2-D network

Let's consider a two dimensional network with dimensions, $N_x x N_y$, where N_x is the number of unit cells in the x-direction and N_y is the number of unit cells in the y-direction. The macroscopic flow direction is parallel to the x-direction.

It is assumed that all the N_y unit cells at the inlet of the network are connected to a reservoir of oil at pressure p,, whereas the N unit cells at the outlet are connected to a sink of pressure $p_o(p_o = 0.)$. The pressure difference is set as

$$Ap = P,-Po=(-VpW_x \tag{4.16}$$

Here, $IN,$ is the length of the system, and V> is the pressure gradient that would be required to drive a flood of oil with capillary number equal to a prescribed value Ca_j in a virtually gas-free (oil saturation $S_a = 1$) sample porous medium. Vp can be find by;

$$Vp = -\text{^}— \tag{4.17}$$

where k is the absolute permeability of the network. Therefore,

$$Ap = {}_{Pr}-Po= \quad \overset{trJN.Ca,}{"^{s}\ ;\ \sim} \tag{4.18}$$

4.8.2. Boundary conditions at the sides of the network

In this work, closed boundaries will be considered for the side boundary. In this way, the unit cells on the side boundaries are considered as zero throat size unit cells (very small value compare to the lowest throat size).

Gas bubbles are placed at least three unit cells away from the boundaries, in order to make sure that boundaries do not affect their movements.

4.9. Development of system of equations (Dias, 1984)

The governing equations of the flow in network model of porous media become linear if flow were under creeping flow condition. In addition, the matrix of the coefficients depends on the location of the interfaces. It means that the motion of an interface depends on the overall pressure difference across a unit cell, and the overall pressure difference depends on the interface location. This makes the governing equations non-linear. In order to make the problem of interest linear, the locations of interfaces were assumed stationary at each time steps and were updated for the next time step based on the current pressure difference and unit cell conductance. By dividing each unit cell to 80 compartments and by controlling the time step such that the interfaces movement does not exceed one compartment, the above assumption was implemented. Assuming quasi-steady state, a system of linear algebraic equations can be

developed to solve the flow problem. In order to use network analysis efficiently, it is necessary to express the network variables in vector form.

The nodes of the network are numbered from left to right and from bottom to top by assigning indices $k = 1,2,\ldots,N_p$, where N_p is the number of interior nodes (excluding the boundary nodes). The number of interior nodes (N_p) could be found as:

$$N_p=(N_x \quad -1) \tag{4.19}$$

where, N_x and N_y are the number of unit cells in the x and y directions, respectively.

The branches (or unit cells) of the network are also given indices, $j = 1,2,\ldots,N_b$, where N_b is the total number of branches and calculated as follows:

$$N_b=(2N_x-1)(N_y-1) \quad + \quad (N_x-1) \tag{4.20}$$

The branch conductance matrix $[G] = (N_b x N_b)$, is formed as follows:

- The off-diagonal elements are set equal to zero.

- Each diagonal element g_n is set equal to hydraulic conductance of the unit cell occupying branch j.

The branch source vector, $v_{(} = (N_b)$ is defined so that $v_{v/}$ is the capillary pressure in the j_{th} unit cell.

- "$v_{v/}$" is equal to zero, if there is no interface in the unit cell.
- It is positive if there is an interface, which tends to propel the wetting phase in the positive direction of the branch.
- It is negative if the interface tends to propel the wetting phase in the negative direction of the branch.
- If the branch j is adjacent to a boundary node, adding the value of the pressure at the boundary node augments to the value of v_{sj}.

The reduced incident matrix $[A] = (N_p$ x $N_b)$describes the manner in which the branches are connected;

- The element a_{kj} is set equal to zero if branch j is not incident on node k.
- The element a_{kj} is set equal to 1 if the fluid in branch j flows toward incident node k.

- The element a_{kj} is set equal to -1 if the fluid in branch j flows away from incident node k.

The node conductance matrix $[Y] = (N_p \text{ x } N_p)\backslash s$ defined as follows:

- y_{kk}, called the self-admittance of node k, is the sum of the conductance of all branches connected to node k.
- $y_{mk} = y_{km}$, called the mutual admittance between nodes m, and k, is the negative of the conductance of the branch connecting nodes m and k.
- y_{mk}, zero if nodes m , and k are not connected directly.

Node-source flow vector q_s, which has N_p elements is given by;

$$q_s=[A]x[G]xv_x \tag{4.21}$$

The node voltage vector $P = (N_p)$ is defined so that p_k is the pressure at node k. Then the instantaneous value of p is obtained as the solution of the below system;

$$[Y]xP = q_t \tag{4.22}$$

The branch pressure drop vector v_{b} and its j_{th} element which is the pressure drop along the positive direction of branch j can be calculated by;

$$v_{\Delta} = A^{T} x P \tag{4.23}$$

where A' is the transpose of matrix A.

Finally, the flow rate vector $q = (N_{p})$, is defined so that q_{j} is the instantaneous flow rate in the j_{th} unit cell. Once P is obtained from solving equation (4.22), vector q is readily obtained from;

$$q = [G] x (y_{b} - v_{s}) \tag{4.24}$$

CHAPTER FIVE

Model features and assumptions

Table 5.1 shows the features of the model used in the current study. In the following sections each of the mentioned features or lack of them is discussed. The discussion is divided in four main categories of porous medium, interested fluids, driving and resisting forces, and pore level processes.

5.1. Porous medium

Porous medium dimensions and size, pore geometries and distribution, and the way that pores are connected to each other are the important parameters in describing a real porous medium. In this section, these parameters are explained.

5.1.1. Model dimensions

Underground reservoir is a three dimensional (3-D) porous medium. Therefore, a 3-D network is suitable for the study of the foamy oil reservoirs. However, a 3-D model is quite complicated and the computation time is much higher than two-dimensional (2-D) network model. Avaraam et al. (1994) have shown that non-planarity has small qualitative but significant quantitative effects. In this study, a 2-D network model has been used. Therefore, the results are qualitatively applicable.

Table 5.1: Model features

Perfect model	This model	Comments/ related references
3 dimensional	2 dimensional	Avaraam et al. (1994)
Random pore geometry	Single pore geometry	Patzek (2000)
Includes pore size distribution	Included	Dias (1984)
Includes random pore size distribution	Included	Dias (1984)
Includes random coordinate number	Fixed number of coordination	Patzek (2000)
Includes random length of periodicity (node-to-node distance)	Constant length of periodicity	Patzek (2000)
Large network size	40 by 40	–
Includes 3 phases	2 phases	Fenwick and Blunt (1998)
Includes capillary forces	Included	All network models
Includes pressure forces	Included	Dias (1984) for oil/water system
Includes gravity forces	Not included	Li (1993)
Applicable for Newtonian and non-Newtonian fluids	Only for Newtonian fluids	Maximenko and Kadet, (2000)
Applicable for compressible and incompressible fluids	Only for incompressible fluids	Alvarado and Rodriguez, (1999)
Includes effects of viscous coupling	Not included	Goode (1991)
Include effect of precursor wetting film	Not included	Constantinides and Payatakes, (2000) for oil/water system
Includes gas bubble nucleation	Not included	Alvarado and Rodriguez, (1999)
Includes gas bubble expansion	Not included	Alvarado and Rodriguez, (1999)
Includes gas bubble movement	Included	Dias (1984) for oil ganglion movement
Includes gas bubble breakup	Not included	Constantinides and Payatakes, (1996) for oil ganglion
Includes gas bubble coalescence	Not included	Valvanides et. al., (1998) for oil/water system

5.1.2. Pore geometry

The pore geometry in natural porous medium is a combination of different irregular shapes. However, mathematical modeling of these irregularities is very difficult. Therefore, a simplified shape is usually considered as the pore geometry of a porous medium and by tuning the parameters, the macroscopic characteristics of the real porous medium are satisfied. Having different regular shapes and random positioning of these regular shapes to a large extent accounts for the irregular shapes of the pores in natural porous medium. In this model a single pore geometry of the converging-diverging form is considered. By changing the defined constants, a good match of the macroscopic characteristics (porosity and permeability) has been obtained. Patzek (2000) developed a model with a combination of different pore shapes (triangular, square, and circle), with random positioning.

5.1.3. Pore size distribution

Pore size distribution curves can be obtained for a real porous medium by different methods such as capillary intrusion, or core scanning. In the capillary intrusion method, an average pore size distribution can be obtained. However, this does not give any information about the location of the pores with different size. Core scanning can give an insight to the position of the different pore size locations.

This model accounts for the variability of pore sizes. A random generator is used to assign a random pore size taken from a pore size distribution curve at different locations. By spending more time and patience the results of a core scan could also be entered into a model.

5.1.4. Coordination number (network connectivity)

Coordination number or the number of the interconnected pores to a certain pore is not the same for each pore in a natural porous medium. Furthermore, it is different from one type to another type of natural porous rocks. Therefore, a complete network model should be able to handle different coordination number and randomly distributed coordination number, in this model, a fixed number of coordination, that is four, is considered for all pores. Patzek (2000), considered variable network connectivity with zero to sixteen coordination number.

5.1.5. Length of periodicity (node-to-node distance)

If we define porous media as the combination of pore bodies and pore throats, it means that throats connect the large pores. The distance between two pores is the length of periodicity. This length is different between any two pore bodies. Patzek (2000) includes random length of periodicity. In the current model, a constant length of periodicity is considered.

5.1.6. Network size

The larger the network size the better would be the representation of a real porous medium. However, there are restrictions due to computer memory and comutation time. Vizika et al. (1994) showed that for the study of residual oil saturation, a 3-D network size of 15 by 6 by 2 could give reliable results. In this study network size up to 100 by 100 have been examined. Most of the results however are based on network size of 40 by 40, which takes reasonable computation time.

5.2. Fluid phases

In this section, model features in terms of the fluids are presented.

5.2.1. Number of fluid phases

There are three phases in underground reservoirs, which are water, oil, and gas. In a water-wet system, water is around the sand grains and it is believed that it is often stationary. Oil is the main fluid and in our study has a very high viscosity. Normally, at the beginning of the life of a reservoir (under-saturated reservoir), there are only two phases, water and oil. When the reservoir pressure declines the solution gas starts to nucleate and liberate. After this time, there are three phases in the reservoir. Therefore, a robust and complete network model should include three phases, and the effect of each phase on another phase should be included too. In this model, water was considered stationary and it was

lumped with the stationary solid phase. Oil and dispersed gas bubbles are included in this model.

5.2.2. Newtonian and non-Newtonian fluids

Among the three available fluids in the reservoir, some heavy oils show non-Newtonian behavior. Maximenko and Kadet (2000) considered non-Newtonian fluids in their network model. In this model, Newtonian behaviour is considered.

5.2.3. Compressible and incompressible fluids

Oil and water are slightly compressible, but gas is compressible. Gas compressibility plays a large role in the bubble expansion and flow behavior of the gas bubbles. This model does not account for the fluid compressibility. However, by considering that the macroscopic pressure difference is low due to the small length of the network model (approximately 4 mm), pressure changes are not very large and the incompressible assumption of fluids even for gas phase might be sufficient.

For the study of bubble expansion, a network model should have the compressible fluid feature.

5.3. Driving and resisting forces

In this section different driving forces that act on gas bubbles to move them will be discussed.

5.3.1. Capillary forces

Due to the low flow rates of the fluid phases and narrow passages in the porous medium, capillary forces are important. This model includes capillary forces. Please refer to Chapter 2 and 4 for further discussion about interface movements and capillary forces.

5.3.2. Viscous forces

Due to the high viscosity ratio between the phases in foamy oil flow the viscous forces play an important role in the movement of the gas phase. Therefore, the effect of viscous forces is included in this study. For further explanation please refer to Chapter 4.

5.3.3. Gravity forces

Due to the large density difference between the phases of interest (oil and gas) in foamy oil flow, it seems that gravity forces are important. However, this model is a horizontal 2-D model. Therefore, despite knowing that gravity forces are important, the effect of gravity forces is not included.

5.4. Pore-level processes

Different phenomena at pore level such as viscous coupling, precursor wetting film, bubble nucleation, bubble expansion, bubble motion, bubble break-up and coalescence of the bubbles will be explained in this section.

5.4.1. Viscous coupling

Viscous coupling or the effect of one phase on the mobility of another phase is an area of active research in petroleum engineering. Viscous coupling between fluid phases for two-phase flow in porous media leads to a matrix of relative permeabilities. This feature is not included in this model. For further discussion about viscous coupling please refer to Goode (1991).

5.4.2. Precursor wetting film

Constantinides and Payatakes (2000) have developed a computer-aided simulator of immiscible displacement in strongly water-wet consolidated porous media that takes into account the effects of the wetting films. Precursor wetting films are assumed to advance through the micro-roughness of the pore walls. Two types of pore wall micro-roughness are considered. In the first type of micro-roughness, the film advances quickly, driven by capillary pressure. In the second type, the wetting film often forms a collar that squeezes the thread of oil causing oil disconnection (they studied oil and water system). Each pore is assumed to have either one of the aforementioned micro-roughness types, or both. The type

of micro-roughness in each pore is assigned randomly. The simulator is used to predict the residual oil saturation as a function of the pertinent parameters (capillary number, viscosity ratio, fraction of pores with each type of wall micro-roughness). These results are compared with those obtained in the absence of wetting films. It was found that wetting film causes substantial increase of residual oil saturation. Furthermore, wetting film causes extensive disconnection and entrapment of non-wetting fluid. The action of wetting film intensifies as the oil/water viscosity ratio increases.

In this study, the precursor wetting film is not included. However, it seems that precursor wetting film acts to entrap the gas bubbles. It means that by modifying the model to account for the precursor wetting film, smaller values of gas relative permeability might be obtained compare to the current study.

5.4.3. Gas bubble nucleation

There have been a lot of challenging efforts in order to define the mechanism of bubble nucleation. There are three main models to describe bubble formation (Jones, 1999); classical model, pseudo-classical (crevice) model, and non-classical model. In classical model, there is no pre-existing gas (nuclei). Pseudo-classical model (crevice model) considers that there is pre-existing gas, but the radius of these pre-existing nuclei are less than the critical bubble size, therefore, macroscopic bubble may or may not form. In non-classical model the

radius of the pre-existing nuclei are larger than the critical radius, therefore, macroscopic bubbles will form.

In this model, gas clusters are assigned in ordered positions. For example, for the case that gas bubble size is 2-CEVS (2-CEVS in x-direction), a few lines from each side boundaries are left free of gas bubbles. Based on the total gas saturation in the network, the gas bubbles are distributed in equal distances in both x and y direction. Figure 5.1 shows a portion of a typical network with 2-CEVS gas bubbles distributed regularly. It is worth to mention that the solution might depend on gas distribution, but ordered and fixed distribution has been chosen to be able to compare the effect of other parameters such as viscosity ratio. The effect of gas bubble distribution is not studied.

5.4.4. **Gas bubble expansion**

In solution gas drive reservoir, the generated gas bubbles would expand with time (depletion) and with distance because of lower pressure close to the wellbore.

Pressure decline rate is a function of the bubble generation and expansion, and

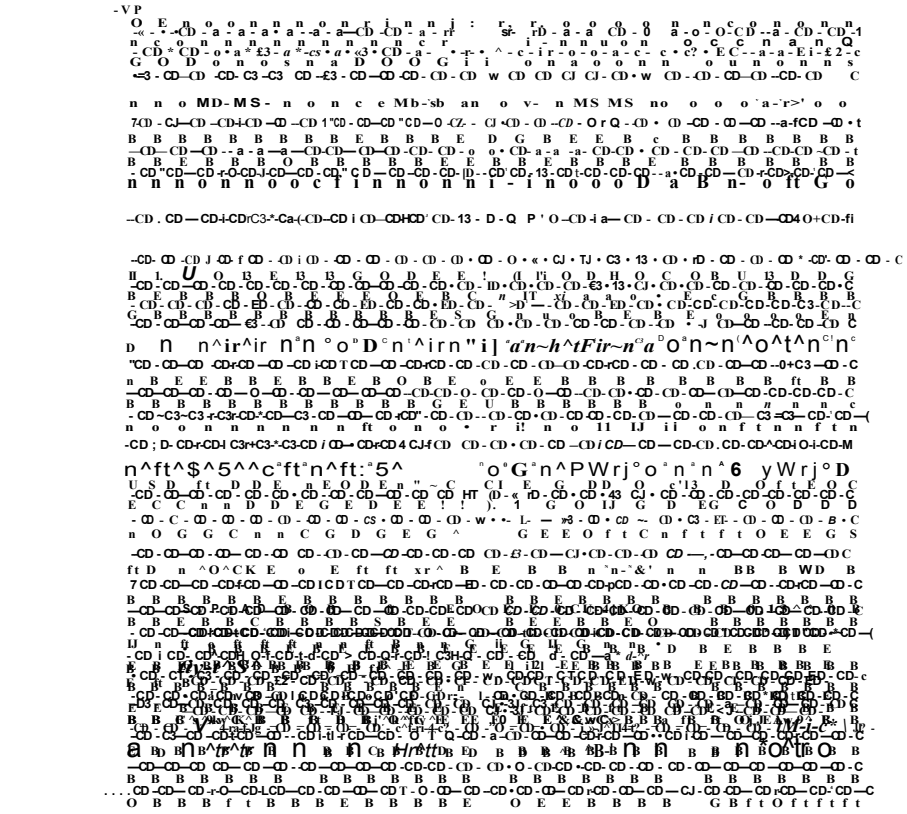

Figure 5.1: A portion of a 2-D model with 2-CEVS bubbles distributed regularly.

bubble growth is a function of mass transfer (diffusion) rate from liquid phase to the gas bubble, and compressibility of the gas. Although the reservoir pressure declines with time, but for the cases that the production is constant, the macroscopic pressure difference over the entire system is constant. In this model, a constant macroscopic pressure difference is considered across the porous element. Bubble expansion is not allowed in this model.

As bubbles move downstream, the pressure will decrease and consequently the bubbles will grow. The length of the network model is usually short (in this study 4

mm). Therefore, the pressure difference is not large. It might be acceptable to assume constant bubble size.

Different gas bubble sizes have been considered. The sizes used in this work are 2-CEVS (in x-direction), 4-CEVS (2 by 2), 9-CEVS (3 by 3), and 16-CEVS (4 by 4).

5.4.5. Gas bubble movement

Ganglion motion and interactions result in an overall dynamic equilibrium giving a time-averaged steady state flow. Such a flow pattern is highly sensitive to the capillary number, viscosity ratio, saturation, contact angle, coalescence, and geometry and topology of the pore network (Constantinides and Payatakes, 1996).

It is well known that the mobility of a phase is related to the saturation of that phase. In this study, different simulation runs have been conducted at different gas saturations to find the gas relative permeability curves versus gas saturation. All the model parameters are kept constant, and only the number of gas bubbles, i.e. gas saturation is changed.

Contact angle is another important parameter that gives some knowledge about the effect of wettability on gas relative permeability curves. In this model,

advancing and receding contact angles are used for the advancing and receding interface movement, respectively. However, the effect of the velocity of the interfaces on the contact angle and also the effect of the mixed wettability (different wettability at different locations) are not included.

Interfacial tension is considered constant in this model. In a foamy oil flow system due to the composition changes of the phases (gas components diffusion from oil to gas by declining the pressure), the interfacial tension between oil and gas could change. However, because the composition variation is likely to be insignificant, interfacial tension could be considered constant.

In Chapter 2, different mechanisms of the gas bubble break-up are explained. From those cases, dynamic break-up seems to be important in heavy oil reservoirs. Once a large gas bubble breaks into two or more daughter gas bubbles, the movement tendency of these small bubbles will decrease. In other words, gas mobility of the smaller bubbles is lower than larger bubbles. The current model does not include the gas bubble break-up feature. In order to investigate the effect of gas bubble size on the gas relative permeability, different simulation runs with different gas bubble sizes have been performed while other model parameters have been kept constant. The obtained results are presented in Chapter 7 to show the effect of gas size on gas relative permeability.

Adding gas bubble break-up feature is highly recommended for the future network studies in foamy oil reservoirs.

Bubble coalescence is another phenomena that may occur during bubble motion in porous media. The main problem of modeling such phenomena in network models arises when two interfaces move toward each other in a gate unit cell. The oil between these two interfaces is trapped, and the gas bubbles could not reach each other to coalesce. By connecting a sink in the center of gate unit cells to drain the trapped oil, this problem could be handled. However, this modification makes the model very complicated. Other investigators (Constantinides and Payatakes, 1996) developed network models that include coalescence.

CHAPTER SIX

Determination of relative permeability and simulation algorithm

In this chapter, the calculation method of gas relative permeability *(k)* based on Darcy equation for two phase flow, the methodology of k_{rk} determination in our network model, and the simulation algorithm will be presented.

6.1. Determination of gas relative permeability *(k^)*

In this section, the methodology of gas relative permeability determination in the developed model is explained.

6.1.1. Background

Experimental observations of steady-state flow of water and oil through planar and non-planar chamber-and-throat pore networks etched in glass (Avraam et al., 1994; Avraam and Payatakes, 1995) have shown that over a broad range of values of the important dimensionless parameters of capillary number $u\ v$, viscosity ratio $(\ \backslash$ nw, and water saturation, oil is disconnected in the form of ganglia in the flooded region. A portion of the oil in the pore network is stationary in the form of stranded ganglia, whereas the flowing part of the oil moves in the form of multisized ganglia by exerting higher macroscopic pressure difference.

Ganglion motion and interactions result in an overall dynamic equilibrium giving a time-average steady state, and can be described as "steady state" ganglion dynamics.

The experimental observations of Avraam et al., (1994), and Avraam and Payatakes, (1995) elucidate the flow mechanisms at pore level during "steady-state" two phase flow experiments and show that moving disconnected oil is solely responsible for the oil flow rate. These observations challenge the common assumption that disconnected portions of oil do not move at all (Honarpour and Mahmood, 1988).

In this study, it is believed that the nucleated dispersed gas bubbles generated in the depletion process of the solution gas drive heavy oil reservoir are moving even at low gas saturations. Therefore, gas relative permeability can be obtained based on the movement of the disconnected dispersed gas bubbles.

6.1.2. Derivation of "steady state" gas pseudo-relative permeability

The governing equation of gas phase flow including the effect of oil phase on the mobility of gas phase (coupling effect) in a gas-oil system is (Kalaydjian et al.):

$$L \qquad (6.1)$$

where, g_g, p_g, p_{o}, A/?$_x$,and A/?$_o$ are the gas flow, gas viscosity, oil viscosity, macroscopic gas pressure difference, and macroscopic oil pressure difference, respectively, k is the effective gas permeability due to flow of the gas phase and k_{go} is the effective gas permeability due to flow of the oil phase. Finding the tensor of the effective gas permeabilities is quite complicated. Therefore, an effective gas permeability which is a combination of both effective permeability tensors is considered in this study and is called gas pseudo-relative permeability after dividing by absolute permeability. Gas pseudo-relative permeability can be obtained using the general form of Darcy equation for two-phase flow in a one dimensional system:

$$Op \qquad \frac{\mu_g v_g}{k k_{rg}} \text{-PggSHITI} \tag{6.2}$$

along with a similar equation for oil. In this equation, $r\backslash$ is the degree of inclination. The attractiveness in obtaining a pseudo-relative permeability for gas is in that, most mathematical models of multi-phase flow and all reservoir simulators use Equation 6.2. In this study, horizontal model is assumed. Therefore, rj is equal to zero, and the gravitational term becomes zero.

Capillary pressure is expressed by $P_c = p_g - p_o$, therefore,

$$a\_Kj P\,\hat{}\, J\_K \qquad (63)$$
$$dx \quad dbc \quad dx$$

From $?\hat{} = \hat{}s\text{-}x\text{—}^{n}$, and assuming uniform gas saturation in entire system, $\frac{\delta S}{dx}$ is equal to zero, therefore, $\frac{\delta P}{dx} = 0$. Equation 6.3 will simplify to Equation 6.4.

$$\frac{d}{dx}\text{-}\hat{}Jj\pm \qquad (6.4)$$
$$dx$$

Equation 6.4 ignores capillary forces. This is a good assumption under flow conditions where capillary forces are negligible compared to pressure forces. Such a assumption is believed to be good in high permeability network model at high pressure gradient.

By knowing that, v_g = — and using equation 6.4 in equation 6.2 and integration of the new equation, the final solution for the gas pseudo-relative permeability will be obtained.

$$k_{,,} = \frac{v_g q_g \; I}{kA \quad A_{Pn}} \qquad (6.5)$$

In which, q_g is the total gas flow rate at each time step and Ap_a is the macroscopic pressure difference along the system in the direction of flow. Tang and Firoozabadi (1999) used the same method to determine the k_{rg} in depletion experiment in a heavy oil sand pack.

6.1.3. Methodology of ^determination in a network model

A gas bubble is shown in Figure 6.1. As it is shown, the interfaces at the upstream and downstream will move after exerting macroscopic pressure difference (Figure 6.1b,c). Line A-A is a reference line for the gas bubble movement at each successive time. The same movements would happen in network model.

Let's consider a network of dispersed gas bubbles as it is shown in Figure 6.2. Now consider a hypothetical line perpendicular to the macroscopic pressure

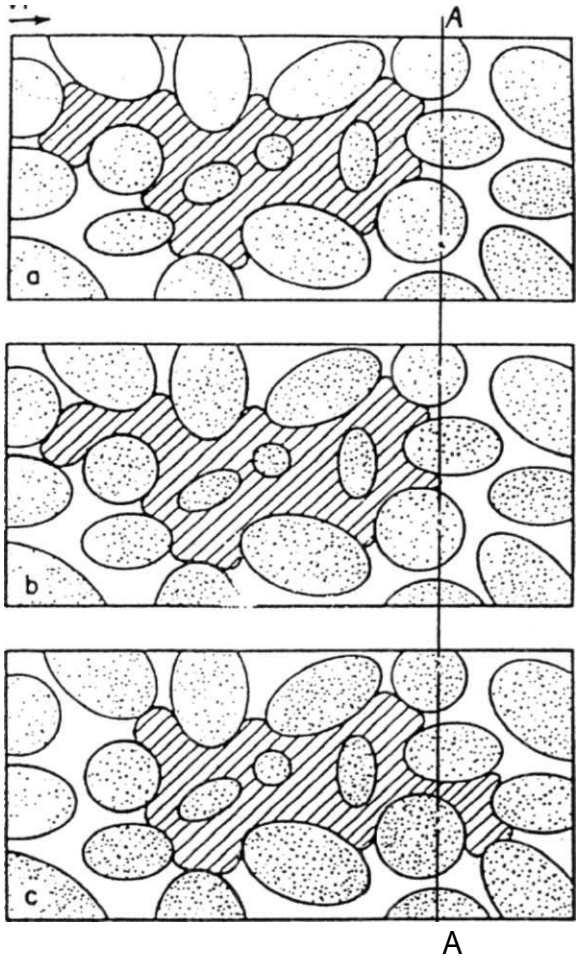

Figure 6.1: Schematic representation of the gas bubble movements. (Modified from Dias, 1984)

difference direction and close to the outlet of the network (line A'-A' in Figure 6.2). This line could be considered at any point perpendicular to the macroscopic pressure difference direction.

As it is shown in Figure 6.2, line A'-A' passing through gate unit cells (the last gate unit cells close to the outlet). At time zero the interfaces assigned to be at

Figure 6.2: Schematic representation of dispersed gas bubbles in a network

the middle of the gate unit cells as it is shown in the inset zoom. Once the simulation starts, the interfaces will move until one or more of the interfaces reach the hypothetical line. In this model, the hypothetical line is assigned at point 0.55 of the gate unit cell. The line A'-A' is slightly to the downstream of the middle point (point 0.5) of the gate unit cells. Once the interface(s) has (have) passed the hypothetical line, the volume of the portion that passed by the line will be calculated (please refer to chapter 4 for further discussions on interface movements). The elapsed time is also calculated as described in Chapter 4. By knowing the volume of the gas that passed through the line and elapsed time, flow rate can be calculated at each time step. Using Equation 6.5, k is then calculated.

It is worth to mention that absolute permeability and porosity of the network can be tuned by the model constants, $\mathbf{c}_{,,}$ $\mathbf{c}_{2}$, and $\mathbf{c}_{3}$. For this study, the experimental data of an unconsolidated sand have been used to find the model constants. The experimental data is given in Table 6.1.

6.2. Simulation algorithm

In this study a two-dimensional converging-diverging network model has been developed to study the effect of oil viscosity on gas relative permeability. The model accounts for random pore sizes, and includes capillary forces, and viscous forces. The model is also capable of handling dispersed gas bubbles with

different sizes. For each bubble size, model was run at different capillary number, viscosity ratio, and gas saturation. This model gives the gas relative permeability based on the movements of the dispersed gas bubbles.

Calculations are performed in two steps, model initialization and two-phase flow calculations. In the next sections a short description of each step is presented.

6.2.1. Model initialisation

In most porous media such as sand-packs or sandstone, both pore-throat and pore body sizes are random variables. This can be accommodated in a converging-diverging unit cell of Figure 6.3, representing a pore-throat and its adjacent half-pore bodies. In a converging-diverging network model, throat diameter, pore body diameter and length of a unit cell are related by some constants, which we would call geometrical constants. For a particular porous medium, the geometrical constants can be found from laboratory measurements such as porosity measurement, initial drainage curve, and grain size distribution. Table 6.1 gives the physical properties and the constants of the porous medium used here.

Table 6.1: Experimental and theoretical analysis of the used porous medium

Parameter	Experimental (Dias, 1984)	Theoretical
Porosity (⌀), %	39.5	40.1
Permeability (K),(j.m^2	3.55	3.50
Mean throat diameter (< d >), |am	20	20
Geometric constants (c,, c_2, c_3)	–	6.1, 4.9, 0.69

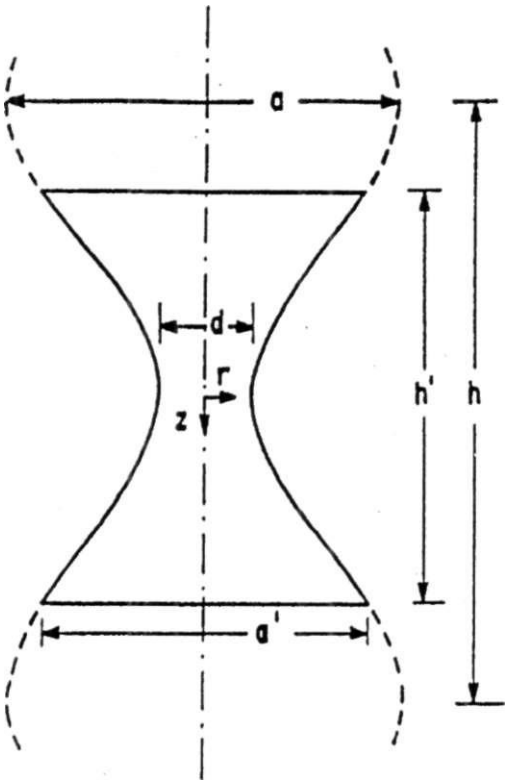

Figure 6.3: Typical unit cell (UC) of the porous medium model (Dias, 1984)

Once the geometrical constants and the pore-size distribution are known, the network model can be set-up. A pore size is randomly selected from the pore-size distribution curve (Figure 6.4). The next pore is chosen similarly, and is placed in the network. The process is continued until the desired space is filled. A two-dimensional representation of a random cubic network of constricted unit cells is given in Figure 6.5a.

Equations have been developed for the conductivity of the unit cells based on their dimensions (further discussion is given in Chapter **4).** Initially, single-phase flow calculations are performed in the

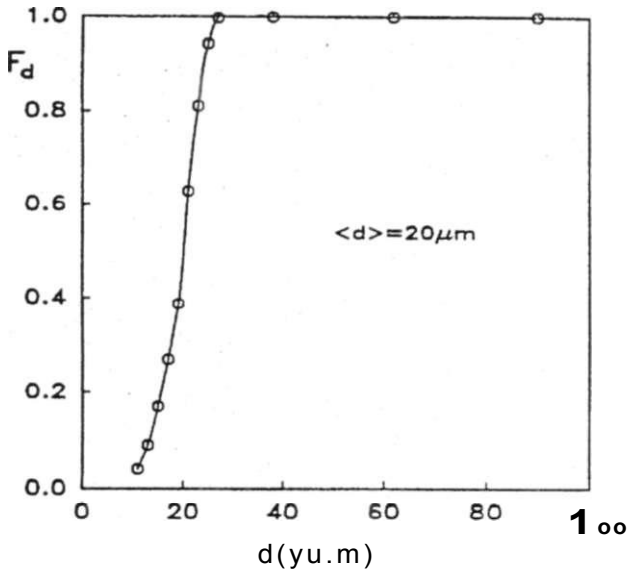

Figure 6.4: Plot of the cumulative throat size distribution function $F_d(d)$ (From Dias, 1984)

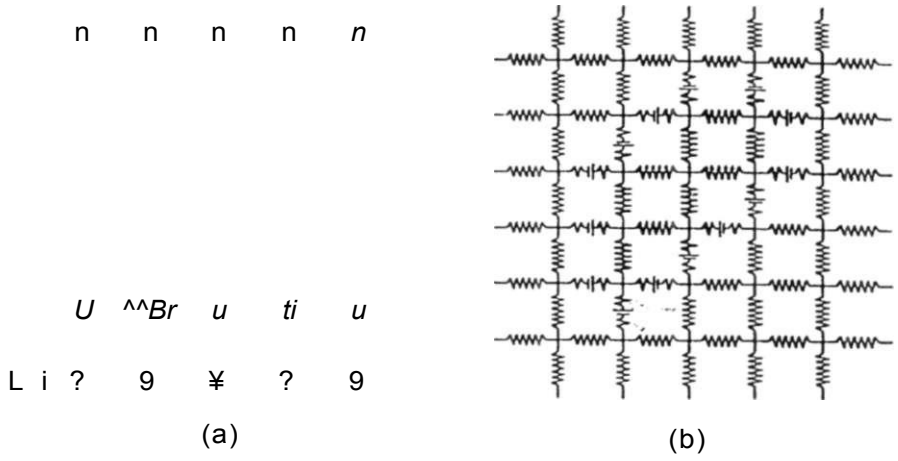

Figure 6.5: (a) Depiction of an 8-CEVS ganglion on a two-dimensional square network and (b) its electric analog network (from Dias, 1984)

following manner. A constant pressure difference is exerted across the network model, and the flow rates are calculated, knowing the conductivity of each unit cell. The total calculated flow rate along with the total pressure drop is used for absolute permeability calculations. The calculated value is compared with the measured permeability of the actual sample. In our calculations, minor adjustment of the geometrical constants was required to match the experimental values of porosity and permeability given in Table 6.1.

Next, some of the unit cells are filled with gas. Figure 6.5a shows part of the network model, with a gas bubble occupying 8-CEVS. A CEVS is composed of four adjacent half unit cell, as shown by the circles in Figure 6.5a. A unit cell occupied by a gas-oil interface is denoted as a Gate Unit Cell (GUC). Gas saturation is obtained knowing the volume and the number of the unit cells occupied by gas and the total space.

In Figure 6.5b, the analogous electric circuit is shown. The unit cells filled with gas and oil are shown by thick and thin line resistors, respectively. Gate unit cells (GUC) are partially thick line resistors. There is a voltage source at each GUC corresponding to the capillary pressure between the interfaces.

6.2.2. Two-Phase fow calculations

Initially, the gas bubbles are distributed uniformly to achieve a particular gas saturation (see Figure 6.2). Two-phase conductivities are then calculated, this time accounting for the viscosity of the particular fluid occupying the unit cell. In this model each unit cell is divided into 80 compartments, such that the location of a gas bubble interface can followed as it moves through a unit-cell. Next, capillary pressure at the gas-oil interfaces is calculated using the radius of unit cell at the interface position, interfacial tension and the contact angles. Interfacial tension, receding and advancing contact angles are input parameters (See Table 6.2). In order to initiate flow, a macroscopic pressure difference is posed. Flow rate through each unit cell is calculated similar to what is performed in electrical circuit analysis. The required input parameters are, the macroscopic pressure drop, the pressure drops due to capillarity and the conductivity of the unit cells. As the gas bubbles move through the unit cells, the pressure drops due to capillarity and the conductivity of the unit cells are updated. When gas bubbles start to move, k will be calculated by the method described in section 6.1.3.

Table 6.2: Input parameters and the range of the investigated parameters

Parameters	Base case	Range
Equilibrium contact angle (9_e)	25	15-25
Advancing contact angle (9_a)	30	20-30
Receding contact angle (9_r)	20	10-20
Interfacial tension (a), mN/m	20	0.1-20
Gas bubble size, CEVS	16	2-16
Gas saturation (S_g), %	12-13	3-23
Capillary number (Ca)	1e-4	0.00001-0.01
Viscosity ratio **(k)**	1e-5	0.000001-0.1
Aspect ratio (AR)	5.8	4.8-6 8
Network size (no. of UC)	40 by 40	40 by 40 and 100 by 100

The calculation flow diagram is depicted in Figure 6.6. A more detailed description of the steps involved is given in the following.

A. Input Data

- Input physical properties of fluids (gas and oil), e.g.: viscosity, interfacial tension.
- Specify porous medium model constants and throat size distribution function.
- Specify network size, and the number of compartments at each UC.
- Specify equilibrium, advancing and receding contact angle.
- Assign unit cell throat sizes.
- Specify the capillary number or macroscopic pressure gradient.

B. Partitioning of unit cells

- Partition unit cell in compartments and calculate volume, position and curvature of interface for each compartment.

C. Gas bubble position, shape, and volume.

- Specify gas bubble position and shape, as well as the volume of gas in each gate unit cell. Calculate the total gas volume and gas saturation.

D. Calculation of unit cell conductance

- Calculate conductance for each unit cell filled with oil and filled with gas, as well as conductance for gate unit cells. Calculate pressure difference due to interface at each Gate Unit Cell (GUC).

E. Network analysis

- Solve the network analysis to determine the pressure at each node.
- Calculate the pressure drop and flow rate along each unit cell.

F. Time increment calculation, and updating

- Calculate the time increment such that the interface in each gate unit cell advances or recedes, at most, one compartment.
- Update the volume of gas in all GUC's.

G. *Motion rules*

- If a unit cell is filled or emptied of gas, apply motion rules.

H. Gas pseudo-relative permeability

- Calculate the gas relative permeability. Report the total time, and gas relative permeability value.

A ***Iteration***

- Repeat steps D through H until the total number of time steps reached.

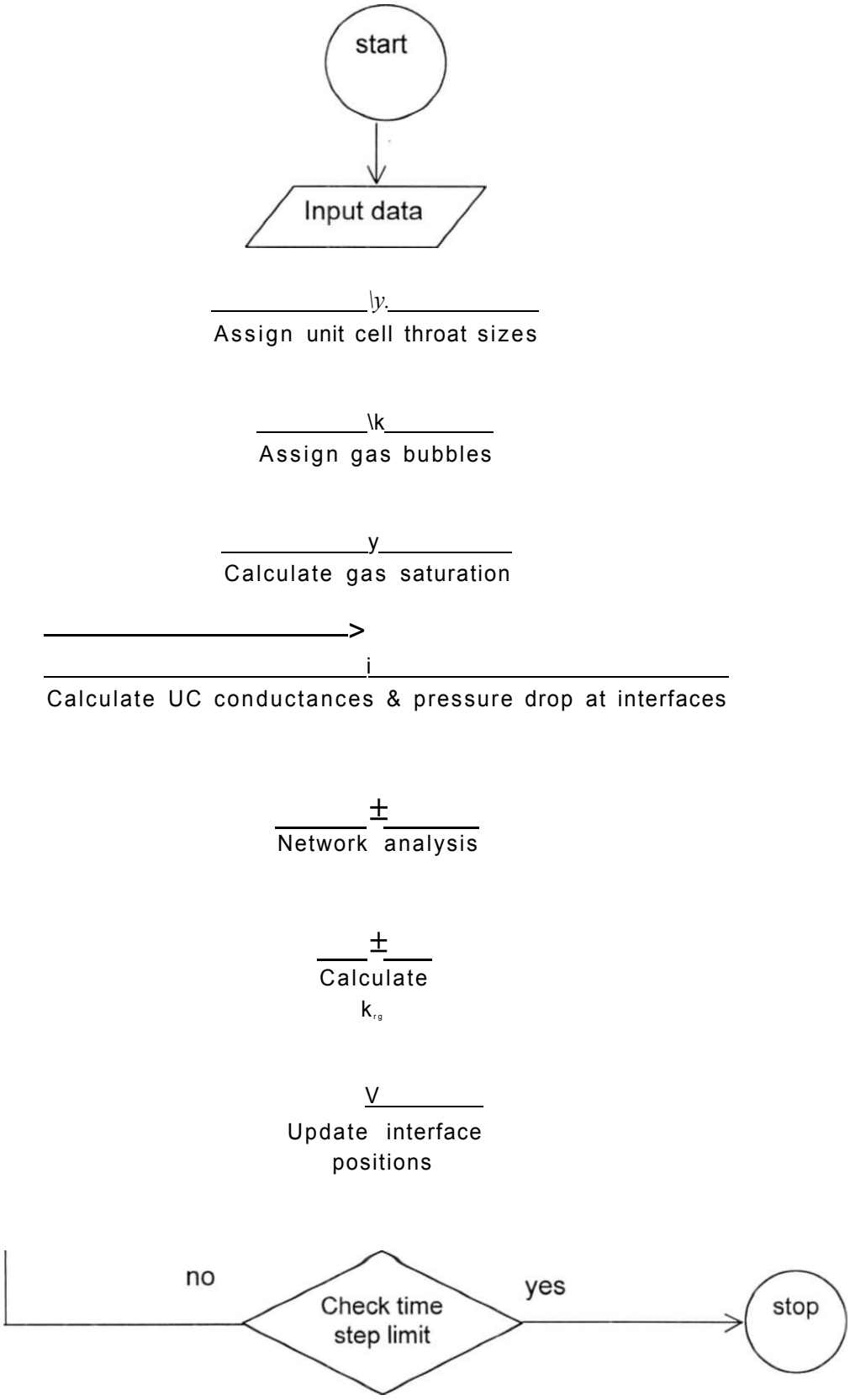

Figure 6.6: Block diagram of the gas relative permeability code

CHAPTER SEVEN

Results and discussion

The developed model is used to investigate gas mobility in heavy oil systems. This is for the first time that a network model has been used to find the effect of oil viscosity on gas mobility. In the next sections the model verifications and obtained results on gas pseudo-relative permeability will be presented.

7.1. Model verification

In order to validate the model a volume balance criterion was added to the model to find total gas and oil volume in the network model. This should remain constant with time prior to gas production. Differences of the order of 1 .e-4 |j.m^3 was observed. For comparison the volume of an average unit cell is about 3.e4 (im^3. Other model verifications will be given along with results and discussion.

In the next section of this chapter, the obtained model results of the effect of different parameters such as network size, gas saturation, viscosity ratio, capillary number, gas bubble size, aspect ratio, contact angles, and interfacial tension on the gas pseudo-relative permeability will be discussed.

7.2. Model results

Figure 7.1 shows a typical gas relative permeability curve versus time. Gas relative permeability is zero at the initial times. This is because the hypothetical line explained in section 6.1.3 is to the downstream of the gas-oil interface and slightly away from it. The last interfaces (close to the outlet) move toward the reference line. After passing through this line, the gas flow rate will be calculated. Figure 7.1 indicates that the

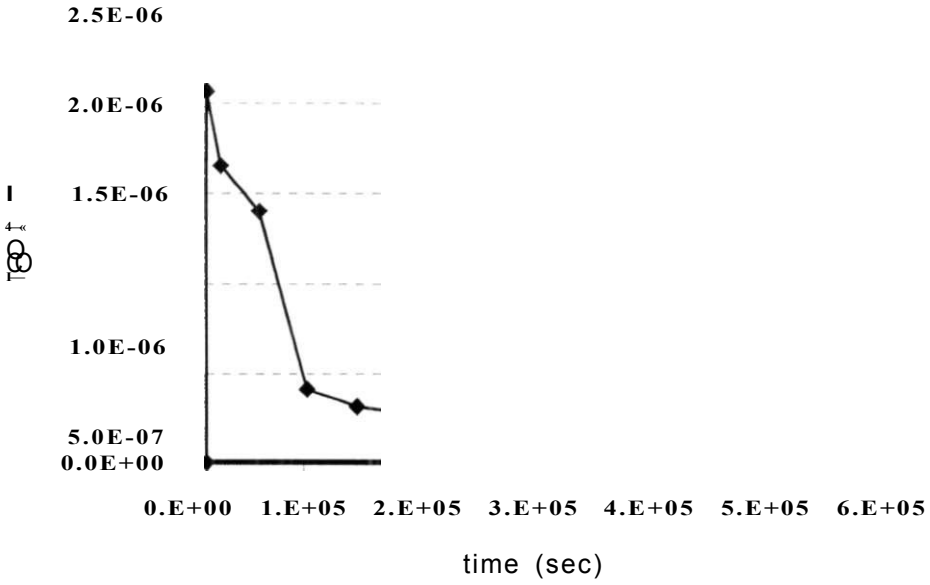

Figure 7.1: Typical model results of k_g versus time (16-CEVS bubble, S_g=13%, IFT=15mN/m, μ / =1e-5, Ca = 1e-4, θ_c = 25)

/ Mo

instantaneous relative permeability to gas (k_{rg}) oscillates periodically around a mean value. Our model showed more oscillations for the cases that capillary number and viscosity ratios were very low.

The k_{rg} value, corresponding to the mean value after the early time response is considered as the obtained k_{rg} value for all the studied cases. In the next sections, the effect of network size, gas saturation, viscosity ratio, capillary number, gas bubble size, aspect ratio, contact angles, and interfacial tension on the gas relative permeability are presented. In order to verify the model results, at each section, the related experimental and modeling results of other investigators is also given.

In all the cases, interfacial tension and advancing, equilibrium and receding contact angles are considered equal to 20 mN/m, 30°, 25°, and 15°, respectively. In Section 7.2.7, however, the contact angles have been changed to do the sensitivity analysis on contact angles. Similarly in Section 7.2.8, the IFT has been changed.

7.2.1. Effect of network size

Figure 7.2 shows the effect of network size on the gas relative permeability for the case that gas bubble size is equal to 16-CEVS (4 by 4) and gas

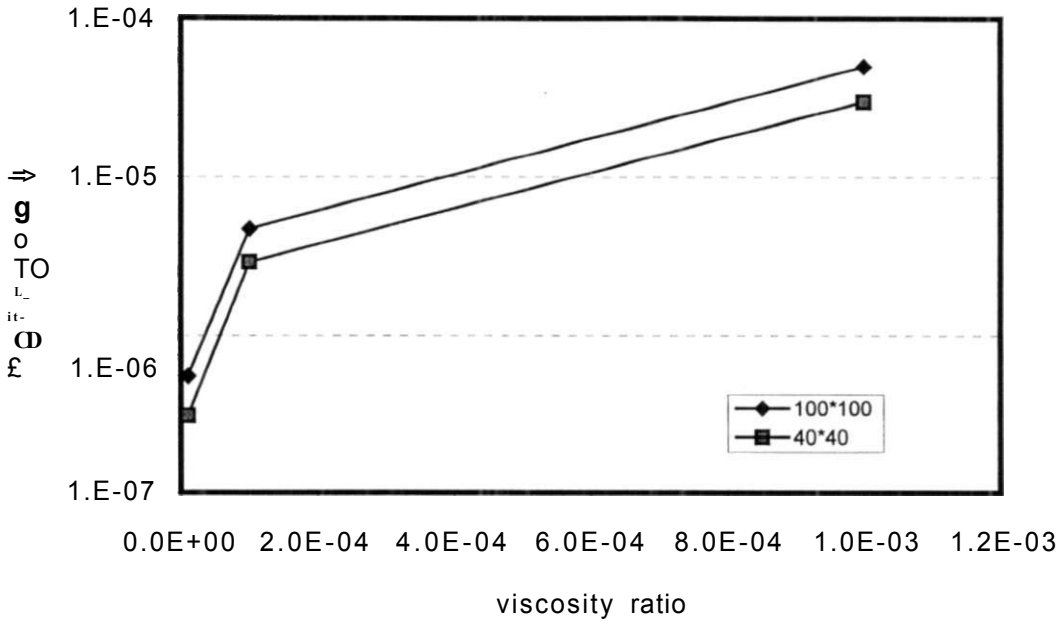

Figure 7.2: Effect of network size on k_{rg} (16-CEVS bubble, S_g=13%, IFT=20mN/m, Cfl=1e-4, θ_e = 25)

saturation around 13%. Other input parameters are given in the figure caption. Figure 7.2 indicates that by increasing network size the value of gas pseudo-relative permeability will increase too. By considering that the larger the network model the better representation of the real porous medium, it can be concluded that larger network size results are more reliable. However, computation time is a limiting factor. As a comparison the computation time of the above 100 by 100 network took 430 minutes to complete 2500 time steps, whereas the above 40 by 40 network took about 15 minutes. By increasing the network size by a factor of 6.25, the computation time increased by a factor of 28. Figure 7.2 shows a similar trend of relative permeability variations with viscosity ratio for both network sizes. Therefore, it is thought that a small network size will exhibit results that are qualitatively correct.

Qualitative investigation of different parameters on gas pseudo-relative permeability is sufficient for this study. Therefore, network size of 40 by 40 was considered and all the simulation runs were performed based on this network size using PC (Geniunintel Pentium Ⅲ processor, 128 MB RAM).

Figure 7.3 shows the results of the network studies, which were conducted by Vizika et al. (1994) to find the effect of network size on residual oil saturation in an oil/water system. This figure shows that by changing the network size, the obtained residual oil saturation is changing too.

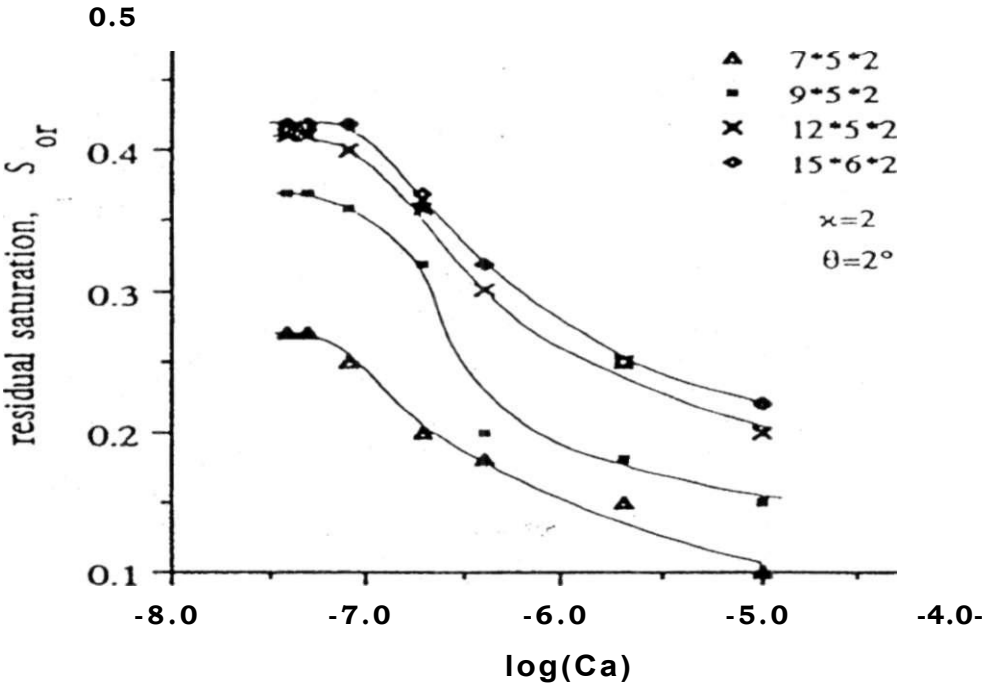

Figure 7.3: Effect of network size on residual oil saturation in oil-water system. (From Vizika et al., 1994)

7.2.2. Effect of gas saturation

Figure 7.4 shows relative permeability values as a function of gas saturation. Figure 7.4 shows that by increasing gas saturation, gas pseudo-relative permeability is increasing. All other cases of varying gas bubble sizes, capillary number, and viscosity ratio showed the same trend of increasing k with increasing gas saturation.

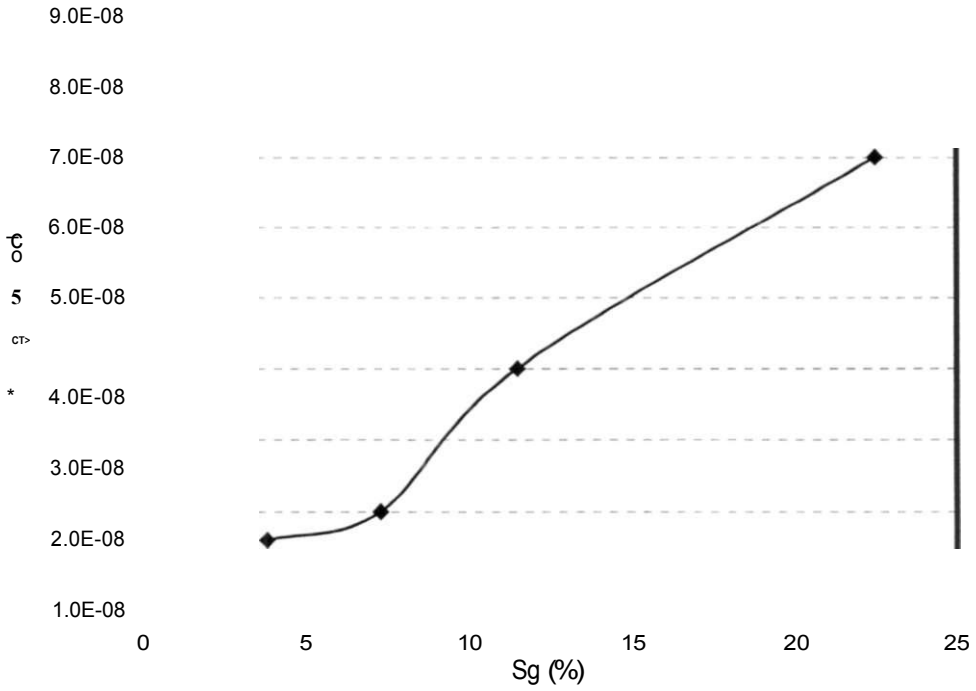

Figure 7.4: k_g, versus gas saturation (9-CEVS bubble, IFT=20mN/m, = 1e-5, Ca = 1e-5,t9, = 25)

7.2.3. Effect of capillary number

Figure 7.5 shows the effect of capillary number on gas relative permeability at different viscosity ratios. The trend lines show that gas relative permeability increases by increasing capillary number. The reason is that by

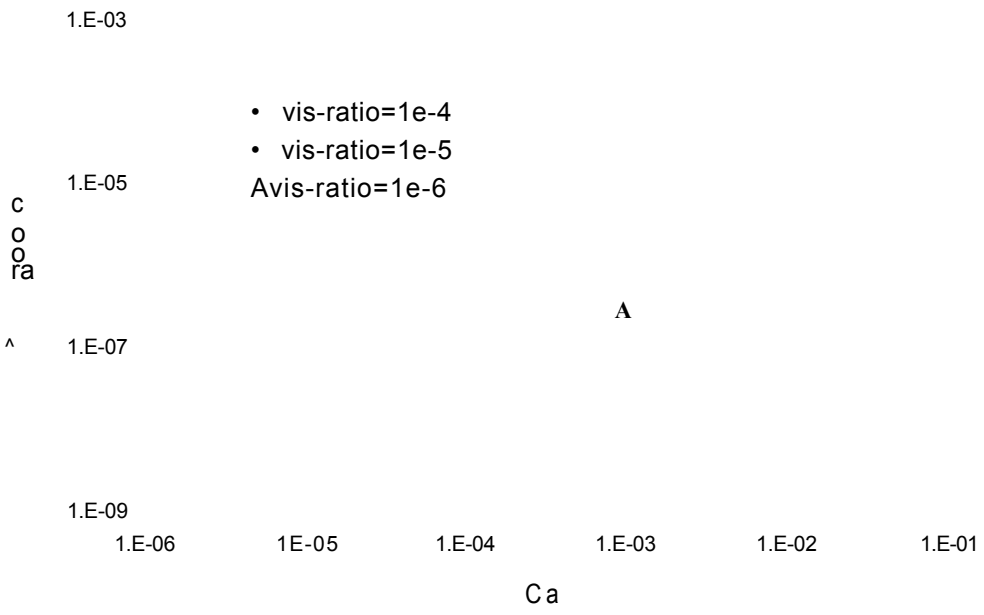

Figure 7.5: Effect of capillary number on gas relative permeability at different viscosity ratios (9-CEVS bubble, S_g=12%, IFT=20mN/m, $9_{,}$ = 25)

increasing capillary number while keeping oil viscosity ($//_{„}$) and interfacial tension constant, flow velocity (v) is increasing, which means that pressure forces are increasing. This tends to increase gas mobility. As it is shown in Figure 7.5, variation of k_{rg} is low, in the regions of capillary numbers less than 1e-4 and more than 1e-3. Between these two regions, the variation of is different. We do not have any explanation for this trend.

Experimental results of the oil relative permeability in oil/water system showed that by increasing the capillary number *(Ca),* oil relative permeability *(k_{ro})* increases (Avraam and Payatakes, 1995). These results are shown in Figure 7.6.

Constantinides and Payatakes (1996) performed network simulation to show the effect of capillary number on k_{ro} in oil/water systems. Figure 7.7 shows their results and indicates that, k_{ro} increases by increasing capillary number.

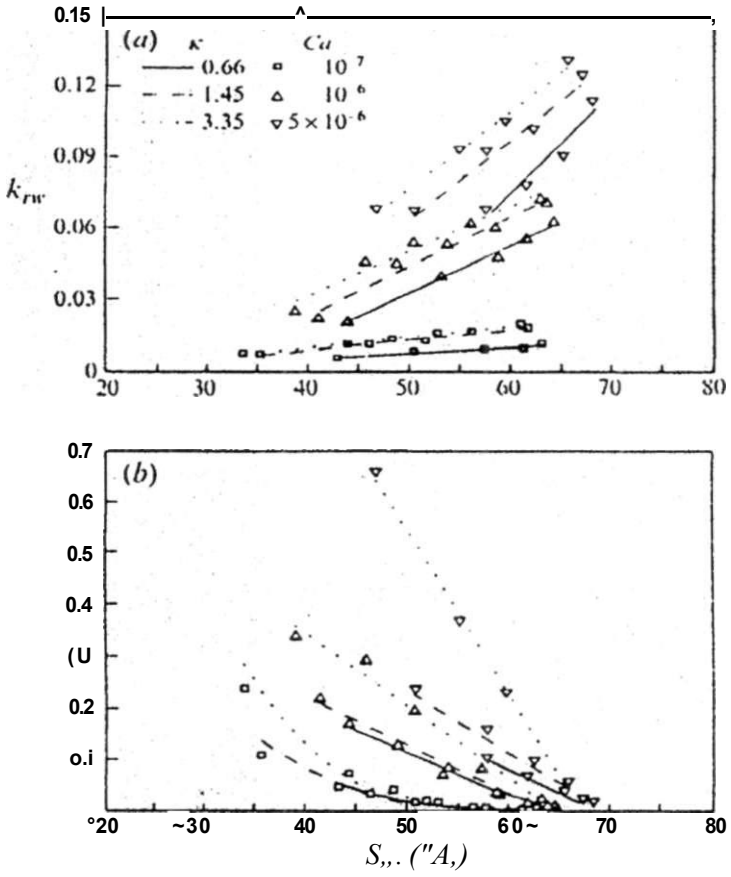

Figure 7.6: Effect of capillary number and viscosity ratio on relative permeability in oil-water system. (From Avraam and Payatakes, 1995)

In a gas-condensate system study, Mott et al. (2000) showed the effect of capillary number on relative permeability of the liquid and gas. The results of relative permeability measurements on a sandstone core from a Northsea gas condensate reservoir are shown in Figure 7.8. As it is shown in this

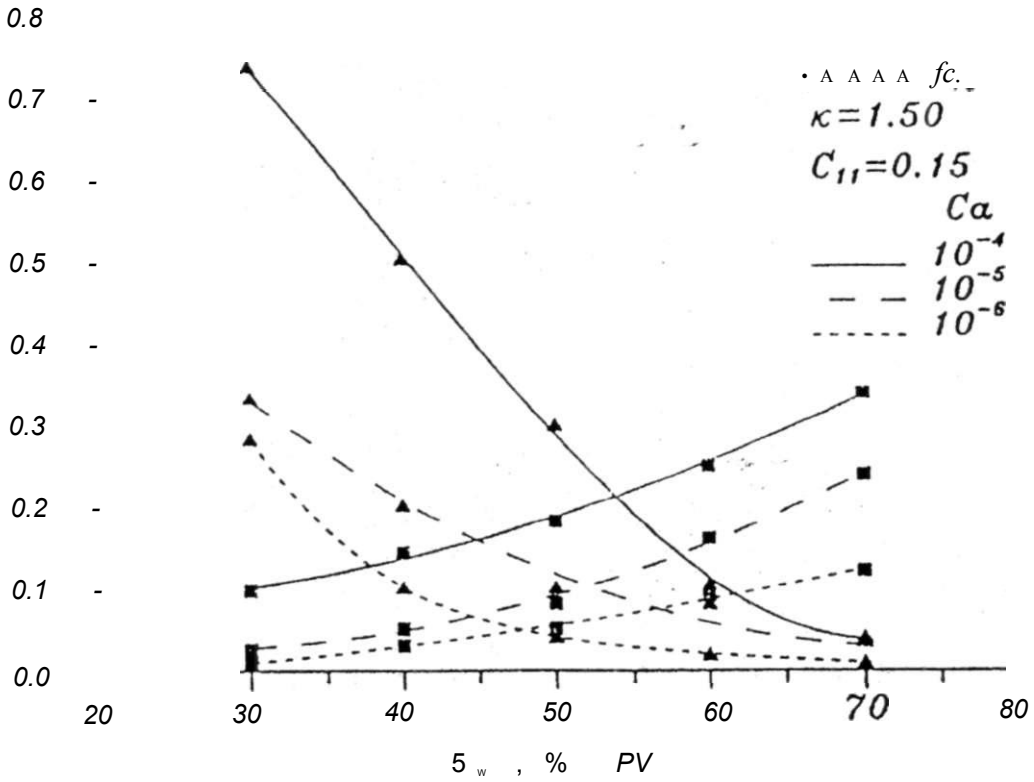

Figure 7.7: Effect of capillary number on relative permeability in oil-water system. (From Constantinides and Payatakes, 1996)

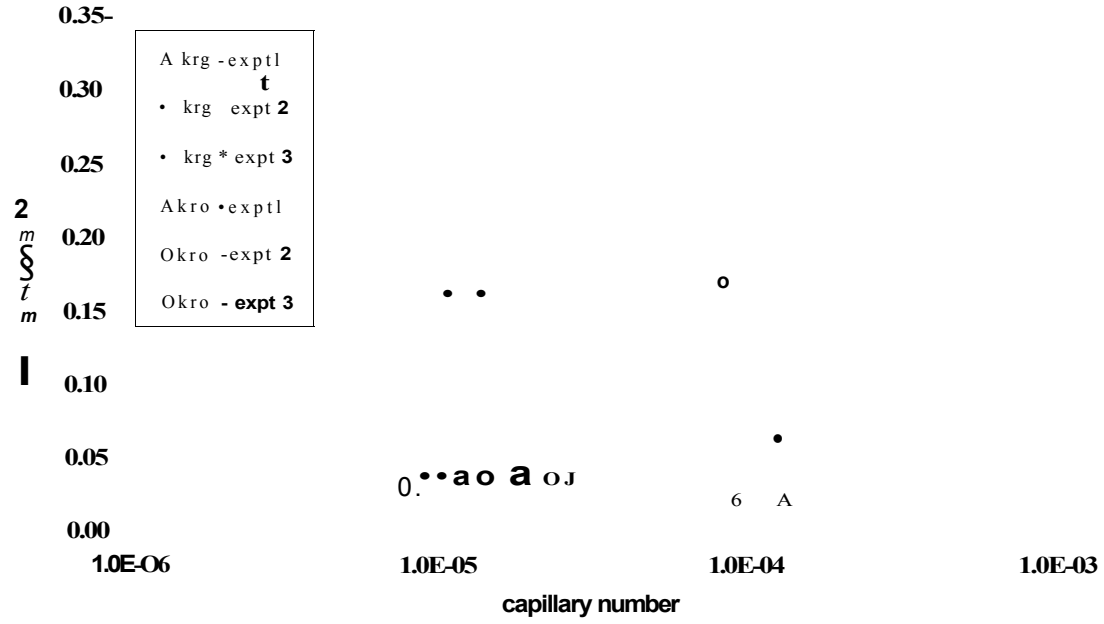

Figure 7.8: Effect of capillary number on relative permeability in gas-condensate system. (From Mott et al., 2000)

figure, by increasing the capillary number, relative permeability to both phases increase.

7.2.4. Effect of gas bubble size

Figure 7.9 shows the effect of gas bubble size on gas relative permeability. As it is shown in this figure, by increasing the gas bubble size at a specified gas saturation and capillary number, the gas relative permeability increases. These graphs are plotted for three different viscosity ratios. All the graphs show that by increasing the gas bubble size, gas mobility is increasing. The physical interpretation is that, larger gas bubbles have larger pressure difference along them, leading to

higher driving force to move the gas bubble. Also higher number of gas bubbles means higher number of interfaces and therefore more resistance to flow.

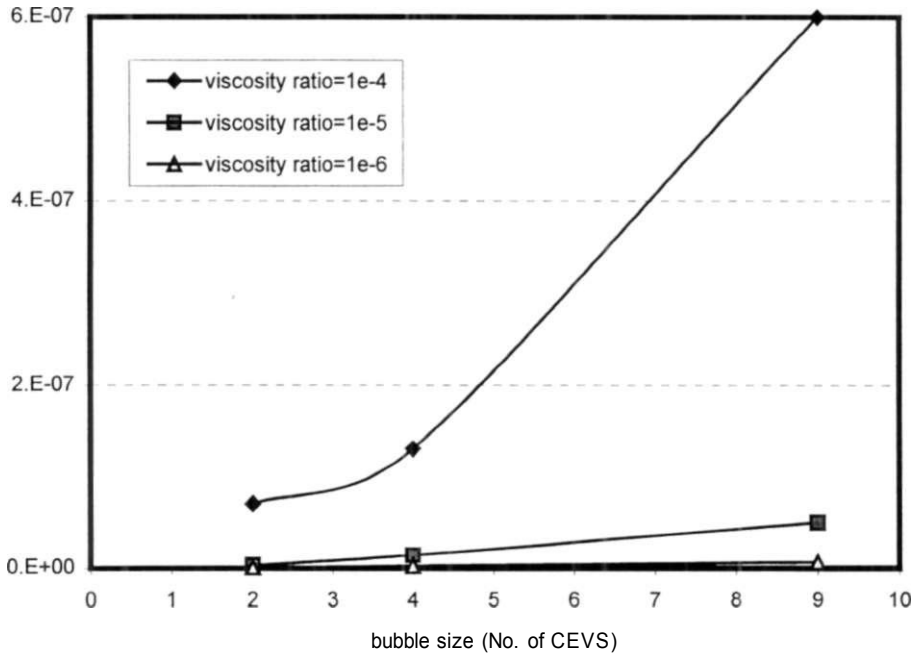

Figure 7.9: Effect of gas bubble size on gas relative permeability (Ca=1e 4, Sg=12%, IFT=20mN/m, O_o = 25)

Kumar and Pooladi-Darvish (2001) showed that gas bubble growth is lower in heavier oils in a depletion process. The results of their work are shown in Figure 7.10. This figure shows that for equal period of time and the same pressure decline, the gas bubble sizes are smaller in heavy oils compare to conventional (light) oil. Lago et al. (2000) conducted a series of pressure depletion experiments in glass micro-model using five Venezuelan oils. They found that during depressurization tests in a micro-model, there are more bubbles in heavy oils than in light oils, while the bubble size is smaller.

Our model results show that smaller gas bubbles move slower than large gas bubbles. By combining these two results, one observe that low gas mobility in heavy oil reservoirs as suggested previously is in line with the fact that (1) the nucleated gas bubbles remain smaller during the depressurizing process in heavy oil systems, and (2) small gas bubbles move slowly.

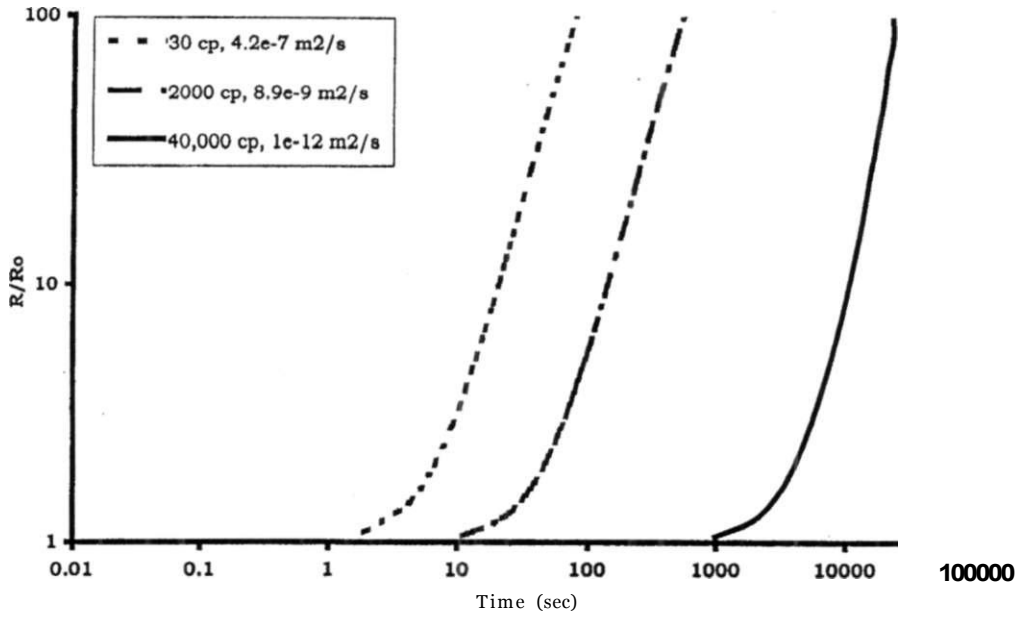

Figure 7.10: **Comparison of bubble growth for gradual decline in pressure** (100 **psi/hr) for various cases. (From Kumar and Pooladi-Darvish,** 2001)

Micro-model studies of Bora et al. (2000) showed that gas bubbles break to smaller daughter gas bubbles at high flow rates (Figure 7.11). Based on our model results on the effect of gas bubble size on gas relative permeability, once a large gas bubble breaks to smaller gas bubbles, the generated small gas bubbles move slower than the original large gas bubble. This might give a clue why high production rates are found a suitable production scheme in cold production of solution gas drive heavy oil reservoirs. Our model does not account for the gas break-up. But it gives the above idea implicitly by running the model at different gas bubble sizes.

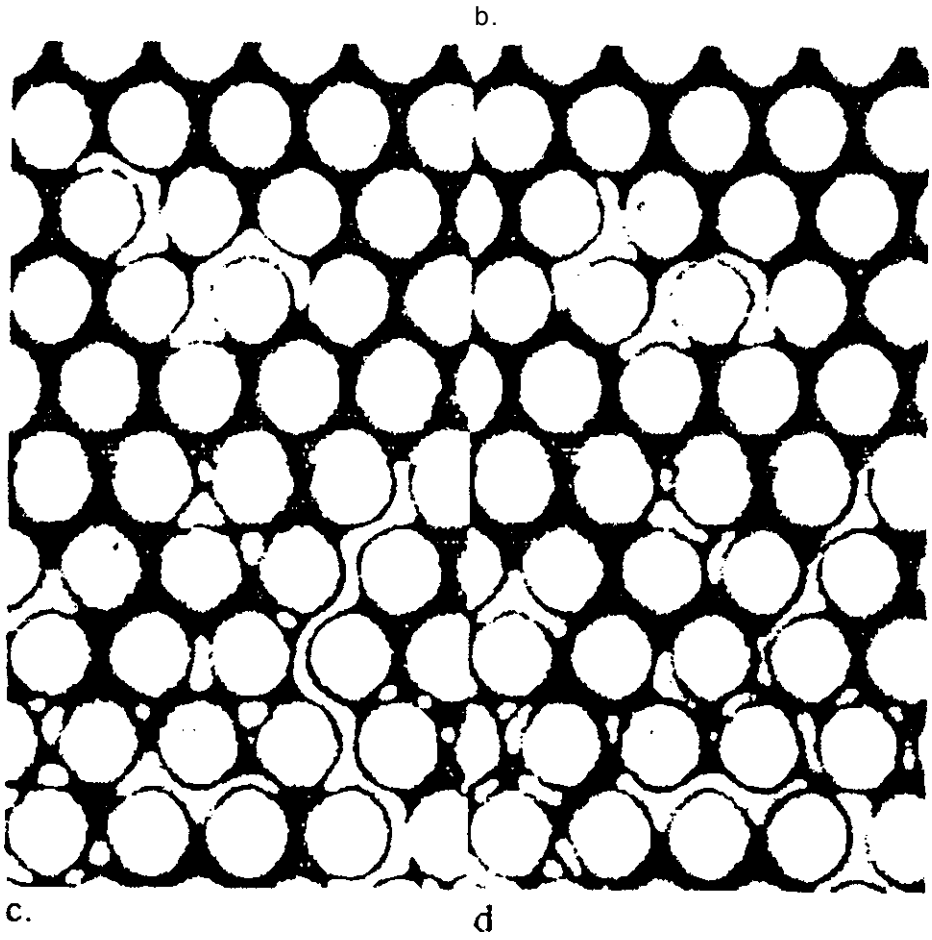

Figure 7.11: Illustration of bubble break-up mechanisms by tip splitting [(a) and (b), and break-up of elongated gas bubbles [(c) and (d)]. (From Bora et al., 2000)

Ettinger and Radke (1992) conducted experimental studies on the influence of texture on steady foam flow in Berea sandstone. The main conclusion of their study was that finer-textured foam leads to larger flow resistance. Figure 7.12 shows the effluent foam texture for a weak foam ($d_{B}i\_$=700 iim) and a strong foam ($d_{B}i\_$=300|im). Figure 7.13 shows the effect of gas bubble sizes on gas velocity. As it is shown in

this figure, gas velocity increases by increasing the gas bubble size. Our model showed the same results.

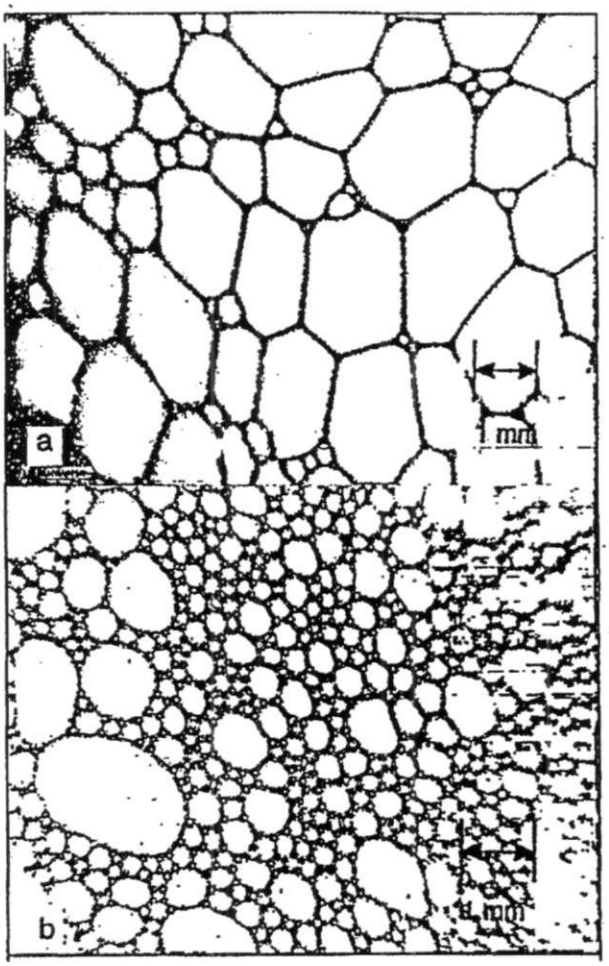

Figure 7.12: Effluent foam texture for (a) a weak foam (d_BL=700 fj,m) and (b) a strong foam (d_BL=300 ^m). (From Ettinger and Rodke, 1992)

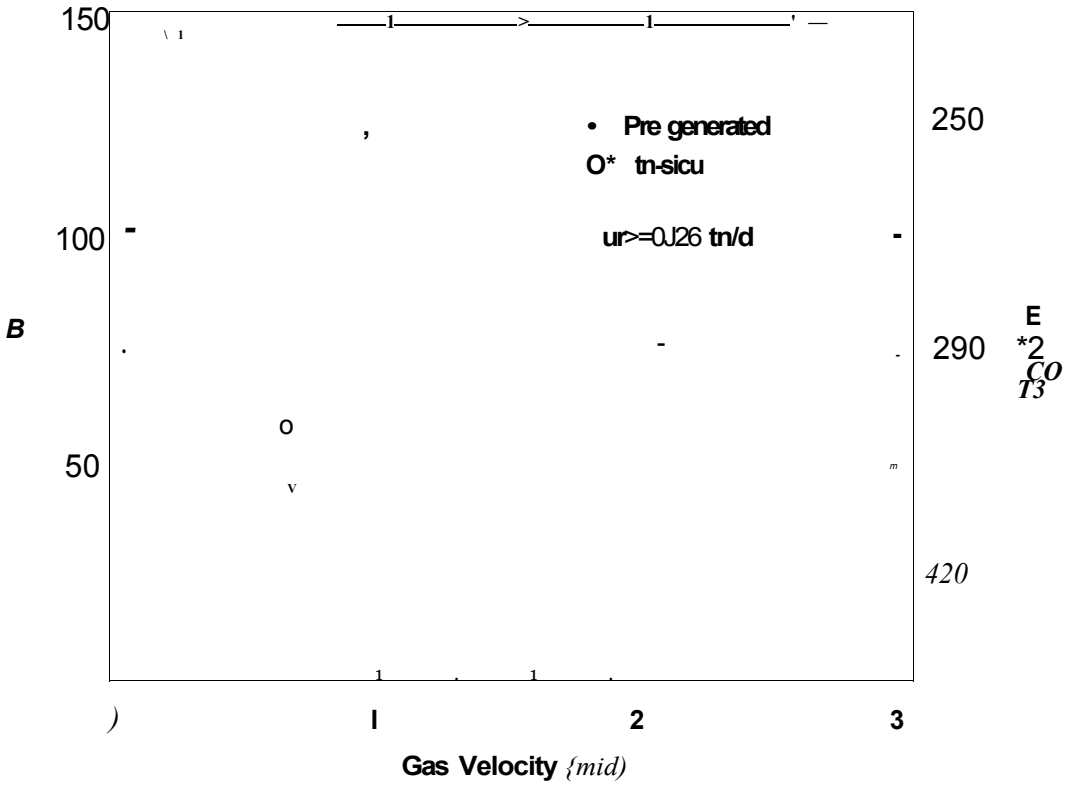

Figure 7.13: Effect of average bubble densities and sizes on gas velocity for pre-generated and in-situ-generated foam flow experiments. (From Ettinger and Radke, 1992)

7.2.5. Effect of aspect ratio (AR)

The effect of aspect ratio or the ratio of the pore body diameter to the pore throat diameter is studied by setting all the variables constants except the value of aspect ratio. The throat sizes are kept constant and the pore body sizes are being changed. Therefore, by increasing the AR, the porosity ($ and absolute permeability (K) of the model increase too, but the gas saturation remains constant. The obtained results are shown in Figure 7.14. As it is shown in this figure, by increasing AR, k_{rk} increases.

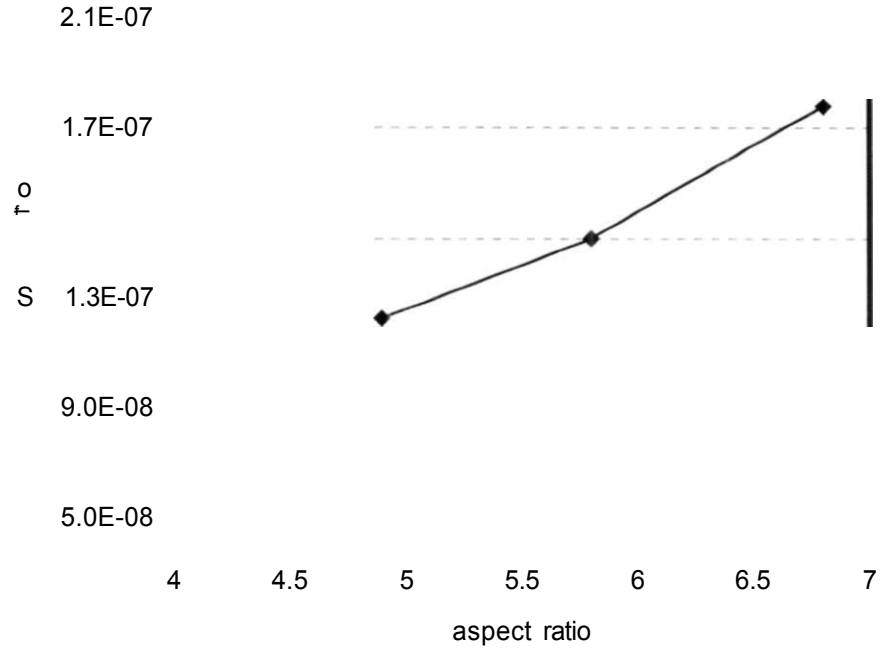

Figure 7.14: Effect of aspect ratio (AR) on gas relative permeability (16-CEVS bubble, Sg=13%, =1e-5, Ca=1e-4, IFT=20mN/m, θ_o = 25)

Unconsolidated sand, which is usually the sand type in Canadian heavy oil reservoirs has lower aspect ratio compared to the consolidated sand type. Therefore, aspect ratio might be one of the reasons that keep k low in these heavy oil reservoirs.

Model gave scattered results of gas relative permeability for the simulation runs of low values of aspect ratio (AR<2.8).

In another set of simulation runs, the effect of aspect ratio is studied by keeping the pore body size constant and change the pore throat sizes. The results showed that

by decreasing pore throat diameter (increasing aspect ratio), porosity and permeability of the network decreased, and the gas pseudo-relative permeability increased, the same as the cases of constant throat sizes and increasing pore body sizes.

7.2.6. Effect of contact angles

In this model, different values are used for the advancing and receding contact angles. Figure 7.15 shows the effect of the contact angles on gas pseudo-relative permeability. As it is shown in this figure, by increasing the contact angles (equilibrium, advancing and receding) the gas relative permeability increases. Advancing and receding contact angle values are 5 degree higher and lower than the equilibrium contact angle, respectively. The explanation is that by increasing the contact angles, capillary forces decrease. Therefore, capillary number (ratio of pressure forces to capillary forces) increases which causes increasing gas relative permeability.

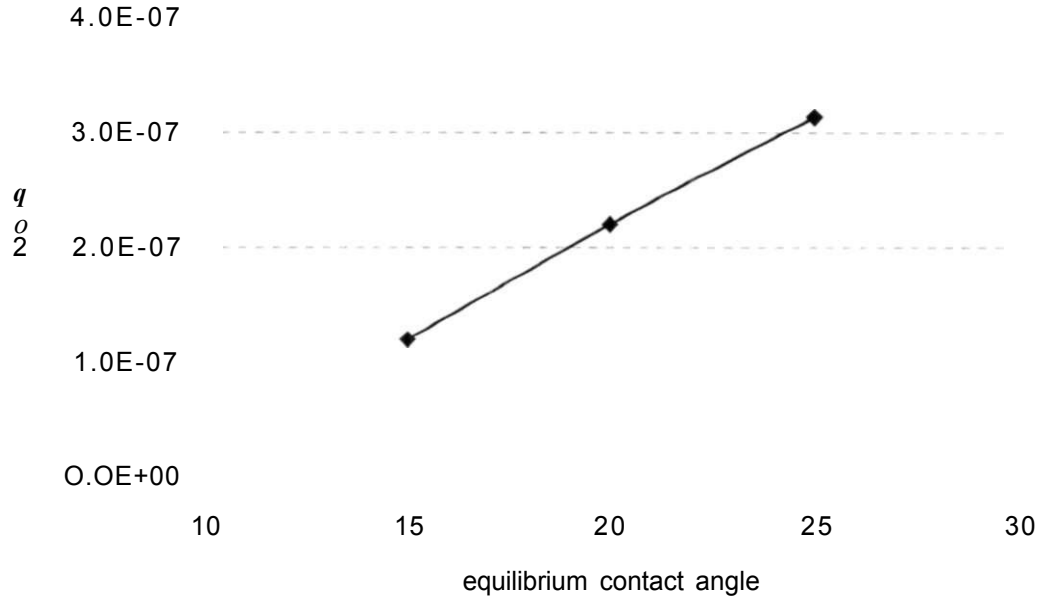

Figure 7.15: Effect of contact angle (equilibrium, advancing, and receding) on gas relative permeability (16-CEVS, Sg=13%, μ_{Mo} = 1e-5, Ca=1e-4, IFT=20mN/m) Advancing and receding contact angles are 5 degrees higher and lower than the equilibrium contact angles, respectively.

7.2.7. Effect of Interfacial Tension (IFT)

Figure 7.16, shows that by increasing interfacial tension between gas bubble and oil, k decreases. In this model by decreasing IFT and keeping the capillary number (\ constant, oil velocity or macroscopic pressure difference will decrease. Therefore, the oil and gas flow will decrease. However, the relative movement of gas bubbles will increase because of reducing capillary forces due to reducing IFT. Li and Firoozabadi (2000) studied relative permeabilities in gas/condensate systems using a network model. Figure 7.17, shows their results. As

it is shown in this figure, relative permeabiities of both phases decrease by increasing interfacial tension. Model for the IFT values less than 0.05 mN/m failed.

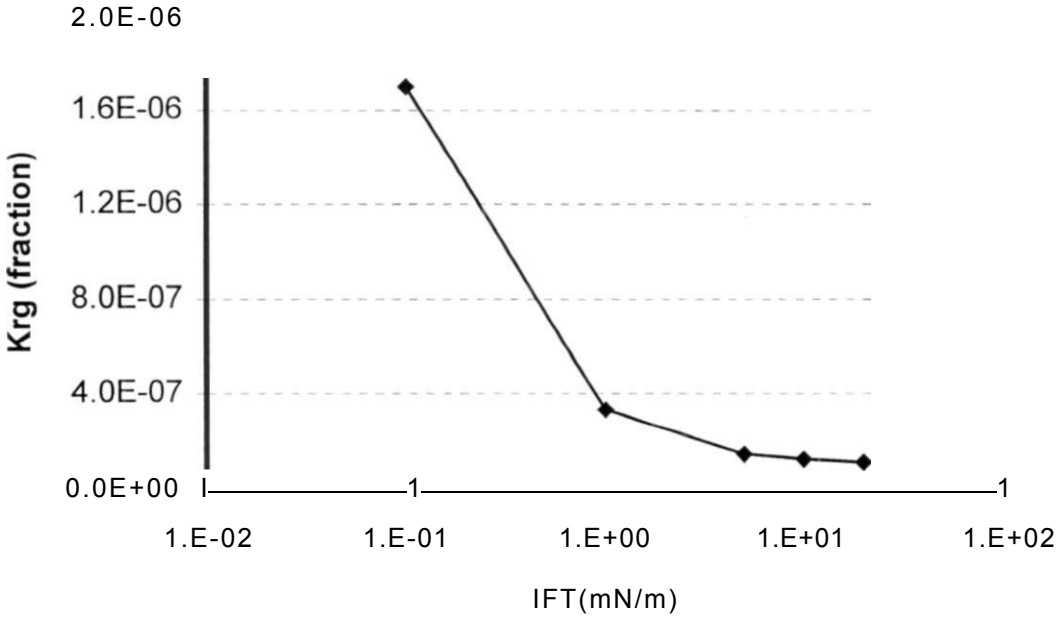

Figure 7.16: Effect of interfacial tension (IFT) between oil and gas on gas relative permeability (16-CEVS bubble, S_g=13%,'"y = 1e-5, Ca=1e-4, 0, **= 25)**

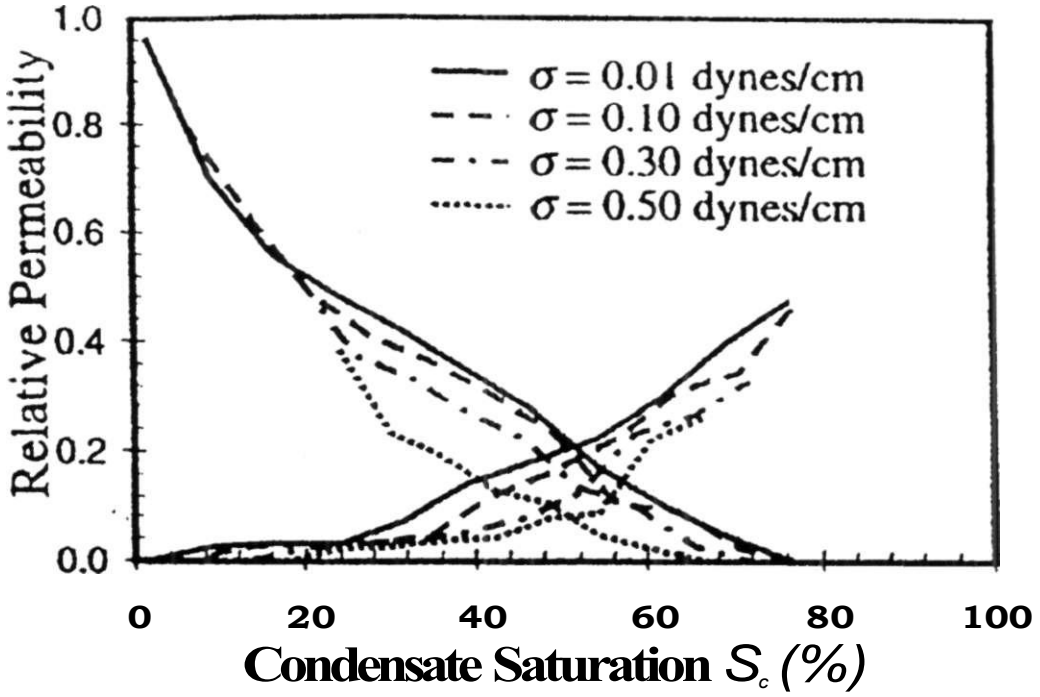

Figure 7.17: Effect of interfacial tension on the relative permeability in gas/condensate system. (From Li and Firoozabadi, 2000)

7.2.8. Effect of viscosity ratio

In this section the effect of viscosity of wetting-phase on the relative permeability to the non-wetting phase is studied.

Odeh (1959) conducted relative permeability experiments at various viscosity ratios for different oil-brine systems and observed that the relative permeability for the non-wetting phase was a function of the viscosity ratio. Figure 7.18 shows the results obtained by Odeh (1959). This figure shows that k_{ro} decreases by

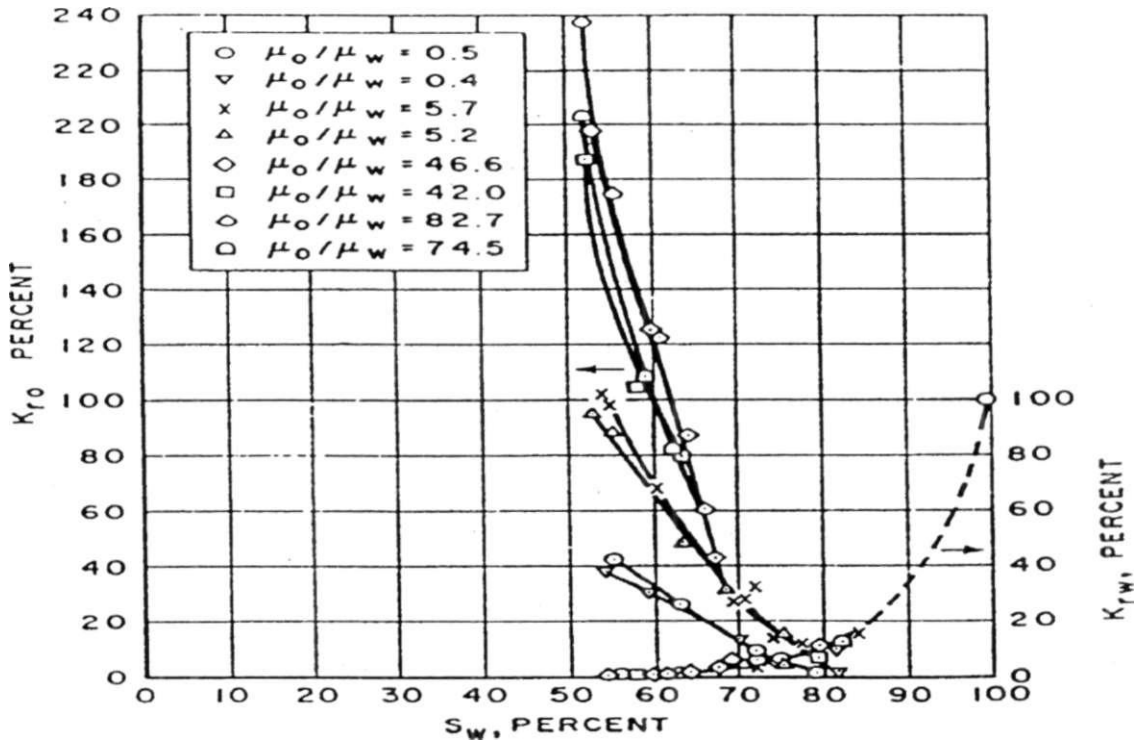

Figure 7.18: Effect of viscosity ratio on relative permeability in oil-water system. (From Odeh, 1959)

decreasing viscosity ratio (—) in a water/oil system. Please note that the symbols in Figure 7.18 are not ordered.

Avraam and Payatakes (1995) conducted experimental studies using a model of chamber and throat type, etched in glass. Some of their results are shown in Figure 7.6. These graphs show the same trends as the experimental works of Odeh (1959), that k_{ro} decreases by decreasing the viscosity ratio ***(K).***

Network simulation results of Constantinides and Payatakes (1996) showed the same trend. Figure 7.19 shows their obtained results. As it is shown in this figure, relative permeability to the disconnected non-wetting phase (oil ganglia) decreases by decreasing the viscosity ratio *(K)*.

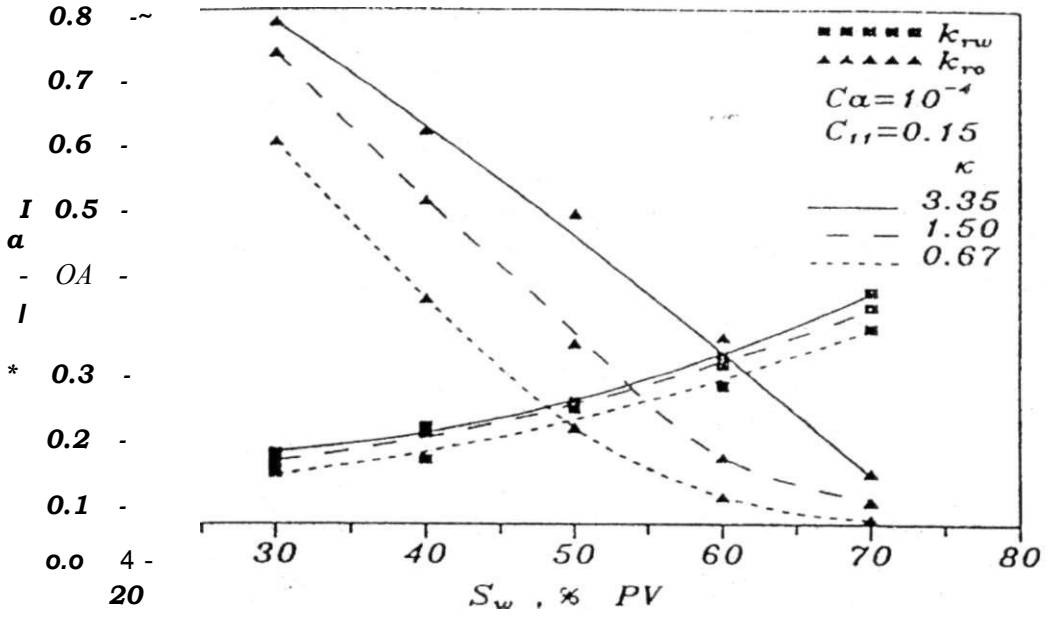

Figure 7.19: Effect of viscosity ratio on relative permeability in oil-water system. (From Constantinides and Payatakes, 1996)

Wall and Khurana (1972) studied the effect of viscosity on relative permeability to gas. They showed that the gas relative permeability decreases with increase in oil viscosity. Figure 7.20 shows their results.

It has been suggested that in gas-oil systems, gas relative permeability is lower in some heavy oil systems than in light oil systems. The experimental and simulation results of Pooladi-Darvish and Firoozabadi (1999) indicate that the gas mobility in a

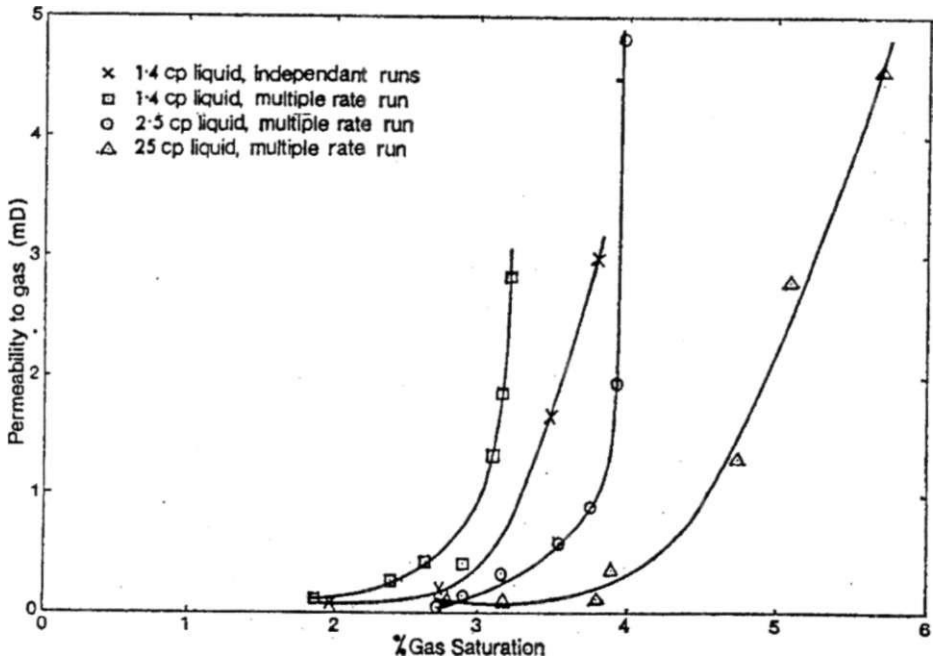

Figure 7.20: Gas relative permeability at different oil viscosities. (From Wall and Khurana, 1972)

heavy oil system is much less than that in a lighter oil system under solution gas drive. Their results are shown in Figure 7.21 in terms of ratio of relative permeabilities, where relative permeability to oil remains constant.

Studying the effect of oil viscosity on gas relative permeability is our main goal in this work. None of the previous network models investigated gas oil system for this purpose. As it is shown in Figure 7.22, by increasing oil viscosity; i.e. by decreasing

the viscosity ratio , relative permeability to gas decreases. This behavior might explain why in heavy oil reservoirs, the tendency of gas bubbles to be produced is lower than that in conventional light oil reservoirs. Figure 7.22 shows this behavior at three different capillary numbers. The same behaviour was found at different gas bubble sizes, and gas saturations.

Figure 7.21: Comparison of relative permeability ratio in heavy and light oil. (From Pooladi-Darvish and Firoozabadi, 1999)

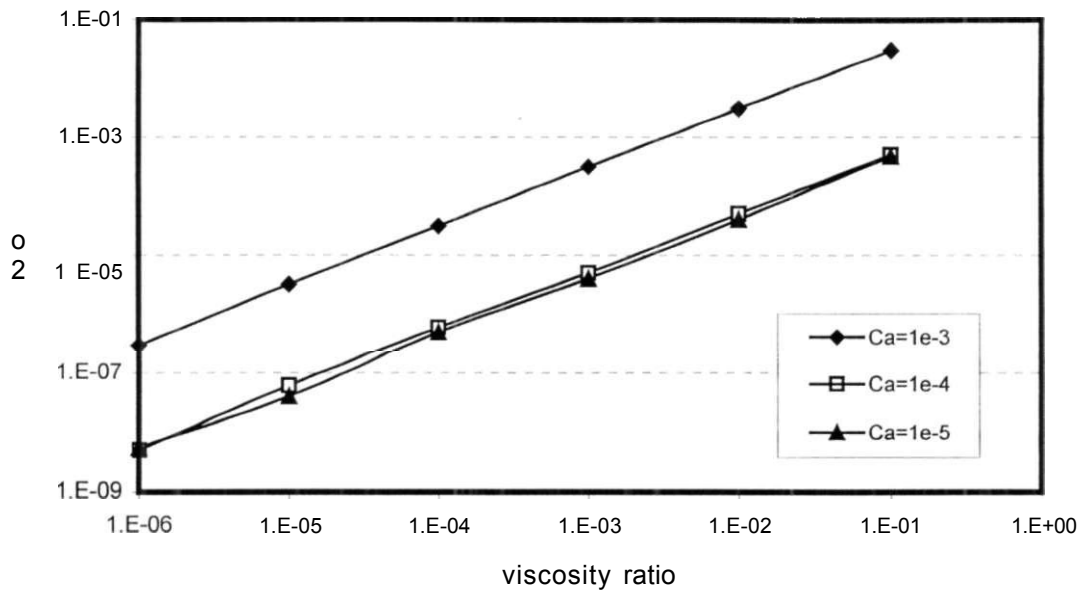

Figure 7.22: Effect of viscosity ratio on gas relative permeability. (9-CEVS bubble, S_g=12%, IFT=20mN/m, θ_c = 25)

The obtained results are in line with the experimental work of Odeh (1959), and Avraam and Payatakes (1995), network modeling of Constantinides and Payatakes (1996), and experimental and simulation results of Pooladi-Darvish and Firoozabadi (1999).

CHAPTER EIGHT

Conclusions and recommendations

8.1. Conclusions

A converging-diverging network model including the capillary and pressure forces was developed. Relative permeability of the dispersed gas bubbles in an oil saturated porous media is simulated using the developed network model. The following conclusions are obtained from the simulation results:

- Gas relative permeability is a function of gas saturation, viscosity ratio *(/jg/ju$_o$),* capillary number, interfacial tension (IFT), contact angle, pore-aspect ratio, and gas bubble size.

- Among the variables studied, viscosity ratio had the largest impact on relative permeability to gas. The results indicated that a ten-time increase in oil viscosity leads to an approximate ten-time decrease in relative permeability to gas, all the other dimensionless numbers remaining the same. This is shown for the first time for the very low values of viscosity ratio (down to 1CT^6), applicable to heavy oil/gas systems. This observation confirms previous hypothesis (Pooladi-Darvish and Firoozabadi, 1999 and Kumar and Pooladi-Darvish 2000) that relative permeability to gas is extremely low in heavy oil systems under solution-gas drive, leading to improved oil recovery.

- Larger gas bubbles showed higher gas relative permeability. This suggests that small gas bubbles in heavy-oil systems under solution gas drive could lead to reduced gas mobility.

Based on the above conclusions the following suggestions can be provided.

- For experimental determination of relative permeability, one should choose the rock and fluids of interest. This would ensure similarity of viscosity ratio, interfacial tension, and aspect ratio. Another dimensionless number that should be properly scaled between the field and the laboratory is the Capillary number. Flow rates in the laboratory should therefore be chosen such that the capillary number is properly scaled with field conditions.

8.2. Recommendations

Our results indicated that a more dispersed gas phase exhibits a lower relative permeability, everything else being similar. Therefore, flow physics that determine bubble size in porous media should be included. One of the important processes affecting bubble size is the dynamic break-up of gas bubbles. The effect of break-up and other similar processes on gas relative permeability and their inclusion in the mathematical models is recommended.

References

ALEXANDROV, A.V., CURRIE, P.K., NGUYEN, Q.P., and ZITHA, P.L.J., Modelling of foam in Porous Media Based on Multivariate Statistics; *SPE 59288, 2000 SPE/DOE Improved Oil Recovery Symposium,* Tulsa, Oklahoma, 3-5 April 2000.

AVRAAM, D.G., KOLONIS, G.B., ROUMELIOTIS, T. C, CONSTANTINEDES, G.N., and PAYATAKES, A.C., Steady-State Two-Phase flow Through Planar and Non-planar Model Porous Media; *Transport in Porous Media,* Vol. 16, pp. 75-101, 1994.

AVRAAM, D.G., and PAYATAKES, A.C., Flow Regimes and Relative Permeabilities during Steady-State Two-Phase Flow in Porous Media; *J. of Fluid Mech.,* Vol. 293, pp. 207-236, 1995.

BOAMIN, X., KAMATH, J., YORTSOS, Y.C., and LEE, S.H., Use of Pore-Network Models to Simulate Laboratiry Corefloods in a Heterogeneous Carbonate Sample; *SPE Journal,* Vol. 4, No. 3, September 1999.

BORA, R., and MAINI, B.B., Flow Visualization Studies of Solution Gas Drive Process in Heavy Oil Reservoirs Using a Glass Micro-model; *SPE 37519, SPE International Thermal Operations and Heavy Oil Symposium, Bakersfield,* CA, 10-12 Feb., 1997.

BORA, R., and MAINI, B.B., and CHAKMA, A., Flow Visualization Studies of Solution Gas Drive Process in Heavy Oil Reservoirs with a Glass Micro-model; *SPE ReservoirEval. & Eng.,* 3 (3), pp. 224-229, June 2000.

BROADBENT, S.R., and HAMMERSLEY, J.M., Percolation Processes I. Crystal and Mazes; *Proc. Cambridge Phil. Soc,* 53, pp.629-645, 1957.

CHANDLER, R., KOPLIC, J., LERMAN, K., and WILLEMSEN, J.F., Capillary Displacement and Percolation in Porous Media; *J. Fluid Mech.,* 119, pp. 249-267, 1982.

CLARIDGE, E.L. and PRATS, M., A Proposed model and Mechanism for Anomalous Foamy Heavy Oil Behaviour; *SPE 29243, International Heavy Oil symposium,* Calgary, AB, Canada, 19-21 June, 1995.

CONSTANTINIDES, G.N., and PAYATAKES, A.C., Effects of Precursor Wetting Films in Immiscible Displacement Through Porous Media; *Transport in Porous Media,* Vol. 38, pp. 291-317, 2000.

CONSTANTINIDES, G.N., and PAYATAKES, A.C., Network Simulation of Steady-State Two-Phase Flow in Consolidated Porous Media; *AIChE Journal,* Vol. 42, No.2, 1996.

CONSTANTINIDES, G.N., and PAYATAKES, A.C., A Theoretical Model of Collision and Coalescence of Ganglia in Porous Media; *Journal of Colloid and Interface Science,* Vol. 141, No. 2, Feb. 1991.

DIAS, M.M., Formation and Dynamics of Oil Ganglia in Porous Media, Ph.D. dissertation, University of Houston, Houston, Texas, 1984.

DIAS, M.M., ALKIVIADES, C, and PAYATAKES, A.C., Network Models for Two-phase Flow in Porous Media, part 1, Immiscible Micro-displacement of Non-wetting fluids; *J. Fluid Mech.,* Vol. 164, pp. 305-336, 1986.

DIAS, M.M., ALKIVIADES, C, and PAYATAKES, A.C., Network Models for Two-phase Flow in Porous Media, part 2, Motion of Oil Ganglia; *J. Fluid Mech.,* Vol. 164, pp. 337-358, 1986.

DIAS, M.M., and WILKINSON, D., Percolation with Trapping; *J., Phys. A: Math. Gen.,* Vol. 19, pp. 3131-3146, 1986.

DIAZ, C.E., CHATZIS, I., and DULLIEN, F.A.L., Simulation of Capillary Pressure Curves Using Bond Correlated Site Percolation on a Simple Cubic Network; *Transport in Porous Media,* 2, pp.215-240, 1987.

DIXIT, A.B., MCDOUGALL, S.R., SORBIE, K.S., and BUCKLEY, J.S., Pore Scale Modelling of Wettability Effcets and Their Influence on Oil Recovery, *SPE/DOE 35451, 1996 SPE/DOE Tenth Symposium on Improved Oil Recovery,* Tulsa, Oklahoma, 21-24 April 1996.

DIXIT, A.B., MCDOUGALL, S.R., and SORBIE, K.S., A Pore-Level Investigation of Relative Permeability Hysteresis in Water-Wet Systems; *SPE 37233, 1997 SPE International Symposium on Oilfield Chemistry,* Houston, Texas, 18-21 February 1997.

DIXIT, A.B., MCDOUGALL, S.R., and SORBIE, K.S., Analysis of Relative Permeability Hysteresis Trends in Mixed-Wet Porous Media Using Network Models; *SPE 39656, 1998 SPE/DOE Improved Oil Recovery Symposium,* Tulsa, Oklahoma, 19-22 April 1998.

DULLIEN, F.A.L., CHATZIS, I., and EL-SEYED, S.; Modelling Transport Phenomena in Porous Media by Networks Consisting of Non-Uniform Capillaries; SPE 6191, 1976.

DUSSAN, V.E.B., The Moving Contact Line: The Slip Boundary Condition; *J. Fluid Mech.,* Vol. 77, pp. 665-684, 1979.

DUSSEAULT, M., Cold Production and Enhanced Oil Recovery; *JCPT,* Vol. 32, No. 9, pp. 16-18, Nov. 1993.

DUSSEAULT, M., and EL-SEYED, S., Heavy Oil Production Enhancement by Encouraging Sand Production; *2000 SPE/DOE Improved Oil Recovery Symposium,* Tulsa, OK, 2-5 April 2000.

DUSSEAULT, M., GEILIKMAN, M.B., SPANOS, T., Mechanisms of Massive Sand Production in Heavy Oils; *7th UNITAR Heavy Crude and Tar Sands International Conference,* Beijing, China, 27-30 Oct. 1998.

ECONOMIDES, E., FERNANDEZ, B.G., and GONGORA, OA., Global Experiences and Practice for Cold Production of Moderate and Heavy Oil, *SPE Formation Damage Control International Symposium,* Lafayette, LA, 23-24 Feb. 2000.

ESSAM, J.W., Percolation Theory; *Rep. Prog. Phys.,* 43, pp.833-912, 1980.

ETTINGER, R.A., and RADKE, C.J., Influence of Texture on Steady Foam Flow in Berea Sandstone; *SPE Reservoir Engineering,* pp. 83-90, Feb. 1992.

FATT, I., The Network Model of Porous Media, Part I: Capillary Pressure Characteristics; *Petroleum Transaction, AIME,* Vol. 207, pp. 144-181, 1956.

FATT, I., The Network Model of Porous Media, Part II: Dynamic Properties of a Single Size Tube Network; *Petroleum Transaction, AIME,* Vol. 207, pp. 144-181, 1956.

FATT, I., The Network Model of Porous Media, Part III: Dynamic Properties of Networks with Tube Radius Distribution; *Petroleum Transaction, AIME,* Vol. 207, pp. 144-181, 1956.

FENWICK, D.H., and BLUNT, M.J., Network Modeling of Three-phase Flow in Porous Media; *SPE Journal,* pp. 86-97, March, 1998.

FIROOZABAI, A.: Mechanisms of Solution Gas Drive in Heavy Oil Reservoirs, *Journal of Canadian Petroleum Technology,* Vol. 40, No. 3, pp. 15-20, 2001.

FLUMERFELT, R.W., CHEN, H-L, RUENGPHRATHUENGSUKA, W., HSU, W-F., and PREIDITIS, J, Network analysis of Capillary and Trapping Behavior of Foams in Porous Media; *SPE Formation Evaluation,* pp. 25-33, March 1992.

FRISCH, H.L., and HAMMERSLEY, J.M., Percolation Processes and Related Topics; *J. Soc. Ind. Appl. Math.,* 11, pp. 894-918, 1963.

GEILIKMAN, M.B., DUSSEAULT, M.B., and DULLIEN, F.A.L, Dynamic Effects of Foamy Fluid Flow in Sand Production Instability; *SPE 30251, International Heavy Oil Symposium,* Calgary, AB, Canada, 19-21 June, 1995.

GOODE, P.A., Momentum Transfer Across Fluid-Fluid Interfaces in Porous Media, PhD. Dissertation, Hariot-Watt University, UK, 1991.

HARTLAND, S., The coalescence of Liquid Drop at a Liquid-Liquid Interface, Part II, Film Thickness; *Trans. Inst. Chem. Engrs. (London),* Vol. 45, T102-T108, 1967.

HEIBA, A.A., DAVIS, H.T., and SCRIVEN, L.E., Statistical Network Theory of Three-Phase Relative Permeabilities; *SPE/DOE 12690,* 1984.

HEIBA, A.A., SAHIMI, M., SCRIVEN, L.E., and DAVIS, H.T., Percolation theory of Two-Phase Relative Permeability; *SPE Reservoir Engineering,* pp. 123-132, Feb. 1992.

HEURTA, M., OTERO, C, RICO, A., JIMENEZ, I., de MIRABAL, M., ROJAS, G., Understanding Foamy Oil Mechanisms for Heavy Oil Reservoirs During Primary Production; *SPE 36749, SPE Annual Technical Conference and Exhibition, Denver, Colorado, USA,* 6-9 Oct., 1996.

HINKLEY, R.E., Experimental Study of Oil Ganglion Motion; MSc. Thesis, University of Houston, 1983.

HONARPOUR, M. and MAHMOOD, S.M.; Relative Permeability Measurements: An Overview, *JPT,* Aug. 1988.

HUGHES, R.G., and BLUNT, M.J., Pore-Scale Modeling of Multiphase Flow in Fractures and Matrix/Fracture Transfer; SPE 56411, *1999 SPE Annual Technical Conference and Exhibition,* Houston, Texas, 3-6 October 1999.

IOANNIDIS, M.A., CHATZIS, I., and DULLIEN, F.A.L., Macroscopic Percolation Model of Immiscible Displacement: Effect of Buoyancy and Spatial Structure; *Water Resources Research,* Vol. 32, No. 11, pp. 3297-3310, 1996.

ISLAM, M. R., and CHAKMA, A., Mechanics of Bublle flow in Heavy Oil Reservoirs; *SPE 20070, 60th California Regional Meeting, Ventura, CA,* 4-6 April 1990.

JEFFREYS, V., and DAVIS, G.A., Coalescence of Liquid Droplets and Liquid dispersions; Recent Advances in Liquid-Liquid Extraction, C. Hanson (ed.), Pergamon Press, 1971.

JONES, S.F., EVANS, G.M., and GALVIN, K.P., Bubble nucleation from gas cavities- A review; Advances in colloid and interface science, 80, pp. 27-50, 1999.

KALAYADJIAN, F., BOURBIAUX, D., and GUERILLOT, D., Viscous Coupling Between Fluid Phases for Two-Phase Flow in Porous Media: Theory Versus Experiment; Institut Francais Du Petrole, France.

KANTZAS, A., and CHATZIS, I., Network Simulation of Relative Permeability Curves Using a Bond Correlated-site Percolation Model of Pore structure; Chem. Eng. Comm., Vol. 69, pp. 191-214, 1988.

KANTZAS, A., and CHATZIS, I., Application of the Preconditioned Conjugate Gradients Method in the Simulation of Relative Permeability Properties of Porous Media; Chem. Eng. Comm., Vol. 69, pp. 169-189, 1988.

KHARABAF, H., and YORTSOS, Y.C., Pore Network Model for Foam Formation and Propagation in Porous Media; *SPE Journal,* pp. 42-53, March 1998.

KOPLIC, J., Creeping Flow in Two-dimensional Networks; J. Fluid Mech., Vol. 119, pp. 21-247, 1982.

KOPLIC, J., and LASSATER, T.J., Two-Phase Flow in Random Network Models of Porous Media; *SPEJ,* pp. 89-100, Feb. 1985.

KRAUS, W.P., McCAFFREY, W.J., and BOYD, G.W., Pseudo-Bubble Point Model for Foamy Oils; *ATM of the Petroleum Society of CIM,* Calgary, AB, Canada, 9-12 May, 1993.

KUMAR, R., Solution-Gas Drive in Heavy Oil- Gas Mobility and Kinetics of Bubble Growth, MSc. Dissertation, University of Calgary, Calgary, Alberta, 2000.

KUMAR, R., and POOLADI-DARVISH, M.; Solution Gas Drive in Heavy Oil: Field Predictions and Sensitivity Studies with Low Gas Phase Relative Permeability, *CIM 2000-63, presented at the 51st Annual Technical Meeting of the Petroleum society of CIM,* Calgary, AB, 9-12 June 2000.

KUMAR, R., and POOLADI-DARVISH, M.; Effect of Viscosity and Diffusion Coefficient on the Kinetics of Bubble Growth in Solution-Gas Drive in Heavy Oil, *JCPT,* Vol. 40, No. 3, pp.30-37, March 2001.

KUMAR, R., POOLADI-DARVISH, M., and OKAZAWA, T.; An Investigation into Enhanced Recovery Under Solution-Gas Drive in Heavy Oil Reservoirs; *SPE 59336,*

presented at the SPE Improved Oil Recovery Symposium, Tulsa, OK, April 2-5, 2000.

I_AGO, M., GOMES, R., and HUERTA, M., Visualization Study During depletion Experiments of Venezuelan Heavy Oils Using Glass Micromodels; *The petroleum society's Canadian International Petroleum Conference,* Calgary, AB, Canada, June 4-8, 2000.

LAROCHE, O, VIZIKA, O., and KALAYDJIAN, F., Network Modeling to Predict the Effect of Wettability Heterogeneities on Multiphase Flow; *SPE 56674, 1999 SPE Annual Technical Conference and Exhibition,* Houston, Texas, 3-6 October 1999.

LARSEN, J.K., BECH, N., and WINTER, A., Three-Phase Immiscible WAG Injection: Micromodel Experiments and Network Models; *SPE 59324, 2000 SPE/DOE Improved Oil Recovery Symposium,* Tulsa, Oklahoma, 3-5 April 2000.

LARSON, R.G., DAVIS, H.T., and SCRIVEN, L.E., Displacement of Residual Nonwetting Fluids from Porous Media; Chem. Eng. Sci., 36, pp. 75-85, 1981.

LARSON, R.G., SCRIVEN, L.E., and DAVIS, H.T., Percolation Theory of Residual Phases in Porous Media; *Nature,* 268, pp. 409-413, 1977.

LI, X, Bubble Growth During Pressure Depletion in Porous Media; Ph.D. Dissertation, University of Southern California, Los Angeles, CA, p.158, May 1993.

LI, K., and FIROOZABADI, A., Phenomenological Modelling of Critical Condensate Saturation and Relative Permeabilities in Gas/Condensate systems, SPE Journal, Vol. 5, No. 2, pp. 138-147, 2000.

LOUGHEAD, D.J., SALTUKLAROGLU, M., Llyodminster Heavy Oil Production- Why So Unusual?; *Ninth Annual Heavy Oil and Oil Sand Technology Symposium, Calgary,* March 11, 1992.

MANI, V., and MOHANTY, K.K., Pore-Level Network Modeling of Three-Phase Capillary Pressure and Relative Permeability Curves; *SPE Journal,* September 1998.

MAXIMENKO, A., and KADET, V.V., Determination of Relative Permeabilities Using the Network Models of Porous Media; *Journal of Petroleum Science and Engineering,* 28, pp. 145-152, 2000.

MCKAY, G.P., and MSON, S.G., The Gravity approach and Coalescence of fluid Drops at Liquid Interfaces; *Canadian Journal of Chemical Engineering,* Vol. 41, pp. 203-212, 1963.

MELROSE, J.C., and BRANDNER, OF., Role of Capillary Forces in Determining Microscopic Displacement Efficiency for Oil Recovery by Water Flooding; *Can. J. Pet. Tech.,* Vol. 13, No. 4, pp.54-62, 1974.

MOGENSEN, K., and STENBY, E., A Dynamic Pore-Scale Model of Imbibition; *SPE 39658, 1998 SPE/DOE Improved Oil Recovery Symposium,* Tulsa, Oklahoma, 19-22 April 1998.

NEIRA, M., ALKIVIADES, O, and PAYATAKES, A. O, Collocation Solution of Creeping Newtonian Flow Through Sinusoidal Tubes; *AIChE J.,* Vol. 25, No. 4, 1979.

NEIRA, M., and PAYATAKES, A. C, Collocation Solution of Creeping Newtonian Flow Through Periodically Constricted Tubes with Piecewise Continuos Wall Profile, *AIChEJ.,* 24, pp.42, 1978.

NG, K.M., and PAYATAKES, A.C., Stochastic Simulation of the Motion, Break-up, and Stranding of Oil Ganglia in Water-Wet Granular Porous Media during Immiscible Displacement; *AIChEJ., Vol. 26, pp. 419-429, 1980.*

ODEH, A.S., Effect of Viscosity Ratio on Relative Permeability, *Petroleum Transaction, AIME, Vol. 216, pp.346-353, 1959.*

OREN, P.E., BILLIOTTE, J., and PINCZEWSKI, W.V., Pore-Scale Network Modelling of waterflood Residual Oil Recovery, *SPE 27814, SPE/DOE Ninth symposium on Improved Oil Recovery, Tulsa, Oklahoma, 17-20 April, 1994.*

PATZEK, T. W., Verification of a complete Pore Network Simulator of Drainage and Imbibition; *SPE 59312, SPE/DOE Improved Oil Recovery Symposium, Tulsa, Oklahoma,* 3-5 April 2000.

PAYATAKES, A.C., Dynamics of Oil Ganglion during Immiscible displacement in Water-wet Porous Media; *Ann. Rev. fluid Mech.,* Vol. 14, pp. 365-393, 1982.

PAYATAKES, A.C., and DIAS, M.M., Immiscible Micro-displacement and Ganglion Dynamics in Porous Media; *Reviews in Chemical Engineering,* Vol. 2, No. 2, pp. 85-174, 1984.

PAYATAKES, A.C., NG, K.M., and FLUMERFELT, R.W., Oil Ganglia Dynamics During Immiscible Displacement, Model Formulation, *AIChE J.,* Vol. 20, pp. 430-443, 1980.

PAYATAKES, A.C., TIEN, C, and TORIAN, R.M., A New Model for Granular Porous Media; *AIChE Journal,* Vol. 19, No. 1, p. 58-76, 1973.

PAYATAKES, A. O, Tien, C, and Turian, R. M., Part II. Numerical solution of Steady State Incompressible Newtonian Flow Through Periodically Constricted Tubes, *AIChE J.,* 19, 67, 1973.

PICKELL, J.J., SWANSON, B.F., and HICKERMAN, W.B., Application of Air-Mercury and Oil-air Capillary Pressure Data in the Study of Pore Structure and Fluid Distribution; *SPEJ,* Vol. 6, pp. 55-61, 1966.

POOLADI-DARVISH, M., and FIROOZABADI, A., Solution-gas Drive in Heavy Oil Reservoirs; *Journal of Canadian Petroleum Technology,* Vol. 38, No. 4, pp. 54-61, 1999.

POON, D., and KISMAN, K., Non-Newtonian effects on the Primary Production of Heavy Oil Reservoirs; *Journal of Canadian Petroleum Technology,* pp. 55-59, September 1992.

SAHIMI, M., Flow Phenomena in Rocks: From Coninuum Models to Fractals, Percolation, Cellular Automata, and simulated Annealing; *Reviews of Modern Physics,* Vol. 65, No. 4, pp. 1393-1534, Oct. 1993.

SARMA, H., and MAINI, B., Role of Solution Gas in Primary Production of Heavy Oils; *SPE 23631, Second Latin America Petroleum Engineering Conference, Caracas, Venezuela,* 8-11 March, 1992.

SATIK, O, and YORTSOS, Y.C., A Pore-Network Study of Bubble Growth in Porous Media Driven by Heat Transfer; *Journal of Heat Transfer,* Vol. 118, May 1996.

SIMON, R., and KELSEY, F.J., The Use of Capillary Tube Networks in Reservoir Performance Studies: II. Equal-Viscosity Miscible Displacement; *SPEJ,* pp. 99-112, June 1971.

SIMON, R., and KELSEY, F.J., The Use of Capillary Tube Networks in Reservoir Performance Studies: II. Effect of Heterogeneity and Mobility on Miscible Displacement Efficiency; *SPEJ,* pp. 345-351, August 1972.

SINGHAL, A.K., and SOMERTON, W.H., Network Model for the Study of Multiphase Flow Behavior in Porous Media; *SPE 2906.* (after 1970).

SHEFFIELD, R.E., and METZNER, A.B., Flow of Non-linear Fluids Through Porous Media; *AlChE J.,* Vol.22, p.736, 1976.

SHEN, C, and BATYCKY, J.P., Observation of Mobility Enhancement of Heavy Oils Flowing Through Sand Pack Under Solution Gas Drive; *Journal of Canadian Petroleum Technology,* Vol. 38, No. 4, pp. 48-53, 1999.

SHENG, J.J., MAINI, B.B., HAYES, R.E., and TORTIKE, W.S., A Non-equilibrium Model to Calculate Foamy Oil Properties; *Journal of Canadian Petroleum Technology,* Vol. 38, No. 4, pp. 38-45, 1999.

SLATTERY, J.C., Interfacial effects in the Entrapment and displacement of Residual Oil; *AIChEJ.,* vol. 20, pp. 1145-1154, 1974.

SMITH, G.E., Fluid Flow and Sand Production in Heavy Oil Reservoirs Under Solution Gas Drive; *SPEPE,* pp. 169-177, May 1988.

STEGEMEIER, G.L., Mechanisms of entrapment and displacement of Oil in Porous Media, *81st AIChE meeting,* Kansas City, Missouri, April 11-14, 1976.

TANG, G. and FIROOZABADI, A., Gas and Liquid-Phase Relative Permeabilities for Cold Production from Heavy Oil Reservoirs; *SPE 56540, 1999 SPE Annual Technical Conference and Exhibition,* Houston, Texas, 3-6 Oct., 1999.

TREINEN, R.J., RING, W. 'W., SPENCE, A.P., MIRABLE, M., and HUETRA, M., Hamaca: Solution Gas Drive Recovery in Heavy Oil Reservoirs, Experimental Results; *SPE 39031, Fifth Latin America and Caribbean Petroleum Engineering Conference and Exhibition,* Rio de Janeiro, Brazil, August 30-September 3, 1997.

TREMBLAY, B., OLDAKOWSKI, K, and SETTARI, A., Geomechanical Properties of Oil Sands at Low Effective Stress; *48th ATM of Petroleum Society,* Calgary, AB, Canada, 8-11 June, 1997.

TREMBLAY, B., SEDGWICK, G„ and FORSHNER, K., Modeling of Sand Production from Wells on Primary Recovery; *47™ ATM of The Petroleum Society, Calgary, Alberta, Canada,* June 10-12, 1996.

TREMBLAY, B., SEDGWICK, G., and VU, D., Cold Production in Heavy Oil Reservoirs; *15th World Petroleum Congress,* Beijing, China, 12-16 Oct. 1997.

VIZIKA, O., AVRAAM, D.G., and PAYATAKES, A.C., On the Role of the Viscosity Ratio during Low-Capillary-number Forced Imbibition in Porous Media; *JOURNAL OF COLLOID AND INTERFACE SCIENCE,* Vol. 165, pp. 386-401, 1994.

WAGNER, G., Use of Invasion Percolation Models to Study the Secondary Migration of Oil and Related Problems; PhD dissertation, University of Oslo, Jan. 1997.

WALL, C.G., and KHURANA, A.K., The Effect of Rate of Pressure Decline and Liquid Viscosity on Low-Pressure Gas Saturations in Porous Media; *Journal of the Institute of Petroleum,* pp. 335-345, Nov. 1972.

WANG, Y., and YUAN, J.Y., Cold Production and Wormhole Propagation in Poorly Consolidated Reservoirs; *7th UNITAR Heavy Crude and Tar Sands International Conference,* Beijing, China, 27-30 Oct. 1998.

WARDLAW, N.C., The Effects of Pore Structure on displacement Efficiency in Reservoir Rocks and in Glass Micro-models; *SPE 8843, First Joint SPE/DOE Symposium on Enhanced Oil Recovery,* Tulsa, Oklahoma, April 20-23, 1980.

WASHBURN, E.W., The Dynamics of Capillary flow; *Phys. Rev.,* Vol. 17, pp. 273-283, 1921.

WEST, G.D., On the Resistance to the Motion of a Thread of Mercury in a Glass Tube; *Proc. Roy. Soc, London,* A86, 20-25, 1911/12.

WILKINSON, D., and WILLIAMSEN, J. F., Invasion Percolation: A New Form of Percolation Theory; *J. Phys. A. Math. Gen.,* Vol. 16, pp.3365-3376, 1983.

YUAN, J.Y., TREBLAY, B., and BABCHIN, A., A Wormhole Network Model of Cold Production in Heavy Oil; *SPE 54097, 1999 SPE International Thermal Operations and Heavy Oil Symposium,* Bakersfield, California, 17-19 March 1999.

YUAN, J.Y., BABCHIN, A., and TREBLAY, B., Modelling Wormhole Flow in cold Production; *49th Petroleum Society ATM,* Calgary, AB, Canada, 8-10 June 1998.

ZARA, R.A., ONODY, R.N., N-steps Invasion Percolation Model; *Physica A: Statistical Mechanics and Its Applications,* Vol. 277, No. 1, 2000.